KERNFORSCHUNGSZENTRUM

KARLSRUHE

November 1975 KFK 2221

Institut für Material- und Festkörperforschung
Projekt Schneller Brüter

The Specifications, Design, Irradiation and Post-Irradiation Examination of a Mixed Oxide Pin of the Mol-8C-Series (Pin No. 5)

M. Zafar Ullah, D. Geithoff, P. Weimar

GESELLSCHAFT
FÜR
KERNFORSCHUNG M.B.H.

KARLSRUHE

GESELLSCHAFT FÜR KERNFORSCHUNG M. B. H.

KARLSRUHE

K E R N F O R S C H U N G S Z E N T R U M K A R L S R U H E

KFK 2221

Institut für Material- und Festkörperforschung

Projekt Schneller Brüter

The Specifications, Design, Irradiation and Post-Irradiation Examination of a Mixed Oxide Pin of the Mol-8C-Series (Pin No.5)

M. Zafar Ullah[+)]

D. Geithoff

P. Weimar

Gesellschaft für Kernforschung mbH., Karlsruhe

[+)] Delegate from the Pakistan Institute of Nuclear Science and Technology (PINSTECH) of the Pakistan Atomic Energy Commission, Islamabad.

K U R Z F A S S U N G

Die Gesellschaft für Kernforschung, Karlsruhe, hat einige Bestrahlungsversuche im BR-2 in Belgien ausgeführt. Die Serie Mol-8C ist eines dieser Experimente. Sie zielt ab auf den Einfluß verschiedener Parameter auf das Bestrahlungsverhalten von Einzelstäben.

Die Bestrahlung wurde unter Cadmium-Abschirmung im epithermischen Fluß in NaK-Kapseln (FAFNIR) ausgeführt. Der Brennstoff bestand aus Mischoxid mit ca. 20 % PuO_2 und aus auf 93 % angereichertem Uran. Die Brennstoffdichte war 86,6 %,und die Säulenlänge betrug 522 mm. Das Hüllmaterial bestand aus austenitischem Stahl 1.4988 (Abmessung 6 mm Außendurchmesser und 0,38 mm Wandstärke). Die Länge des Brennstabes betrug 1.024 mm. Die Bestrahlung wurde über 22 BR2-Zyklen in 4 verschiedenen Kanälen über 427,8 Tage (Volleistungsäquivalent) ausgeführt. Die maximale Hüllaußentemperatur betrug 575 ^{o}C, die lineare Leistung des Stabes 393 W/cm und der mittlere Abbrand 9,6 % FIMA.

Der Bericht gibt im Detail die Ergebnisse der kompletten Nachuntersuchung des Stabes 5 der Mol-8C-Serie wieder. Weiterhin werden ebenfalls einige notwendige Angaben über Spezifikation, Fabrikation und Bestrahlungsgeschichte des Stabes gemacht.

A B S T R A C T

The Karlsruhe Nuclear Centre (GfK) has undertaken some irradiation experiments in BR-2 at Mol/Belgium. The Mol-8C series is one of these experiments and is aimed at investigating the influence of various parameters on the irradiation behaviour of some pins.

The irradiation was performed in the epithermal flux of the reactor in a cadmium shielded and NaK cooled capsule, called FAFNIR. The fuel was $(U, Pu)O_2$ with about 20 % PuO_2 and 93 % enriched uranium. The fuel density was 86.6 % theoretical density and the fuel column length was 522 mm. The cladding material was an austenitic stainless steel (no.1.4988) tube of 6 mm outer diameter and of 0.38 mm wall thickness. The pin length was 1024 mm

The irradiation was completed in 22 cycles in four different channels of the reactor for a total of 427.8 full power days. The clad outside maximum temperature was 575°C. The pin linear power was 393 W/cm and mean burn-up was about 9.6 % fima.

The present report describes in detail the post-irradiation behaviour of one of the pins of the Mol-8C series. Some necessary information regarding the specifications, fabrication and irradiation history of the pin is also given.

ACKNOWLEDGEMENTS

We wish to thank Mr. Bauer for his help in making the diagramms and supervising the printing of this report and Mrs. Hauth and Mrs. Ratzel for typing the manuscript in a short time.

One of us (MZU) specially wishes to thank Dr. K. Kummerer, head of the Institut für Material- und Festkörperforschung for accepting him to work in his institute and GfK for the generous grant received during his stay in the centre. He is also grateful to the Pakistan Atomic Energy Commission for nominating him to work at GfK.

M. Zafar Ullah
D. Geithoff
P. Weimar

CONTENTS

1. INTRODUCTION

The Karlsruhe Nuclear Centre (GfK) has conceived a large number of irradiation experiments for research and development of satisfactory fuel elements for the future fast breeder reactors. Accordingly, a comprehensive work on making different specifications and fabrication of the fuel pins to investigate the influence of numerous parameters on the irradiation behaviour was undertaken by GfK. Since only limited space is available in the fast reactor test facilities in Europe, it was, therefore, envisaged that some additional experiments may be performed in the thermal reactor BR-2 at Mol. However, it was deemed necessary that the irradiations be carried out under conditions closely approaching the conditions to be encountered in the fast reactors. It was, therefore, decided that the capsule to be used for irradiation should be cadmium shielded so that all the thermal neutrons are screened out by the cadmium shield and the irradiation is carried out in the epithermal and fast flux of the reactor. One such capsule, called, FAFNIR was developed at CEN-Mol and was used for the irradiation of numerous pins. The capsule was internally cooled by a stagnant NaK alloy.

Table 1 summarizes the designation and objectives of various irradiation experiments performed in FAFNIR capsules:

Table 1 Objectives of Mol 8-Irradiation Experiments

Experiment	Objectives	No. of Pins	Fuel
Mol-8A	Performance test	2	enriched U and Pu mixed oxide
Mol-8B	Fission gas pressure measurement	2	
Mol-8C	Parameter tests	10	
Mol-8D	Central temperature measurement	12	

The Mol-8C experiment was undertaken to investigate the influence of certain parameters, such as, smear density, axial restraint of the fuel column, and fuel clad gap on the irradiation behaviour of 10 fuel pins.[+)] Table 2 gives certain pertinent details of these pins.

Table 2 Details of the 10 pins of the Mol 8C-series

Pin No.	Density T.D. %	Pellet Diameter (mm)	Radial Gap (/um)	Axial Restraint.
Mol-8C-1	95	5·10	70	with
-2	95	"	"	"
-3	95	"	"	without
-4	95	"	"	"
-5	87.6	"	"	with
-6	87.6	"	"	"
-7	87.6	"	"	without
-8	87.6	"	"	"
-9	87.6/90.8/95	5.19/5.10/4.986	25/70/127	with
-10	"	"	"	"

The present report describes in detail the post-irradiation behaviour of Mol-8C-5 Pin.

Some other information regarding specifications, fabrication and irradiation history of the pin are also given. Since any such task of this magnitude involves a large number of persons at various stages of the experiment, therefore, the following table has been included to show the contribution made by various persons during the course of this experimentation.

+) The main feature was a continuous measurement of the fission gas pressure.

Table 3 Time Schedule of the Mol 8C-Experiment

Period	Activity	Main worker/s	Institution/Department and Centre
1967	Preparatory Consideration and Conception of experiment	Gerken and Karsten	+) IAR - GfK
1968	Irradiation Capsule	von der Hardt	Tech. Dept.-CEN
1968	Specifications	Kummerer, Gerken	++) IMF - GfK
1970	Fabrication of Specimens	Dippel and Kummerer	IMF - GfK
1970-73	Organization and Supervision of Irradiation in BR-2	von der Hardt Freund, AG Mol-GfK	Tech.Dept. - CEN IMF - GfK
1975	Destructive and Non-Destructive Examination in Hot Cells	Scheeder, Enderlein, Pejsa, Tucek, Schweigel, Ziegler, Weih, and Bossert	Hot cells- GfK
1975	Burnup analysis	Wertenbach	+++) IRCh - GfK
1975	Organization and Supervision of Examination in Hot Cells and Interpretation and Documentation of results	Zafar Ullah Geithoff Weimar	IMF - GfK (Delegate from PAEC) IMF - GfK " "

+) Institute of Applied Reactor Physics

++) Institute of Material Research

+++) Institute of Radio-Chemistry

2. SPECIFICATIONS AND DESIGN OF THE PINS

2.1 Objectives

The objectives of the Mol-8C irradiation experiments were:

a) to design experimental fuel pins with a typical mixed oxide fuel composition for a sodium cooled fast reactor,

b) to irradiate the pins under conditions fully or partially characteristic of a fast reactor, and

c) to undertake the post-irradiation examination of these pins.

The pins were designed to contain a fuel zone, a blanket zone and a fission gas plenum in the upper part of the pin. The fuel in the form of pellets was made of UO_2/PuO_2 mixed oxide (80 %/20 %) the uranium being enriched to 93 % U-235. Natural UO_2 pellets were used as the blanket material. An austenitic stainless steel of 6 mm outer diameter was used as the cladding tube. With a fluence of 7.5×10^{22} n/cm^2 ($E > 0.1$ MeV), the burn-up was expected to reach a value of 9 % fima. The irradiation examination was intended to elucidate the following aspects of the pin behaviour:

i) The pin integrity after the target burn-up has been reached,
ii) The axial and radial dimensional changes of the pin,
iii) The amount of fission gas released and retained by the fuel,
iV) The fuel restructuring with the formation of a central channel and various regions of different grain sizes,
V) The distribution of fission products in radial and axial directions and
Vi) The mechanism and the extent of internal and external damage of the clad material
Vii) The fission gas pressure-built-up during irradiation in oxide-fuel.

2.2 General Design Specifications

The detailed information has been published previously, /1,2/, however, the composition, shape, density and length of fuel and blanket column are given below. The type and dimensions of cladding material and the overall length of the pin are also given below:

Fuel material	=	$UO_2 - PuO_2$
PuO_2 content	=	20 $\pm$ 1 wt-%
U-235 content in UO_2	=	93 wt-%
O/M ratio	=	2.0 $\pm$ 0,03
Fuel shape	=	pellets, centreless ground without dishing
Fuel pellet density	=	87.6 $\pm$ 2 (% T.D.)
Smear density	=	83.0 (% T.D.)
Fuel pellet length	=	6.5 $\pm$ 1 mm
Fuel pellet diameter	=	5.1 $\pm$ 0.03 mm
Blanket material	=	natural UO_2, pellets
Blanket pellet density	=	95 $\pm$ 2.0 (% t.D.)
Cladding material	=	stainless steel no. 1.4988
Clad inside diameter	=	5.24 $\pm$ 0.03 mm
Clad thickness	=	0.38 $\pm$ 0.03 mm
Fuel clad radial gap	=	70 μm
Fuel column length	=	520 mm
Blanket column length	=	195 mm
Fission gas plenum length	=	250 mm
Total pin length	=	1024.4 mm
Max. clad inner temp.	=	680 ^{o}C
Average target burn-up	=	9 % fima

2.3 Pin Specifications

The Pin is 1024.4 mm long starting from the bottom of lower end plug to the top of the upper end cap. The fuel column is isolated from the lower end plug by two blanket pellets and is followed by a blanket column of natural UO_2 pellets. A sintered metallic filter fixed in a metallic plug separates the blanket column from the fission gas plenum. The top of the pin is closed by an outer upper end plug with arrangements for housing a metallic filter. The outer plug is welded to the end cap. The detailed pin design also indicating the material of construction of the various pin components is given in fig. 1. The overall length with the length of various internal parts of the pin are given below:

	mm
lower end plug	20.0
two isolation pellets	13.0
fuel column	520.0
blanket column	195.0
filter housing plug	4.0
gas plenum	250.0
upper outer plug + end cap	22.4
Total	1024.4

The sintered metallic filters have been used to avoid any contamination of the fission gases going into the gas plenum and subsequently to the outside measuring circuit through a capillary tube. The capillary tube has been brazed to the end cap and has the following dimensions:

	mm
outer diameter	1.1
wall-thickness	0.2
length	3000.0

The fuel column has been axially restrained by a tube placed inside the gas plenum between the filter housing plug and the upper outer end plug. The pin outside diameter is 6.0 $\pm$ 0.03 mm.

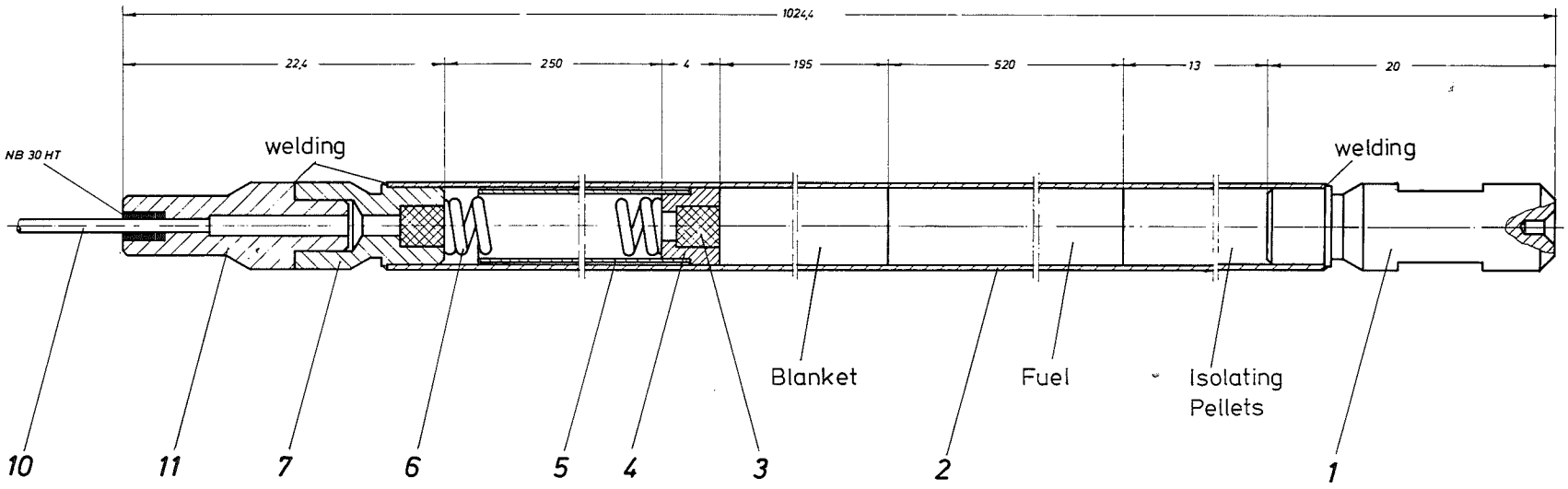

		Schweißprüfling			LBZ8/2/12
11	1	Endkappe	4988		LBZ8/2/11
10	1	Kapillare	4401	1,1 x 0,2 x 3000	
7	1	Oberer Endstopfen	4988		LBZ8/1/07
6	1	Druckfeder	4310	Lo = 255, d = 0,8, D_m = 4, i_f = 200 Wdg.	
5	1	Stützrohr	4988	5 x 0,25 x 244	
4	1	Führungsstück	4988		LBZ8/1/04
3	2	Sinterstahlfilter	Cr Ni	28 x 3	
2	1	Hüllrohr	4988		LBZ8/1/02
1	1	Unterer Endstopfen	4988		LBZ8/1/01

Teil	Stück	Benennung	Werkstoff	Abmessung	Zeichngs. Nr. Norm	Bemerkung

Oberflächenzeichen	~	▽	▽▽	▽▽▽	▽▽▽▽	Freimaßtoleranz	bis 6	über 6 bis 30	über 30 bis 100	über 100 bis 300	über 300 bis 1000	über 1000 bis 2000
Rauhtiefe max. in µ	1000	40	10	4	1,6		± 0,1	± 0,2	± 0,3	± 0,5	± 0,8	± 1,2

	Tag	Name	Werkstoff
1970			
gez.	30.7.	Pauli	
gepr.			
gen.			

Gesellschaft für Kernforschung m. b. H.
7500 Karlsruhe
Postfach 947

Zugeh. Zchng.

Ersatz für LBZ 8700

Ersetzt durch

Maßstab 5:1

Benennung

Zeichnungs Nr. LBZ8/2/00

Mol 8C Fuel Pin

Fig. 1

2.4 Fuel

2.4.1 Fuel Chemical Composition

The fuel used is a mechanically mixed and sintered Uranium-Plutonium oxide. The various specified values are as follows:

PuO_2 content	(wt %) =	20 ± 1
U-235 content in UO_2	(wt%) =	93
O/M ratio	=	2.0 ± 0.03

The impurities are permissible up to 1000 ppm with the following maximum values for certain elements.

impurity	max. ppm
C	150
N	100
F	50
H_2O	100
O_2	50

The uranium dioxide with 93.16 % U-235 obtained by the direct conversion method was supplied by NUKEM and PuO_2 was supplied by Hanford Laboratories of USA. Both these starting powders were analysed for the various chemical impurities. The results obtained are given in the following table 4.

Table 4 Impurities of the Fuel

	PuO_2 Hanford/USA (ppm)	UO_2 with 93.16 % U-235 NUKEM (ppm)
Ag	-+)	0,16
Al	100	29
B	1	< 0,08
C	-	-
Ca	90	-
Cd	< 1	< 0,07
Cl	-	32
Co	-	-
Cr	< 5	12
Cu	< 1	0,5
F	-	-
Fe	40	75
Cd	-	-
Mg	45	-
Mo	< 10	-
Mn	5	3
N	-	-
Ni	5	180
P	-	-
Pb	< 10	-
Si	< 10	< 5
Sn	< 5	< 5
Th	-	< 10
V	< 10	< 3
Zn	< 50	< 20
Zr	-	-

+) not analysed

These powders were mechanically mixed and further analysed for the Pu-content of the mixed powder. The results are given below (Table 5).

Table 5 Pu-Content in the Powder Mixture

wt of UO_2 with 93.16% U-235 (g)	wt of PuO_2 (g)	Total wt (g)	Pu/Pu + U %		
			calculated	Analysis 1	Analysis 2
770.22	193.22	963.45	20.06	19.98	20.15

2.4.2 Fuel Isotopic Composition

As already mentioned the Pu with a nominal concentration of 7.7 % Pu-240 was obtained from Hanford/USA. The material was further analysed at GfK and results obtained are given below (Table 6) along with the Hanford results.

Table 6 Isotopic Composition of Plutonium

Isotopes	Isotopic wt %	
	Hanford results	GfK results
Pu-239	90.519	90.498
Pu-240	8.238	8.278
Pu-241	1.133	1.127
Pu-242	0.061	0.061

The isotopic composition of U was as follows

U-235 = 93.16 wt %

U-238 = rest

2.4.3 Fuel shape

The fuel was made in the form of cylindrical pellets. The U and Pu oxide powders were mechanically mixed, pressed and sintered to make the desired pellets. Smooth surface was obtained by grinding the pellets on centreless grinding machines using water as lubricant, The pellet geometry etc. are given below:

- Pellet diameter 5.10 ± 0.03 mm
- Pellet length 6.50 mm
- Edge spalling 0.30 mm
- Micro flaws (max) 2.00 mm in length and 0.10 mm in width.

The finished pellets were further analysed. The Pu/Pu + U content was found to be 19.98 wt % and the various chemical impurities analysed are given below:

Elements	ppm	Elements	ppm
C	47	Co	< 5
Cl	1	Al	150
F	70 - 140	Mo	< 10
B	0,1	Cu	< 1
Mg	< 5	Cd	< 1
Mn	35	Na	< 10
Pb	< 10	Ag	< 5
Cr	30	Zn	< 5
Sn	< 5	Si	
Fe	400	Ca	10
Ni	110	V	< 10

A total number of 80 pellets was used an the details such as weight, length, diameter and density of each pellet are summarized in Table 7. The individual pellet length may vary by 1.5 mm, however, the total fuel column length should remain within the specified limits given in Art. 2.2.

Pellets		wt (g)	Lenght (mm)	Diameter (mm)	Geom.Density (% T.D.)
lower end of fuel column	1	1,2952	6,625	5,100	87,11
	2	1,2925	6,555	5,110	87,52
	3	1,2879	6,585	5,100	87,15
	4	1,2845	6,570	5,110	86,78
	5	1,2699	6,510	5,100	86,92
	6	1,3024	6,605	5,110	87,52
	7	1,2221	6,320	5,100	86,17
	8	1,2682	6,435	5,100	87,82
	9	1,2656	6,585	5,090	85,97
	10	1,2613	6,595	5,080	85,89
	11	1,3007	6,655	5,105	86,92
	12	1,2871	6,495	5,100	88,29
	13	1,2803	6,510	5,100	87,64
	14	1,2930	6,545	5,100	88,03
	15	1,2918	6,535	5,100	88,08
	16	1,2774	6,615	5,095	86,22
	17	1,2569	6,560	5,085	85,88
	18	1,2783	6,475	5,100	87,97
	19	1,2637	6,560	5,100	85,84
	20	1,2429	6,440	5,105	85,83
	21	1,2804	6,560	5,095	87,14
	22	1,2755	6,520	5,105	87,00
	23	1,2740	6,515	5,100	87,14
	24	1,2943	6,570	5,105	87,61
	25	1,2673	6,505	5,100	86,81
	26	1,2829	6,585	5,105	86,64
	27	1,2773	6,535	5,110	86,75
	28	1,2878	6,555	5,100	87,54
	29	1,2626	6,505	5,100	86,49
	30	1,2669	6,510	5,100	86,72
	31	1,2784	6,580	5,100	86,58
	32	1,2483	6,490	5,095	85,88
	33	1,2826	6,540	5,095	87,56
	34	1,2556	6,500	5,100	86,08
	35	1,2538	6,360	5,110	87,50
	36	1,2368	6,365	5,100	86,59
	37	1,2794	6,580	5,100	86,64
	38	1,2673	6,550	5,100	86,22
	39	1,2632	6,520	5,095	86,50
	40	1,2708	6,500	5,100	87,12
	41	1,2815	6,550	5,110	86,84
	42	1,2835	6,580	5,105	86,75
	43	1,2318	6,370	5,100	86,17
	44	1,2854	6,550	5,110	87,11
	45	1,2349	6,385	5,105	86,01
	46	1,3091	6,700	5,100	87,07
	47	1,2502	6,390	5,100	87,18
	48	1,2587	6,470	5,110	86,35
	49	1,2394	6,370	5,105	86,53
	50	1,2716	6,500	5,110	86,83
	51	1,2613	6,535	5,100	86,00
	52	1,2750	6,570	5,100	86,48
	53	1,2841	6,540	5,110	87,15
	54	1,2862	6,725	5,080	85,88
	55	1,2681	6,575	5,105	85,77
	56	1,2725	6,545	5,110	86,30
	57	1,2964	6,620	5,110	86,79
	58	1,2930	6,550	5,105	87,79
	59	1,2951	6,500	5,100	88,78
	60	1,2320	6,320	5,095	87,04
	61	1,2925	6,545	5,110	87,65
	62	1,2194	6,335	5,070	86,79
	63	1,2724	6,570	5,090	88,06
	64	1,2923	6,565	5,090	88,06
	65	1,2920	6,520	5,110	87,96
	66	1,2757	6,540	5,105	86,75
	67	1,2762	6,550	5,100	86,82
	68	1,2836	6,565	5,110	86,78
	69	1,2460	6,375	5,105	86,92
	70	1,2432	6,390	5,115	86,19
	71	1,2739	6,550	5,110	86,33
	72	1,2619	6,515	5,100	86,31
	73	1,3293	6,810	5,105	86,81
	74	1,3127	6,635	5,110	87,82
upper end of fuel column	75	1,2588	6,520	5,110	85,70
	76	1,2683	6,570	5,105	85,85
	77	1,2688	6,385	5,105	88,38
	78	1,2854	6,580	5,085	87,56
	79	1,2770	6,570	5,105	86,44
	80	1,2970	6,565	5,110	87,69
Total		101,6531	522,32		
Average				5,102	86,685

Table 7

Mol 8C-5

Fuel Pellets data

2.5 Blanket Material

2.5.1 Blanket Chemical Composition

The blanket material was natural UO_2 in the form of pellets with 0.7205 wt % of Uranium-235. The O/M ratio was specified to be 2.0 $\pm$ 0.03. The upper limit of impurities was 1000 ppm and for water content to be $\leq$ 1000 ppm.
The total gas content of the blanket material released at 1600 ^{o}C was specified to 0.1 cm^3/g at STP.

2.5.2 Blanket Shape and Density

The blanket pellets were of the following dimensions:

Diameter	5.10 $\pm$ 0.03 mm
Length	6.5 mm (nominal)

The nominal pellet length may vary by 1.0 mm, however, the total blanket column length should remain within the defined specifications given in Art. 2.2. The pellet surface finish should be same as mentioned in Art. 2.4.3.

The pellet density was specified to be 95.0 $\pm$ 2.0 (% T.D.)

2.6 Cladding Material

2.6.1 Clad Chemical Composition

The austenitic stainless steel X8CrNiMoVNb 1613 (material no. 1.4988) was used as the clad and end plugs material.
It was further specified that the clad material should be 10 - 20 % cold worked and also given a thermal treatment (40 h - 150^{o}C). The expected clad composition was as follows:

Element	wt %
C	$\leq$ 0,1
Si	0,3 - 0,6
Mn	1,0 - 1,5
Cr	15,5 - 17,5
Ni	12,5 - 14,5
Mo	1,1 - 1,5
V	0,6 - 0,85
N_2	0,1
Nb - Ta	$\leq$ 1,2
P	$\leq$ 0,02
S	$\leq$ 0,02
Fe	Rest

2.6.2 Clad Tube Dimensions and Quality

Outer diameter	6.0 $\pm$ 0.03 mm
Inner diameter	5.24 $\pm$ 0.03 mm
Wall thickness	0.38 $\pm$ 0.03 mm
Straightness	1:1500 for each 10 cm length
Roughness	$\leq$ 2 µm
Surface flaws	$\leq$20 µm
Inner flaws	$\leq$10 % of wall thickness
Inclusions	$\leq$0.05 µm or 10^{-3} mm^2.

3. IRRADIATION OF PIN (Mol-8C-5)

3.1 Irradiation Facility

The pin was irradiated in the BR-2 reactor at Mol. The BR-2 is a light water cooled and moderated reactor. The fuel in the form of concentric tubes is made of 90 % enriched uranium. A hyperboloid configuration and its high neutron thermal flux are the two main design and operational features of the reactor. The fuel elements, central rods or experiments are located in the moderating matrix of beryllium placed in the central section of the reactor pressure vessel. Any unoccupied matrix position is filled with beryllium plugs. Due to the special configuration of the core, any one of the above mentioned items may be removed from the reactor without influencing the others.

Twenty-six fuel elements of the reactor contain about 5.6 kg of U-235 and even with large experimental loadings, the reactor can operate at a power level of 57.6 MW. The maximum heat flux in the fuel plates and the maximum thermal neutron flux in the central 200 mm of the experimental channel are 425 W/cm^2 and 10^{15} n/cm^2 s, respectively.

3.2 Irradiation Capsule

The pins were irradiated in FAFNIR [+)] capsule developed by CEN/Mol /3/. A general view of the capsule and its cross-section are shown in figs. 2 and 3 respectively. The capsule is shielded by an 8.8 mm thick Cd-Ag alloy clad in stainless steel annular tubes of 1.6 mm thickness. The outer and inner diameters of the"shield-clad" are 25.4 mm and 13.4 mm, respectively. The pin is cooled by a stagnant NaK alloy. A maximum unperturbed thermal neutron flux (FAFNIR capsule replaced by a beryllium plug in SV/1 fuel element)of 3 x 10^{14} n/cm^2. s was used as a standard. Fig.4 shows that all the neutrons with energies less than 0.683 ev are absorbed by the Cd shielding and that the maximum neutron flux is with energies close to 1 Mev. It may be seen that the thermal flux has been completely screened out and that only the epithermal flux and fast flux are available.

[+)] FUEL ARRAY FAST NEUTRON IRRADIATION RIG (FAFNIR)

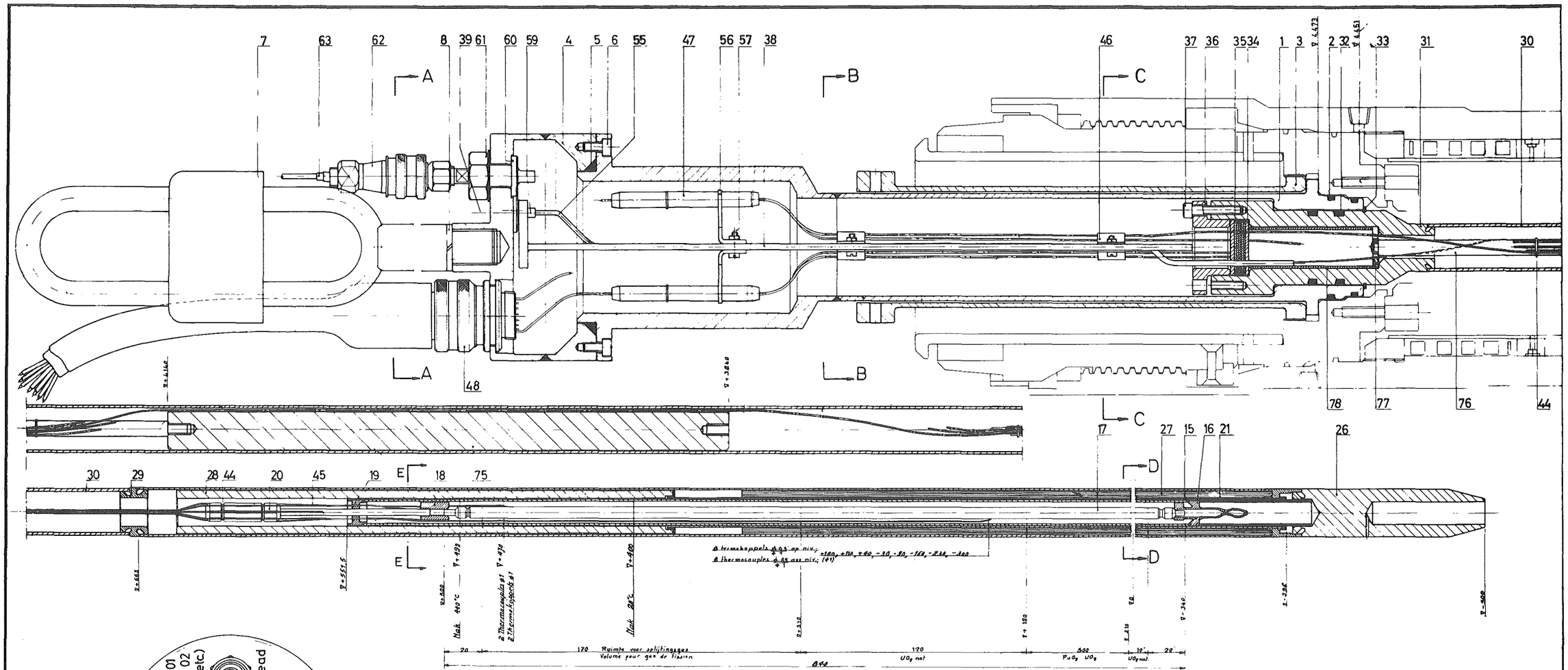

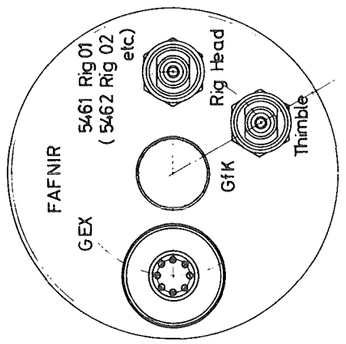

Doorsnede "AA. Coupe

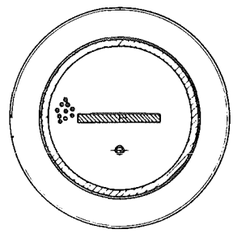

Doorsnede "BB. Coupe

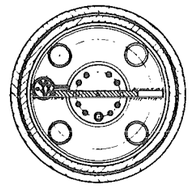

Doorsnede "CC. Coupe

Coupe EE Doorsnede.

Doorsnede "DD. Coupe

Voor stuklijst zie plannen N 22 413 1/2 & 2/2
Voir nomenclature voir plans N 22 413 1/2 & 2/2

D	18-10-68	Med. position des thermocouples		
C	6-5-1968	Modifié cup 18 - Ajouté coupe EE. Changé niveau No.	L.D.	
B	7-2-68	Afschermring		
A	11.11.67	Verbreering ringen naald		
Ind.	dat.	Modifications - Wijzigingen	Par.	Appr.

N°	Dénomination	Benaming	Q	Mat.	Observ.
Etat de surface : / Afwerkingsgraad :		Cotes non tolérancées / Maten zonder tolerantie	< 6 / ± 0,1	> 6 < 30 / ± 0,2	> 30 < 100 / ± 0,3	> 100 < 300 / ± 0,5	> 300 < 1000 / ± 0,8	> 1000 < 2000 / ± 1,2	> 2000 / ± 2

GROUPE D'EXPLOITATION DU RÉACTEUR BR 2 ET DE SES INSTALLATIONS CONNEXES

GROEP VOOR EXPLOITATIE VAN DE REAKTOR BR 2 EN ZIJN BIJHORENDE INSTALLATIES

Service - Dienst : Tech.st. Dossier : 71.5460

Dessiné Getekend : Beeckmans dat. : 12.10.1967 FAFNIR Mk III

Vérif. : Swinnen J. dat. : 16-10-67 GfK

Approb. : W. des Marchi dat. : 17-10-67 Echelle Schaal : 1/1 N° GEX 23[illegible] D

BESTRALING VAN EEN BRANDSTOFNAALD. Samenstelling.
IRRADIATION D'UNE AIGUILLE DE COMBUSTIBLE. Ensemble.

Fig. 2 Irradiation Capsule „FAFNIR"

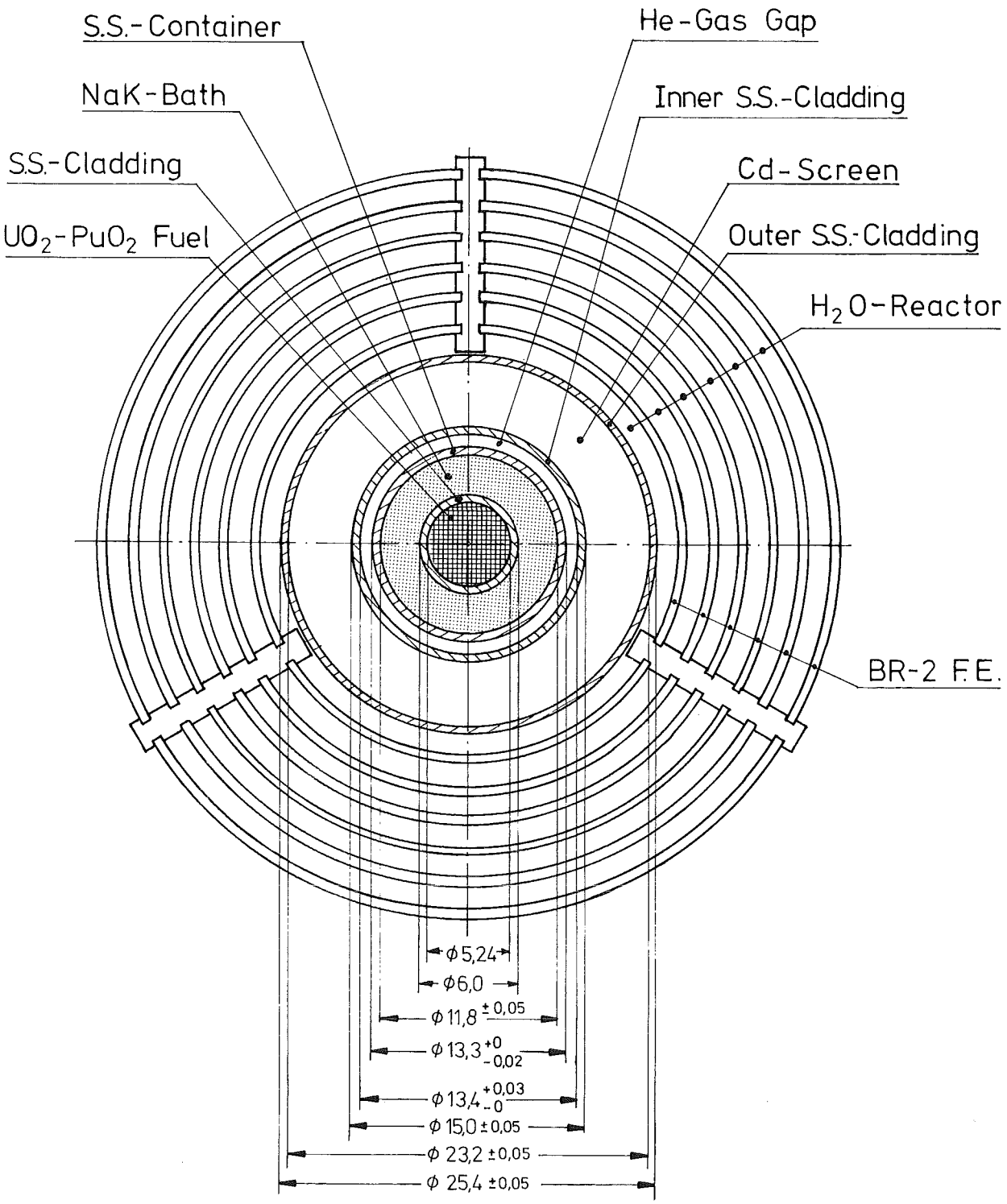

Fig: 3 FAFNIR Capsule Cross Section

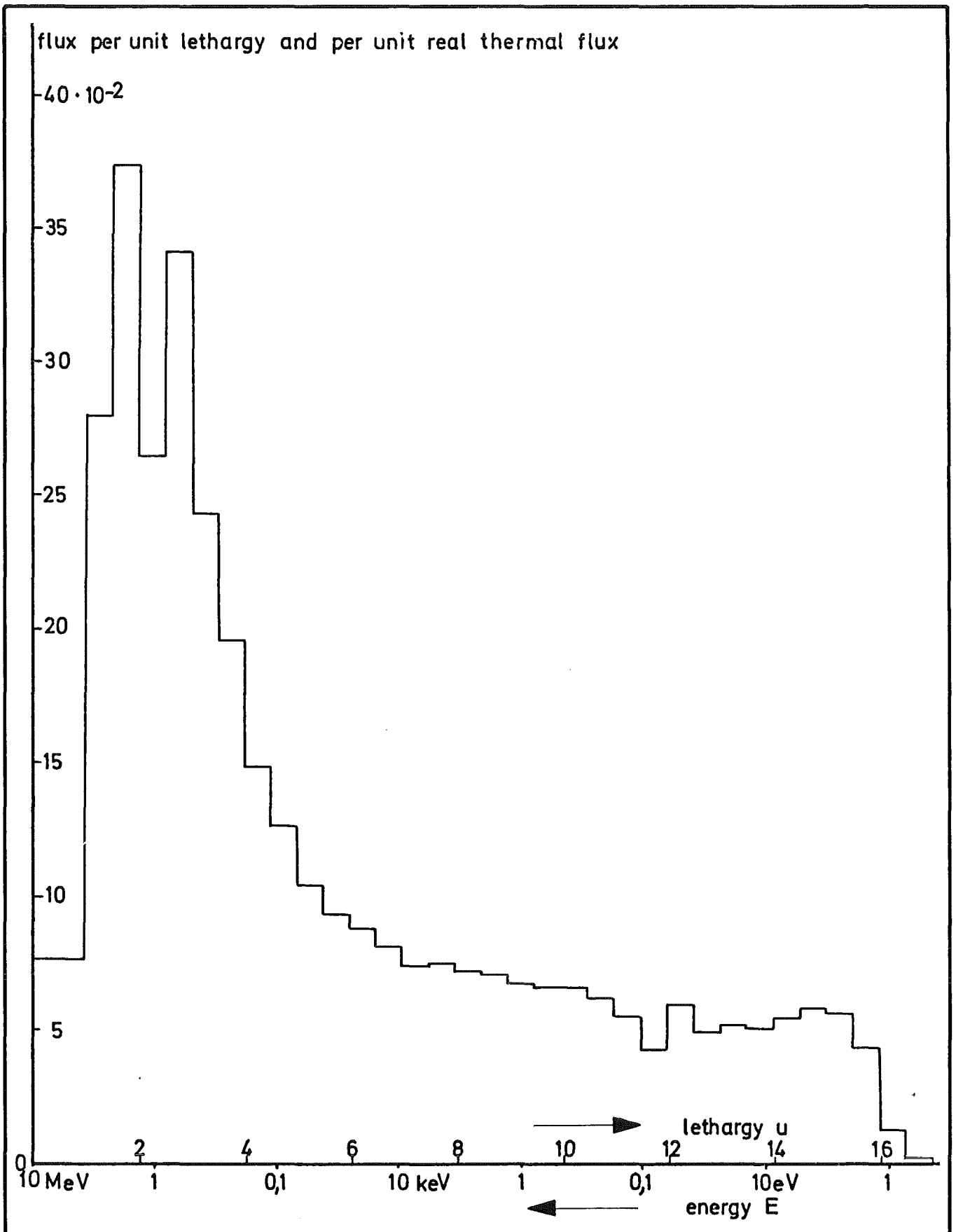

Average neutron flux spectrum in the fuel pin

Fig. 4

It may be further seen from fig. 5 that the maximum number of fissions are caused by neutrons of energies close to 10 eV and, therefore, it may be concluded that inspite of the availability of the fast flux within the capsule, the fissions are mainly caused by the epithermal flux of the reactor.

3.3 Irradiation History

The FAFNIR capsule was irradiated in four different channels of the BR-2 and their positions in the reactor core are shown in fig. 6 . The capsule irradiation was started on 20.3.71 in channel G-240 and was completed on 12.3.73 in channel E-30 in twenty-two irradiation cycles with a total irradiation time of 427.8 full power days. During each irradiation cycle, the pertinent data such as given below were recorded:

i) Neutron flux (fast and thermal)
ii) Gamma heating
iii) Reactor power
iV) Irradiation time
V) Irradiation position
Vi) Temperature at measuring points
Vii) Rod power
Viii) Burn-up
iX) Fission gas pressure

The detailed information is summarized in table 8 and further information on irradiation history may be found elsewhere /4/.

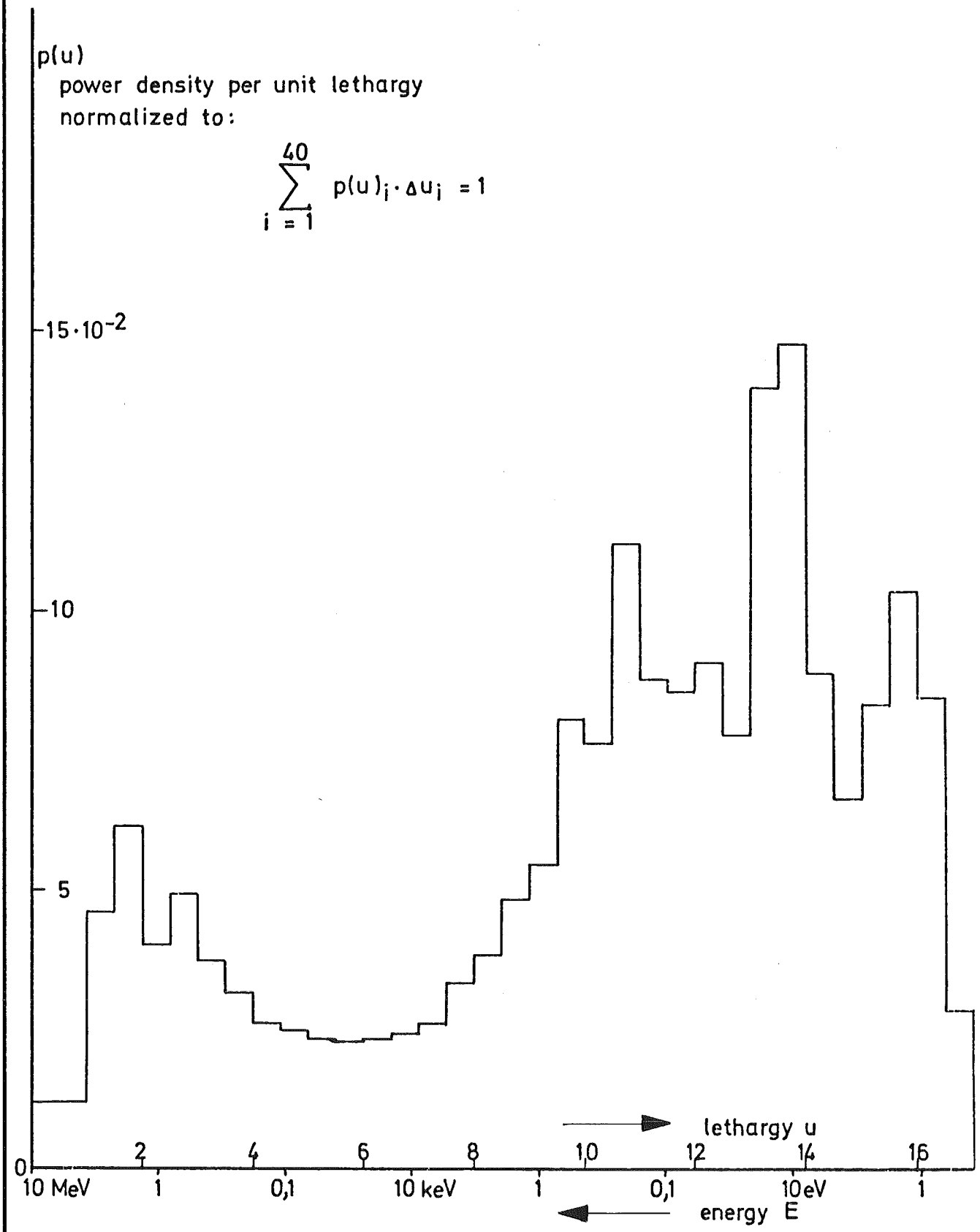

Average power density spectrum in the fuel pin

Fig. 5

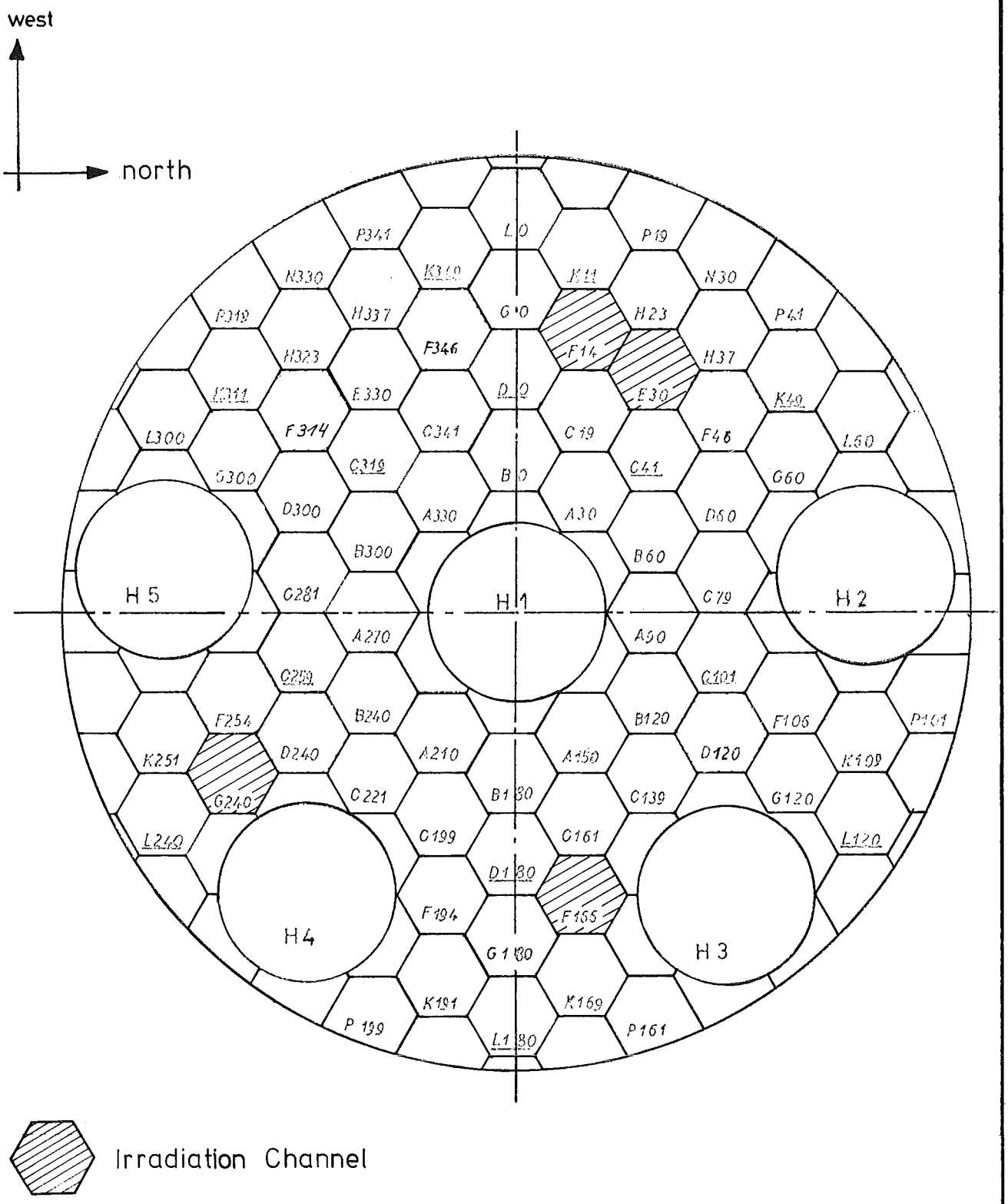

Mol 8C-5 Fuel Element Position in BR-2

Fig. 6

Table 8 Irradiation History of Pin 5

BR-2 Cycle No.	Channel No.	Burn-up of Driver Fuel (%)	Max. Undisturbed Flux and Fluence				Y-Heat W/gr Al	Released Energy M W D	Reactor Power (MW th)	Full Power Days	Max. Temp. in each Cycle °C	Rod Power W/cm			Burn-up MWD/kg Me				Fission gas pressure at end of Cycle	Fractional gas release
			Thermal		Fast							Max. Point value in each Cycle	Average hot spot value in each Cycle	Axial Average value of pin in each Cycle	Average hot spot value in each Cycle	Cumulative hot spot value in each Cycle	Average pin value in each Cycle	Cumulative pin value		
			10^{14} n/cm^{2}s	10^{20} n/cm^2	10^{14} n/cm^{2}s	10^{20} n/cm^2														
3/71	G240	18	1.79	2.77	3.02	4.66	7.0	1252.7	70	17.15	496	384	362	289	3.577	-	2.852	-	4.6	-
4/71	F 166	16	2.04	3.87	3.39	6.43	7.4	1537.6	70	22.10	519	413	361	300	4.594	8.171	3.816	6.668	4.8	0.069
5/71	F 14	37	2.15	3.77	2.62	4.58	6.4	1419.7	70	18.93	612	544	470	378	5.132	13.303	4.119	10.787	5.6	0.212
6/71	-	14	2.15	3.90	4.06	7.36	9.5	1468.2	70	20.97	621	558	519	439	6.271	19.574	5.303	16.090	5.5	0.128
7/71	-	17	1.81	1.79	3.30	3.26	7.9	800.6	70	11.96	571	485	461	384	3.177	22.751	2.647	18.737	5.2	0.073
8/71	-	16	1.77	2.60	3.27	4.80	7.7	1191.3	70	16.37	597	521	492	417	4.644	27.395	3.932	22.669	-	- ②
9/71	-	14	1.84	2.76	3.52	5.28	7.9	1215.6	70	16.95	587	502	491	371	4.794	32.189	3.629	26.298	-	-
10/71	-	0	1.56	2.30	3.43	5.05	7.9	1194.6	70	16.17	603	530	454	397	4.228	36.417	3.698	29.996	7.2	0.118
11/71	-	0	1.51	2.89	3.31	6.33	8.4	1548.2	70	21.37	622	558	523	446	6.442	42.859	5.496	35.492	10.15	0.357
1/72	-	0	1.66	3.11	3.66	6.85	9.3	1516.1	70	20.09	634	576	525	440	6.072	48.931	5.089	40.581	12.0	0.417
2/72	-	0	1.66	2.45	3.66	5.41	9.1	1195.4	70	16.09	606	534	489	407	4.538	53.469	3.778	44.359	12.7	0.417
3/72	-	0	1.67	3.03	3.64	6.6	9.4	1468.7	70	19.91	646	594	553	468	6.344	59.813	5.375	49.734	15.6	0.506
4/72	-	0	1.63	3.30	3.58	7.24	9.4	1640.5	70	21.83	622	558	502	413	6.316	66.129	5.194	54.928	17.8	0.549
5/72	-	0	1.59	4.22	3.51	9.3	9.2	2148.2	70	29.25	596	520	429	374	7.232	73.361	6.306	61.234	19.4	0.552
6/72	-	0	1.51	3.20	3.32	7.04	8.5	1802.3	73.5	23.09	554	460	421	335	5.599	78.960	4.455	65.689	21.0	0.571
7/72	-	0	1.50	3.23	3.31	7.12	8.6	1829.0	73.5	22.98	585	503	450	355	5.965	84.925	4.698	70.387	23.6	0.617
8/72	E 30	37	2.17	4.11	3.83	7.25	9.1	1611.1	73.5	20.56	602	528	465	398	5.512	90.437	4.711	75.098	25.2	0.627
9/72	E 30	29	1.94	4.67	3.97	9.55	9.3	2047.4	73.5	25.53	609	539	493	373	7.251	97.688	5.481	80.579	25	0.579
10/72	-	18	1.70	3.35	4.14	8.17	9.7	1678.8	73.5	20.02	617	550	531	458	6.125	103.813	5.282	85.861	27.2	0.602
11/72	-	18	1.70	1.26	4.12	3.06	9.6	631.0	73.5	7.88	621	556	505	449	2.295	106.108	2.041	87.902	28.7	0.627
1/73	-	23	1.8	3.11	4.09	7.08	9.4	1471.3	73.5	17.86	598	520	468	394	4.812	110.920	4.050	91.952	28.4	0.592
2/73	-	27	1.88	3.86	3.99	8.2	9.4	1747.4	73.5	20.75	575	486	444	370	5.305	116.225	4.421	96.373	30.7	0.619
Total				69.5		140.6		32415.7		427.8						116.225		96.373	30.7	0.619
											Average value		473	393.4	Irradiation Data of MOL 8C 5.					

4. DIMENSIONAL MEASUREMENTS

4.1 Introduction

The diameter of the fuel pin was measured, at two orientations 90 degrees apart, before and after irradiation as a continious diameter profile scan along the entire length of the pin. The transducer contacting point was tungsten carbide wire of 1.0 mm diameter and the measuring head was moving at a constant speed of 80 mm/min. The results of these scans before and after irradiation with percentage increase in diameter at two orientations are given in fig. 7 and fig. 8. Percentage increase in diameter in the fuel section was calculated at each pellet interface i.e. at about 6.5 mm intervals, while in the remaining part of the pin at intervals ranging from 10 mm to 20 mm apart. It was seen that, in general, no significant increase in diameter had occurred. However, a sharp increase in the form of a hump (cf. fig. 7 + 8 - detail II) corresponding to about 0.6 % increase in diameter is seen at about 22 cm from the isolation pellet/fuel interface.

The length of the pin measured before and after irradiation between the same end points of pin has shown an increase of less than 0.06 % of the pin. Since this increase is very small, therefore, its further evalution is not undertaken.

The following points are considered to explain some of the minor variations in diameter:

4.2 Thermocouple Contact Points

The upper part of fig. 9 shows the arrangement for thermocouples attachment to the fuel pin. The exact thermocouple distances are shown in fig. 7 + 8. The bigger "star" rings are loose and move freely over the pin. They are used for holding the thermocouples close to the pin and also for centering the pin in the FAFNIR capsule. The contact of the thermocouple is made by winding a wire near the head of the thermocouple. Some variation in diameter near the vicinity of the thermocouples is noted. It is difficult to explain but it could be that the winding of the wires is causing some chemical/mechanical interaction at these points.

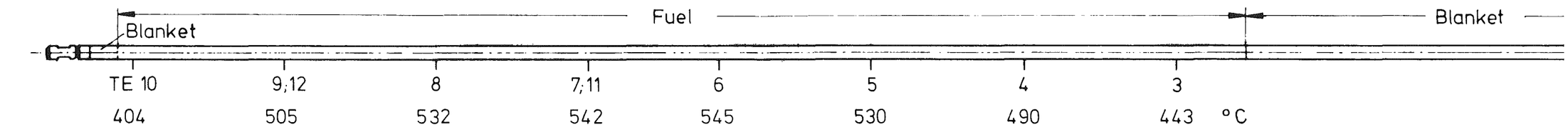

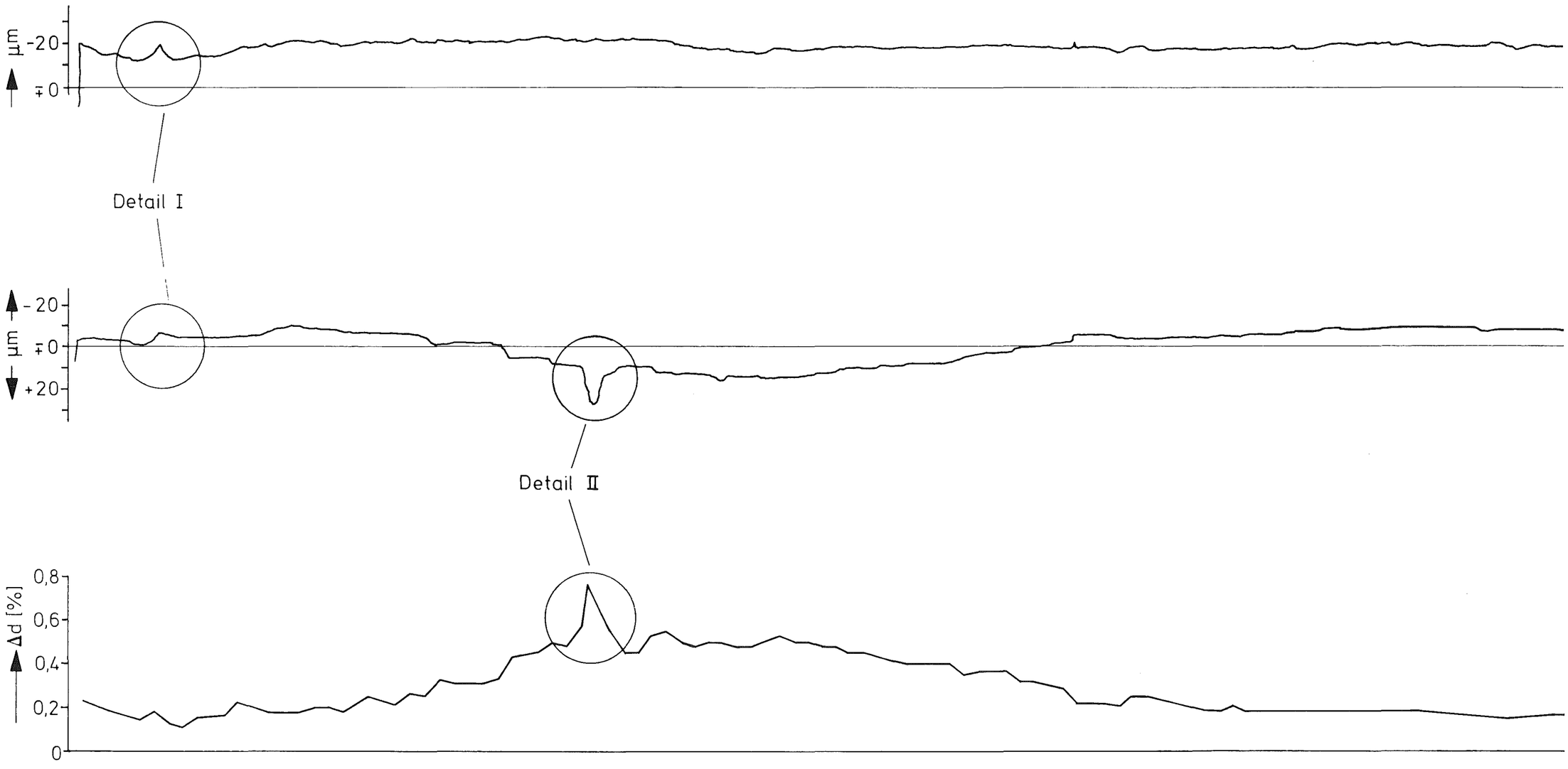

GfK Karlsruhe

IMF/III

Diameter Profiles for Mol 8C-5

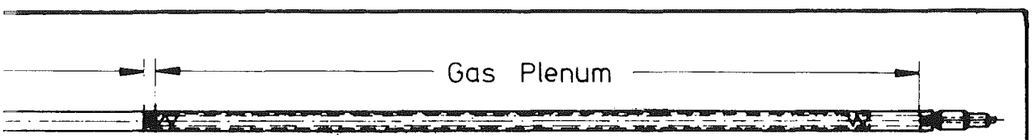

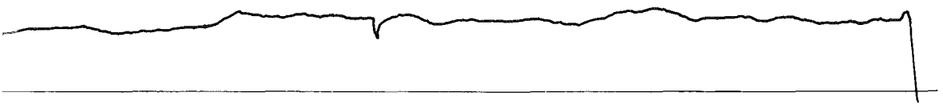

Pre - irradiation

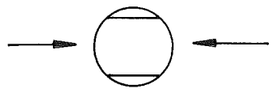

Post - irradiation

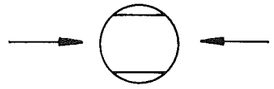

Fig: 7

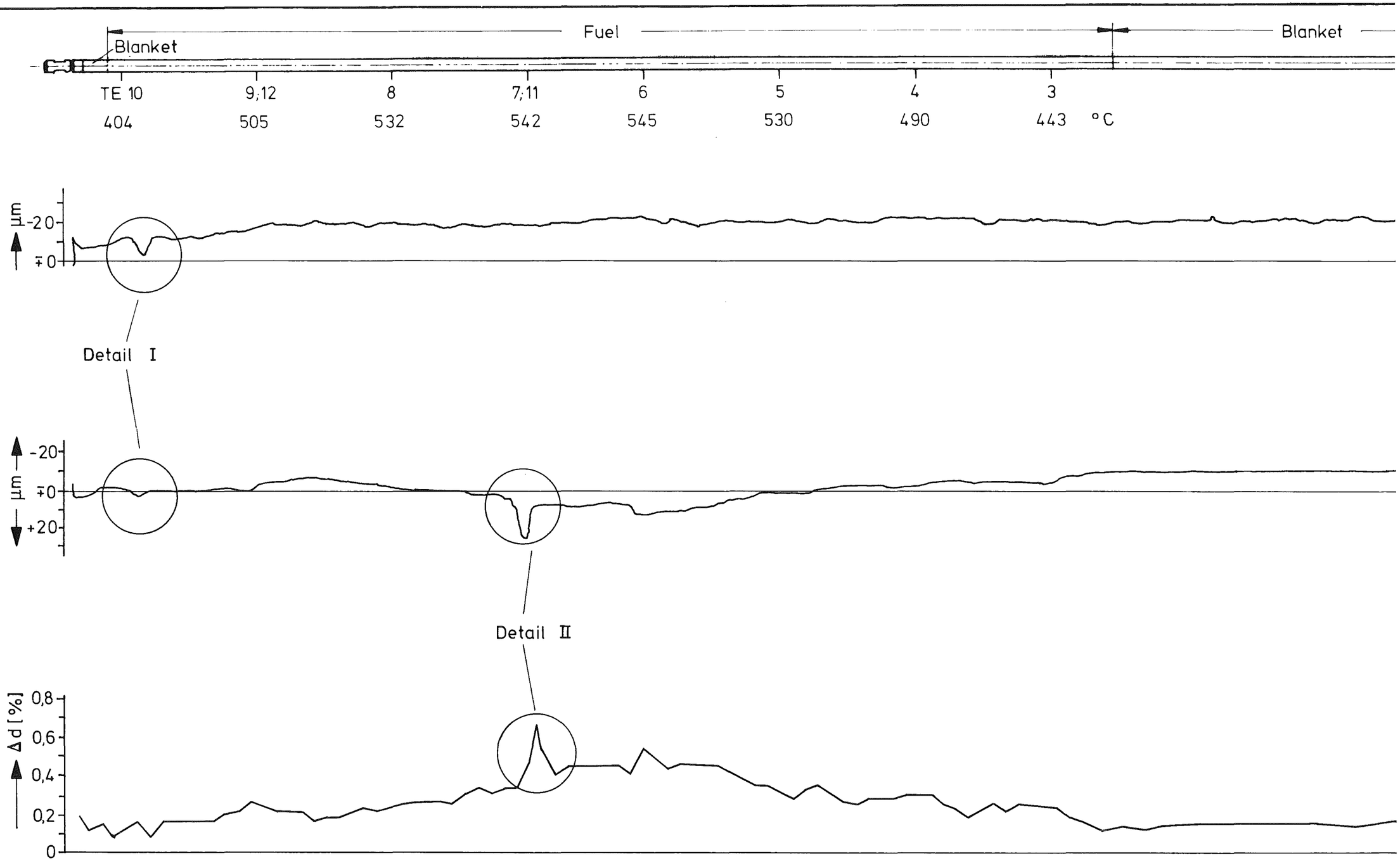

GfK Karlsruhe

IMF/III

Diameter Profiles for Mol 8C-5

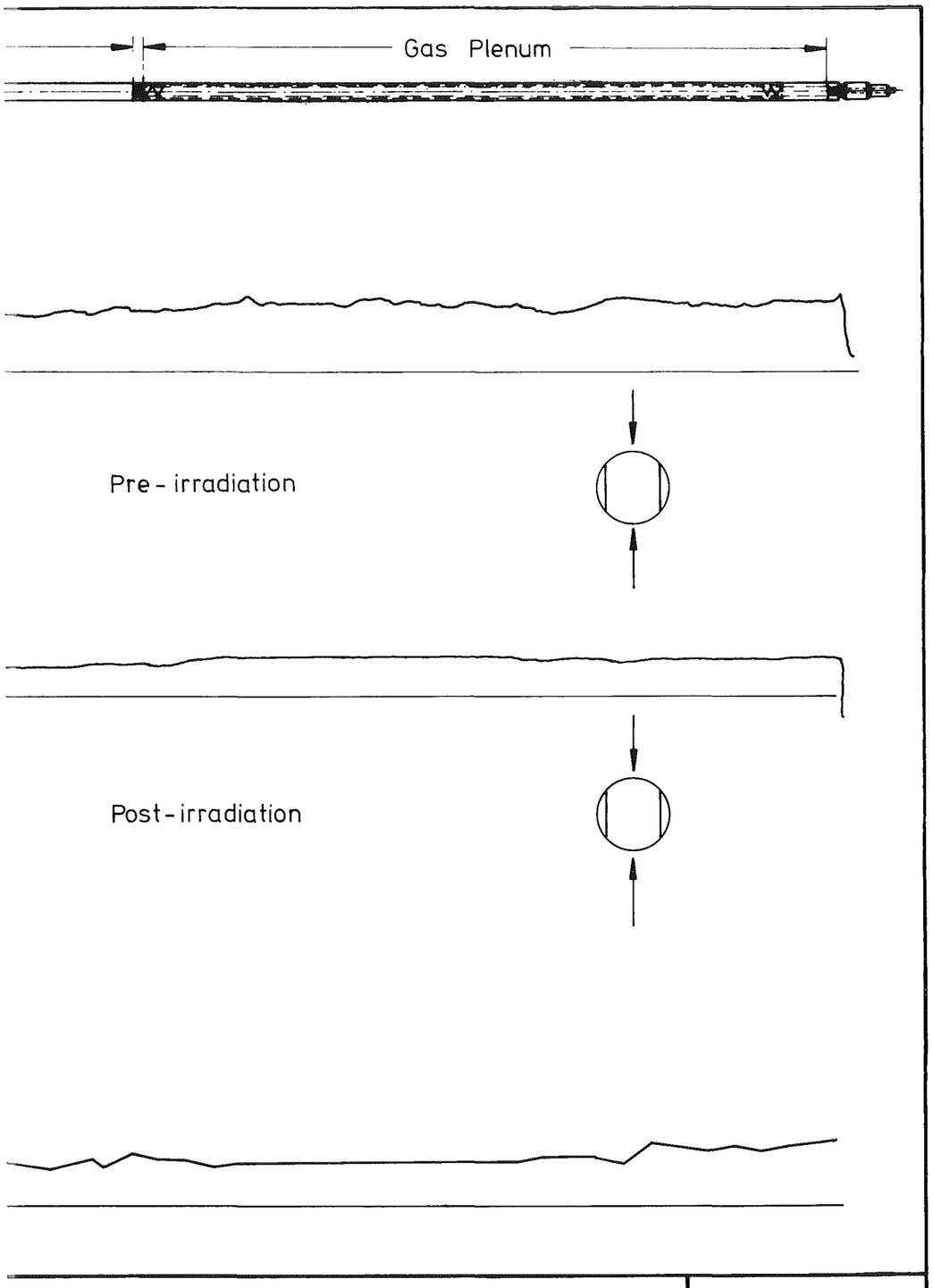

Fig: 8

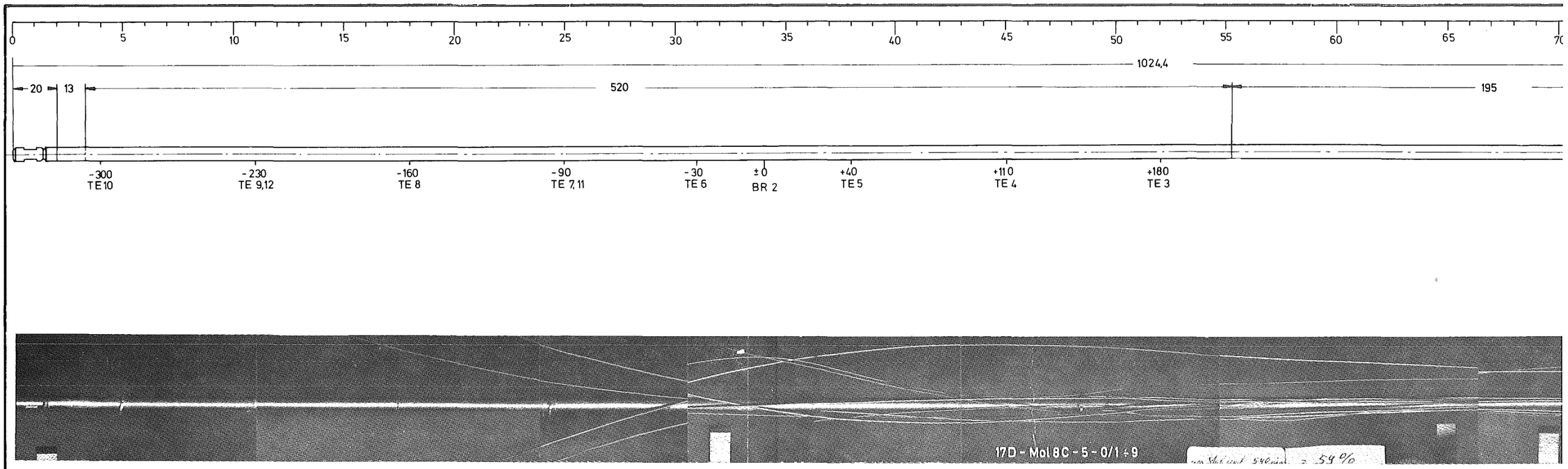

Visual Inspection of the Fuel Pin with Thermocouples

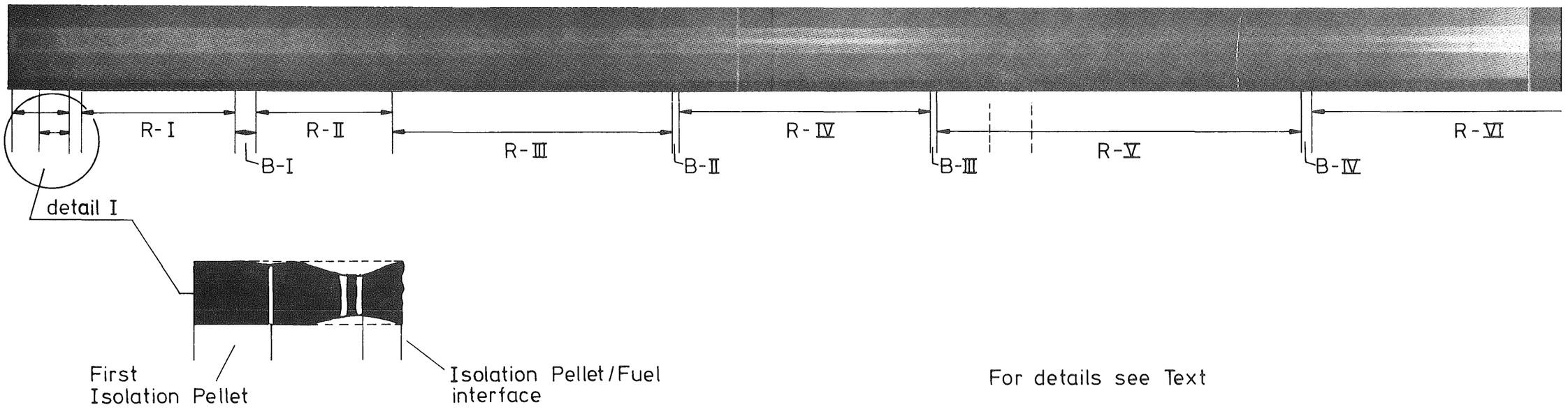

For details see Text

GfK Karlsruhe

IMF/III

Betatron Pictures

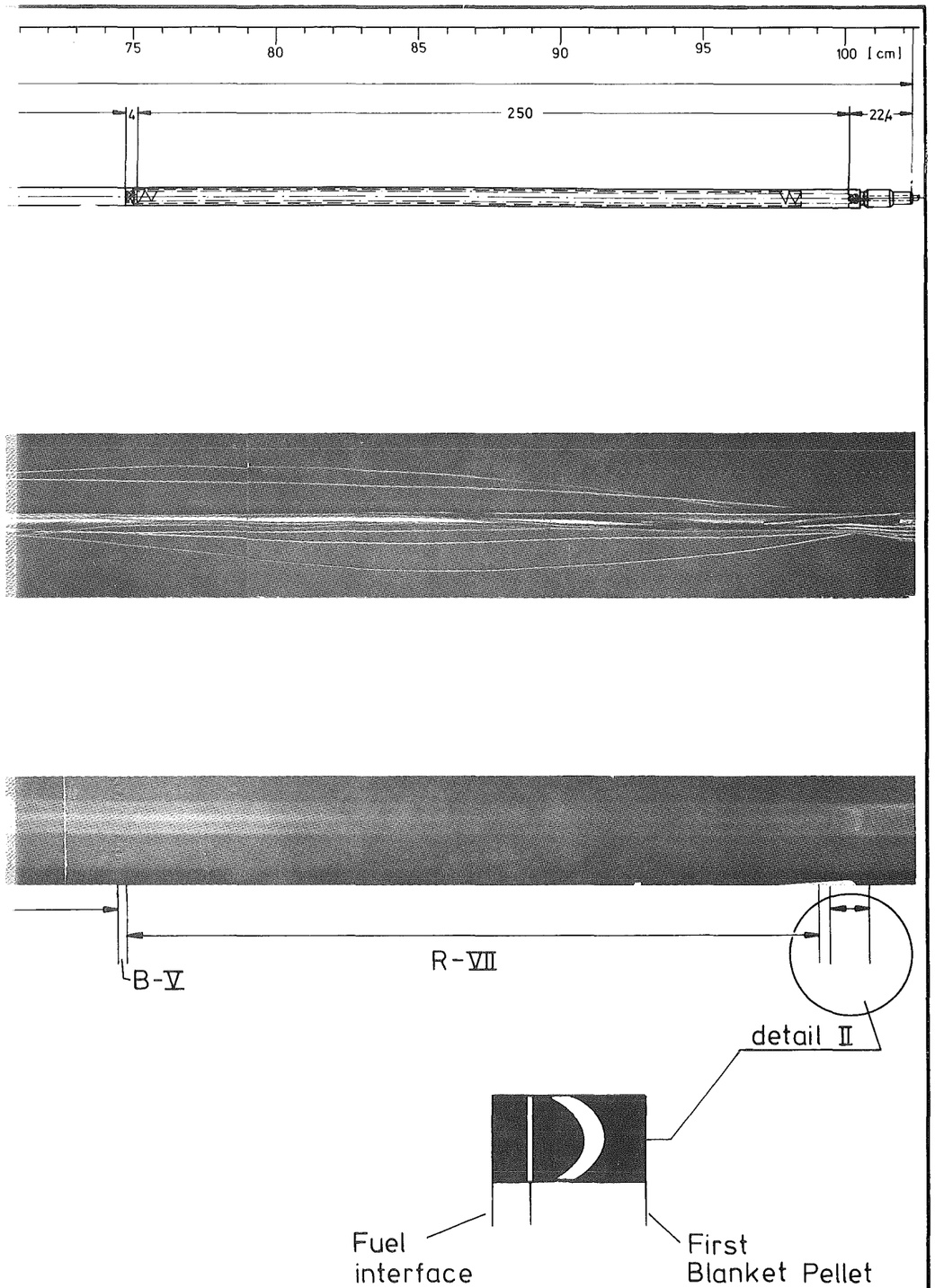
75
80
85
90
95
100 [cm]
4
250
22,4
B-V
R-VII
detail II
Fuel
interface
First
Blanket Pellet

Fig. 9

4.3 Ovality

A comparison of the scans before and after irradiation in fig. 7 + 8 (detail I) would show that the decrease in diameter is coming from the ovality defect of the tube. However, some "recovery" of diameter seems to have taken place possibly because of the fuel/clad mechanical interaction at higher temperatures.

4.4 Betatron Picture:

In the betatron picture (Fig. 9) the central channel in the fuel column has been studied in detail. The regions of the radial cracks and of the sharp and diffused "bridges" formed in the central channel do not appear to have any noticable effect on the diameter increase of the fuel pin.

4.5 γ-Scanning:

In the gross γ-scan upper part and Zr/Nb trace shown in fig. 10, the two peaks observed in the middle of the graphs do not correspond to the region of sharp diameter increase of the fuel pin (figs. 7 + 8 - detail II) It may, therefore, be inferred that no accumulation of fission products has taken place here and also that the burnup in this region is the same as that of the fuel pin in general.

4.6 Pellet Density and Diameter:

The effect of density and diameter of each pellet was studied in detail but no meaningful correlation of the sharp increase in pin diameter with the pellet density or its diameter could be made. The pellets fall in the following range of values:

	Diameter		Density (% T.D.)
max.	5.115 mm	max.	88.78
min.	5.070 mm	min.	85.77

The pellet in the region of sharp increase of diameter has 5.10 mm diameter and 86.08 density, and, thus, it falls into fairly average range of the large number of pellets. Therefore, the pellet density and its diameter do not appear to be the cause for sharp increase of pin diameter.

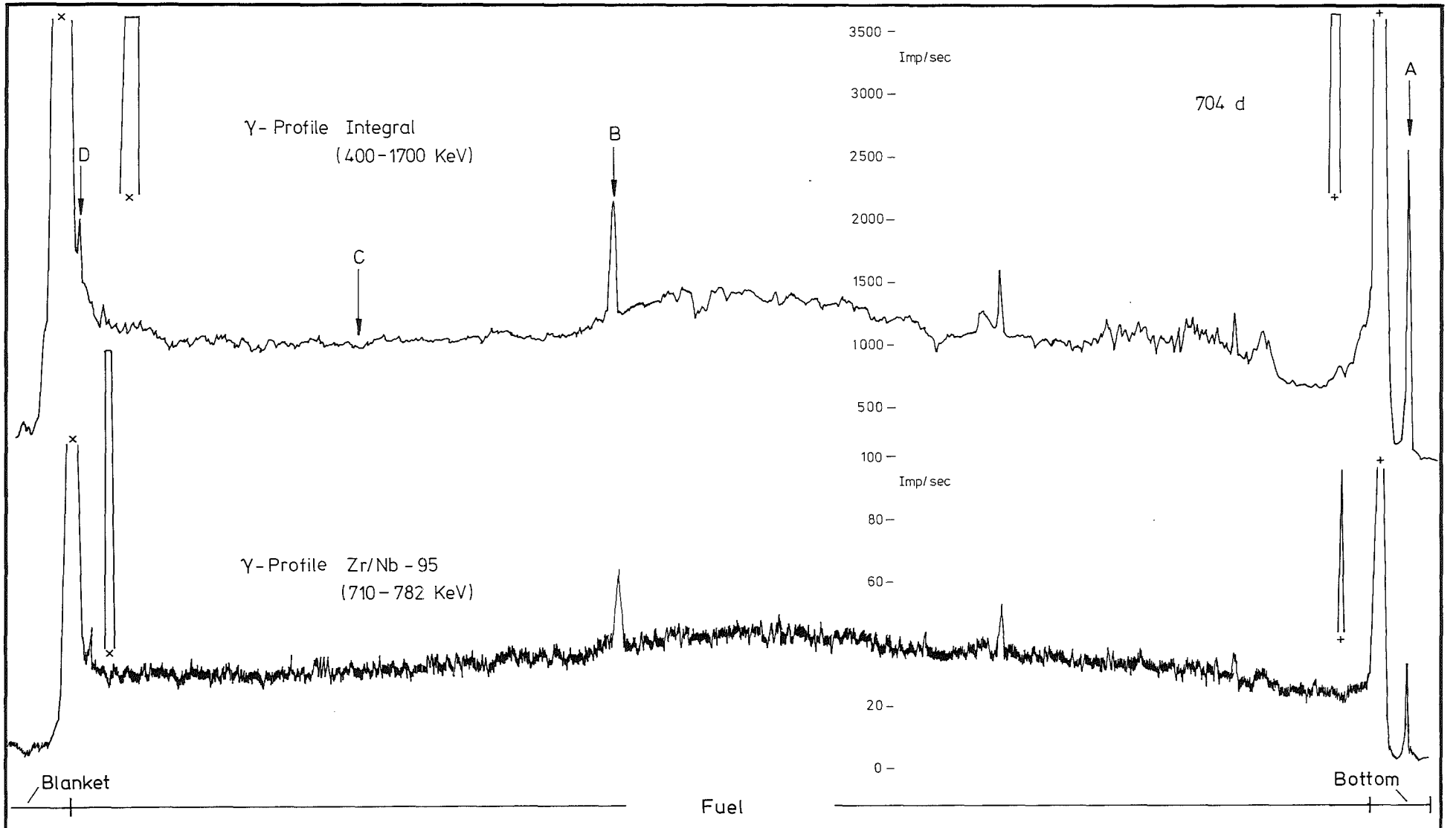

GfK Karlsruhe IMF/III	γ- Scanning Profiles Fuel Pin Mol 8C-5	Fig: 10

4.7 Swelling:

Clad swelling and clad inelastic strain can cause considerable dimensional changes during irradiation. Clad swelling and thus inelastic strain determination by the immersion density measurement was not undertaken because of the following reasons:

i) the irradiation was done in soft, epithermal flux and thus no significant swelling of the clad can be expected, and

ii) since all the fission gas produced during irradiation was being collected outside the pin, therefore, no strain could be expected without any pressure arising from fission gas production.

Thus, it would appear that clad swelling and clad inelastic strain are not significantly contributing to the sharp increase of fuel diameter.

4.8 External Effects:

In the foregoing discussion, the sharp increase of pin diameter does not appear to be the consequence of the internal characteristics of fuel. Thus, it would seem that some external effects such as remains of the wire used for thermocouple contacting etc. could be the possible cause of this sharp increase of fuel pin diameter.

5. BETATRON PICTURES

5.1 Introduction

The pin has been radiographed by using an 18 MeV betatron. The equipment details and the experimental procedures have been described previously /5, 6/. The radiography of the pin was obtained by exposing for 6 - 7 minutes the Kodak-M film placed behind a 1.5 mm thick tantalum intensifier foil. The image magnification of 1.4 was obtained. The formation of the central channel starting with a smaller diameter at the bottom and ending with a larger diameter at the top of the fuel pin is seen. Some local irregulaties of the diameter and the blockage at various places of the central channel are also observed. A strong reaction at both ends of the fuel column is noted. Thus, the detailed examination of the betatron pictures fig. 9 revealed that the fuel behaviour can be characterized into the following three groups:

i) Reaction at fuel column extremities,
ii) Formation of central channel, and
iii) Formation of sharp and diffused "bridges".

5.2 Reaction at Fuel Column Extremities

5.2.1 Reaction at the bottom of fuel column:

Strong reaction at the fuel pellet/isolation pellet interface seems to have taken place (Fig. 9 - detail I). The fuel pellet edges appear slightly rounded off, whereas the upper half of the isolation pellet has undergone severe damage with the formation of:

i) some areas of different density around the diameter of pellet, and
ii) appearance of two radial gaps closed at the outer edges.

The integral γ-scan (Fig.10) has shown a sharp increase in activity near this lower interface, thus, indicating the migration of some fission products to this part of fuel pin. Further γ-scanning for Cs-137 (Fig. 11) has also indicated a sharp peak in this region.

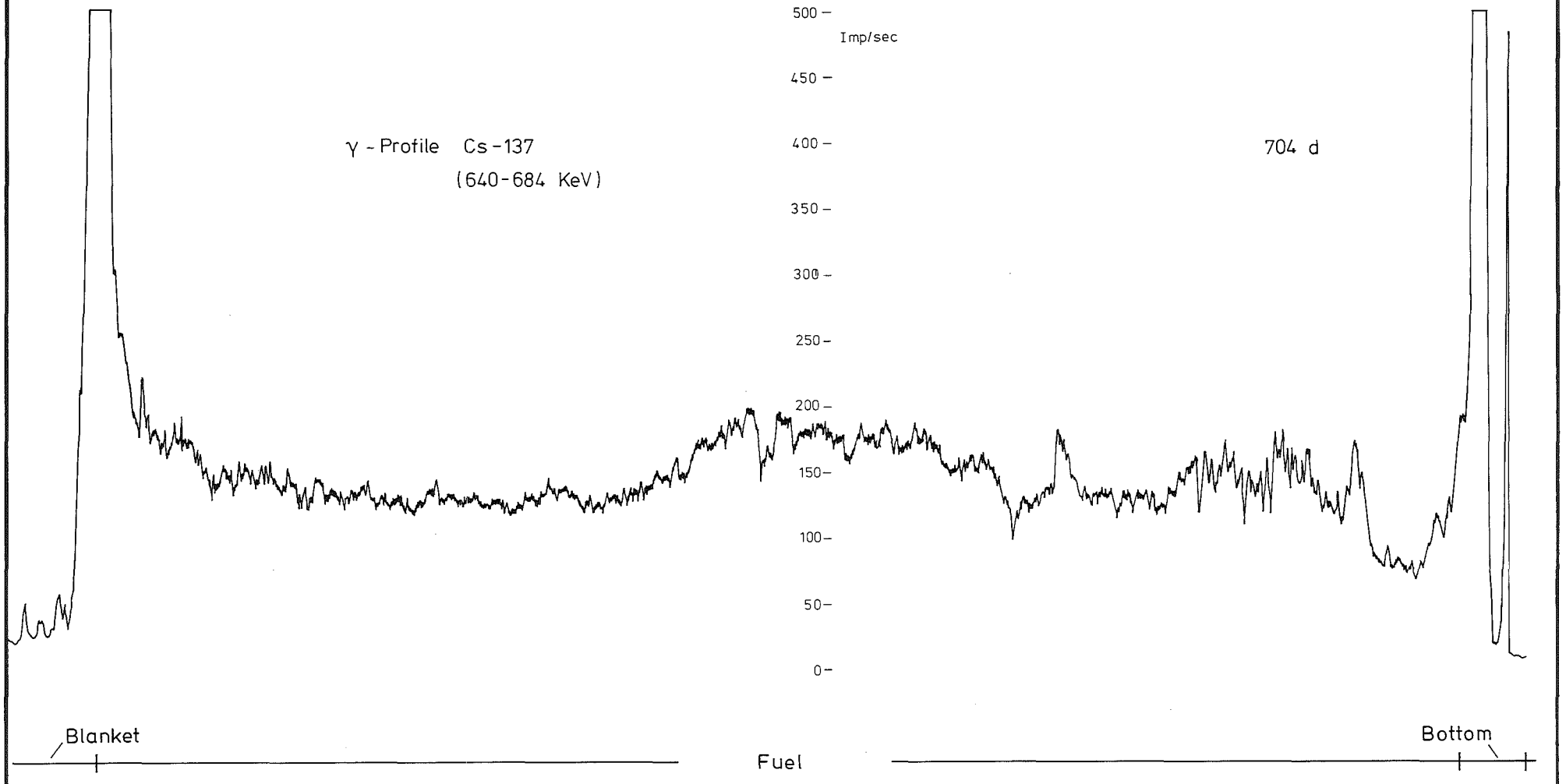

GfK Karlsruhe IMF/III	γ - Scanning Profiles Fuel Pin Mol 8C-5	Fig: 11

Therefore, it appears that Cs-137 has migrated from the hot fuel to this colder part of the fuel and has reacted with the isolation pellet. This would also explain the areas of different density seen around the outer edges of the pellet.

5.2.2 Reaction at the top of fuel column:

An analysis similar to that of art 5.2.1 has confirmed that Cs-137 has also accumulated in this part of the fuel. No radial gaps can be seen here, however, a half moon shaped area of lower density (Fig. 9 - detail II) in the first blanket pellet is seen. This also, then, appears to be some reaction product of Cs-137 and the UO_2 of the blanket pellet.

5.3 Formation of Central Channel

The formation of central channel of non-uniform diameter can be clearly seen in the betatron pictures (Fig. 9). The fuel column has been divided into seven region to help better explain the various parts of the pin.

5.3.1 Region R-I

The central channel starts at the left with a small hole, remaining constant upto the middle of this region from where the diameter steadily increases upto the right side and is finally blocked.

5.3.2 Region R-II

The central channel reappears with a uniform diameter slightly larger than R-I. A large number of radial cracks are also seen on both sides of the channel.

5.3.3 Region R-III

The radial cracks are not visible any more. The central channel diameter seems to have increased but remains constant in this region. The central channel is blocked at the right side of this region.

5.3.4 Region R-IV

The central channel reappears with slightly enlarged diameter than R-III and is again blocked at the right side of this region.

5.3.5 Region R-V

The central channel reappears with almost same diameter as R-IV. Nevertheless, a small area near the left side of this region (within dotted lines), although with clear channel boundary lines, does appear to have some porous material inside the channel. The channel is blocked at the right side of this region by a sharp "bridge".

5.3.6 Region R-VI

The central channel reappears with diameter slightly larger than R-V and remains constant in this region. However, beyond this region, some fluctuations in diameter are noted. The channel is again blocked at the right side of this region.

5.3.7 Region R-VII

The central channel reappears and some variations in its diameter are noted. This region has been divided into five areas, demarcated by dotted lines, and they are described below, starting with first area from left side:

i) The diameter appears to be even larger than R-VI region.
ii) The diameter has decreased a little bit and appears to be same as R-VI.
iii) Same as (i) above.
iv) Same as (ii) above.
v) The diameters seems to be the largest in this area. The clear channel boundaries have vanished with the appearance of a coarse and corrugated central channel.

5.4 Formation of Sharp and Diffused "Bridges"

Five sharp and diffused "bridges" are seen in the betatron picture along the entire length of the fuel column. They are discussed below:

5.4.1 Bridge B-I

This is the longest blockage of the central channel and the "bridge" formation is observed with ill-defined or diffused edges on its both sides.

5.4.2 Bridge B-II

This is a narrow "bridge" with well defined and sharp edges on both sides.

5.4.3 Bridge B-III

The length of this "bridge" is same as that of B-II but it has diffused edges on both sides.

5.4.4 Bridge B-IV

This "bridge" is smaller than B-I but larger than B-II and is also formed with sharp edges on both sides.

5.4.5 Bridge B-V

This is identical to B-III.

5.4.6 Integral and Zr/Nb Scan

The integral γ-scan (Fig.10) has shown sharp increase in activity only above B-II and B-IV and that the activity at B-IV is higher than at B-II. Thus, it indicates that the "bridges" formed with sharp edges are a consequence of the accumulation of metallic fission products in the form of "ingots" etc., whereas, the "bridges" formed with diffused edges arise from the agglomeration of non-metallic fission products or from fuel itself. The γ-spectrum of "bridge" B-IV is shown in fig. 12 (B) and it is seen that the activity is mainly due to the accumulation of Ru/Rh-106.

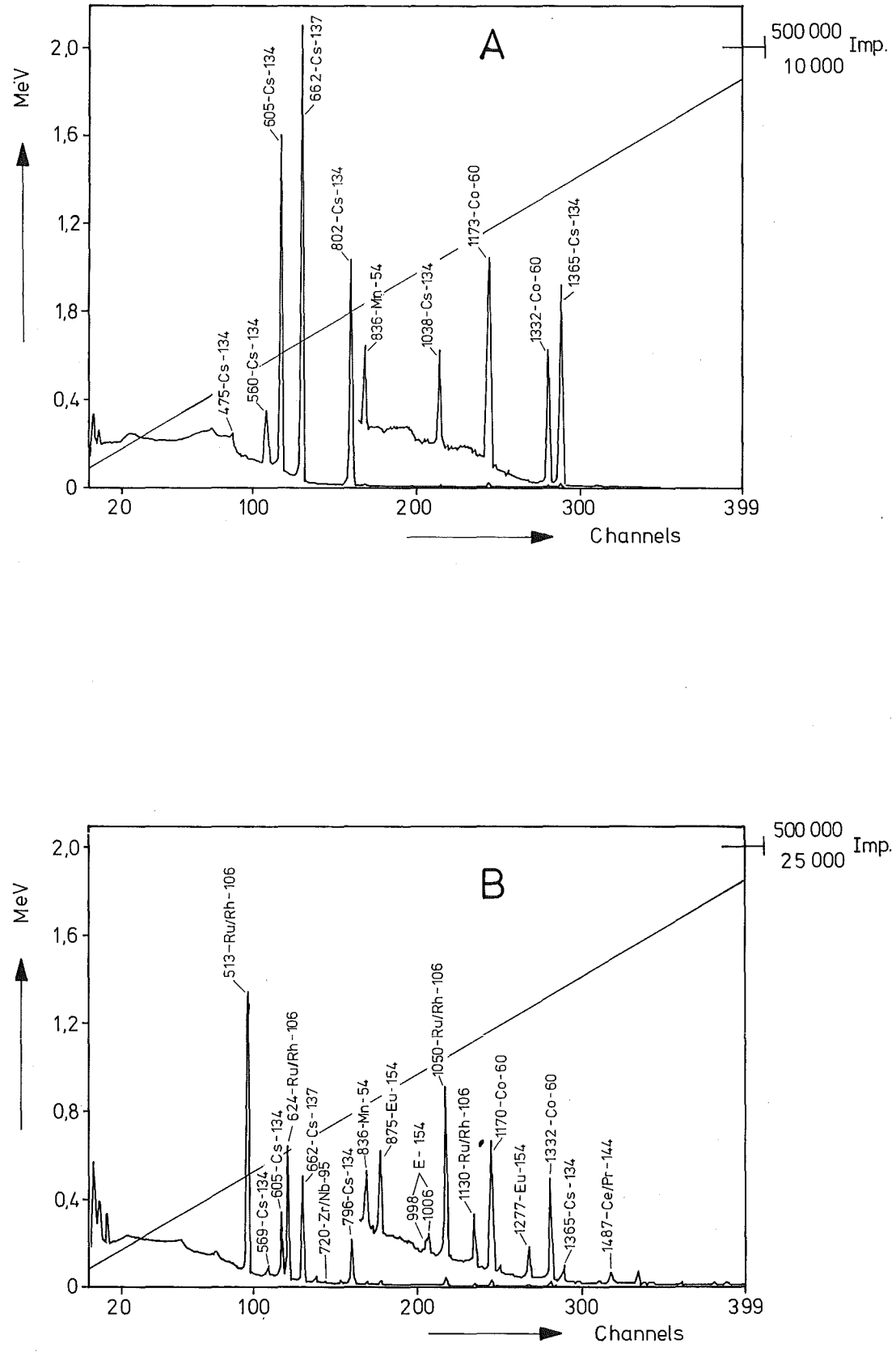

GfK Karlsruhe IMF/III	Pin Mol 8 C - 5 γ-Spectrum at Point A and B	Fig: 12

6. GAMMA SPECTROSCOPY

6.1 Introduction

Axial distribution of the fission products in the fuel has been studied by taking an integral γ-scan and γ-scans for Zr/Nb-95 and Cs/Ba-137. Additional gamma spectra of four points of interest have been measured to study the local accumulation of the various fission products in the fuel. The results do not indicate any gross relocation of the fuel, however, cesium is seen to have accumulated at the colder extremities of the fuel column. A sharp increase in activity at certain parts of the fuel has been noted and it is believed to arise from some irregularities of the central channel. Further analysis has shown that the fission product Ru/Rh-106 is mainly responsible for such sharp increases of activity in the fuel column.

The γ-scans and γ-spectra have been measured by using a Ge-Li detector and a 400 channel analyzer. All these measurements were made by using the same collimator (5.0 x 20 x 700 mm) with a 20 mm plexiglass window in front of it as α ß-absorber. The detector voltage was 1400 volts in all the cases.

6.2 Gamma-Scanning:

6.2.1 Integral Gamma-Scan:

The integral γ -scan of the pin is shown in Fig.10. The count rate was 5 x 10^3 impulses/sec. The following points of interest are noted:

i) The γ-activity at the extremeties of the fuel column is very high, thus, indicating the accumulation of some volatile fission products at the colder parts of the fuel.

ii) Two sharp peaks are observed in the fuel column and these are attributed to the irregularities of the central channel. A comparison with betatron pictures (chapter 5) has shown that these peaks are exactly above the points where "bridges" with sharp edges are seen. This observation, thus, confirms the accumulation of some fission products in the central channel.

iii) Since the trace is fairly uniform, therefore, no gross axial relocation of the fuel seems to have taken place.

6.2.2 Cs/Ba-137, Gamma-Scan:

The γ-scan for Cs-137 is shown in Fig.11. The count rate was 5×10^2 impulses/sec. The following points are noted:

i) A very high activity of Cs-137 and Cs-134 at both ends of the fuel column is seen. Since these are the colder parts of the fuel, it is, therefore, believed that cesium evaporated from the hotter parts of the fuel has condensed at the extremeties of the fuel. Some similar results have also been reported by Smailos and Geithoff /7/.

ii) Cs-137 activity in the middle of fuel column is slightly higher, thus, indicating that a relatively lesser amount of cesium has migrated to the extremities from the central region of the fuel.

iii) In the upper half of the fuel column, a smooth cesium trace is seen, whereas, some fluctuations in its activity are noted in the lower part of the fuel column. This variation in activity is believed to arise from the migration of Cs-137 to the colder outer parts of the pellet through numerous radial cracks formed during and after various irradiations cycles. It may be mentioned here that some radial cracks, although only in small area, have been seen in the betatron pictures (chapter 5) in the lower part of the fuel column.

6.2.3 Zr/Nb-95 Gamma-Scan:

The Zr/Nb-95 γ-scan is shown in Fig. 10. The count rate was 2×10^2 impulses/sec. The gamma-activity observed here is believed to arise from the fissions in the last cycle or the latter parts of the last cycle of irradiation. The smooth trace with a fairly constant activity level, thus, indicates an uniform burnup along the entire length of the fuel pin. Since the gross γ - activity of pin is much higher as compared to the Zr/Nb-95 trace, therefore, the various peaks seen in Fig. 10 are believed to arise from secondary Compton radiations and not from the higher isotopic concentrations of these fission products.

6.3 Gamma-Spectra:

The gamma spectra of four points marked as A, B, C and D in Fig. 10 were measured and the same are discussed below. The time of measurement in each case was 20 minutes. Decay time was 705 days.

6.3.1 Gamma-Spectrum at Point A:

This is shown in Fig.12. The following points are noted:

i) The main gamma-activity sharp peak is found to be from Cs-137 and this is in agreement with the results discussed in 6.2.2.

ii) A substantial contribution to gamma-activity from the activation product Cs-134 is also noted.

iii) The presence of other activation products such as Mn-54 and Co-60 is also detected. Their contribution to gamma-activity, however, is very small.

6.3.2 Gamma-Spectrum at Point B:

This is shown in Fig.12 and the following points are observed.

i) The gamma-activity is mainly from fission product Ru/Rh-106 at this point, although, Cs-137 is also contributing to some degree. Other fission products such as Ce/Pr-144 and Zr/Nb-95 are also detected.

ii) Contribution from activation products such as Cs-134, Mn-54, Eu-154, and Co-60 is very small.

iii) Since the sharp increase in activity at this point is considered to arise from some irregularities of the central channel, therefore, a comparison with betatron pictures (chapter 5) was made. It is seen that the sharp peak is exactly above the area where a "bridge" with sharp edges is noted and, thus, it may be infered that fission and activation products mentioned above are present in high concentrations in the "bridge" material.

6.3.3 Gamma-Spectrum at Point C:

This is shown in Fig.13 and the following points are discussed.

i) The same fission and activation products as noted in 6.3.2 are also identified here, however, the gamma-activity due to various isotopes is substantially different in both cases. The counts from Ru/Rh-106 are about five times less in the present case than that noted in Fig.12.

ii) As expected from the facts discussed in 6.2.2, the activity of Cs-137 at this point is less than that of its activity at Point B, thus, indicating that a relatively larger amount of Cs-137 has migrated from this part to the colder upper end of the fuel. A strongly depleted area near the lower end of the fuel is seen. This is understandable provided it is believed that the "make up" Cs was not available any more because it was trapped in certain cracks near the peripheries of the pellets or at some places in the blocked fuel-clad gap. Thus, a depleted zone near each end of the fuel column would be expected, however, it appears that the cracking and trapping behaviour of the fuel would determine the exact location of these zones.

6.3.4 Gamma-Spectrum at Point D:

This is shown in Fig.13 and the following points are considered:

i) The fission and activation products are same as detected at points B and C, however, the gamma-activity due to various isotopes is substantially different from both the other locations.

ii) Cs-137 activity has increased again and in fact is even higher than its value detected at Point B, thereby, indicating an increase in its concentration as the colder end is approached.

iii) The gamma-activity due to Ru/Rh-106 has also increased to more than three times its activity detected at Point C. As mentioned in chapter 5, the central channel in this region has become very coarse and corrugated and, therefore, it appears that the factors which are influencing the Ru/Rh-106 concentrations are also operating in the formation of central channel irregularities.

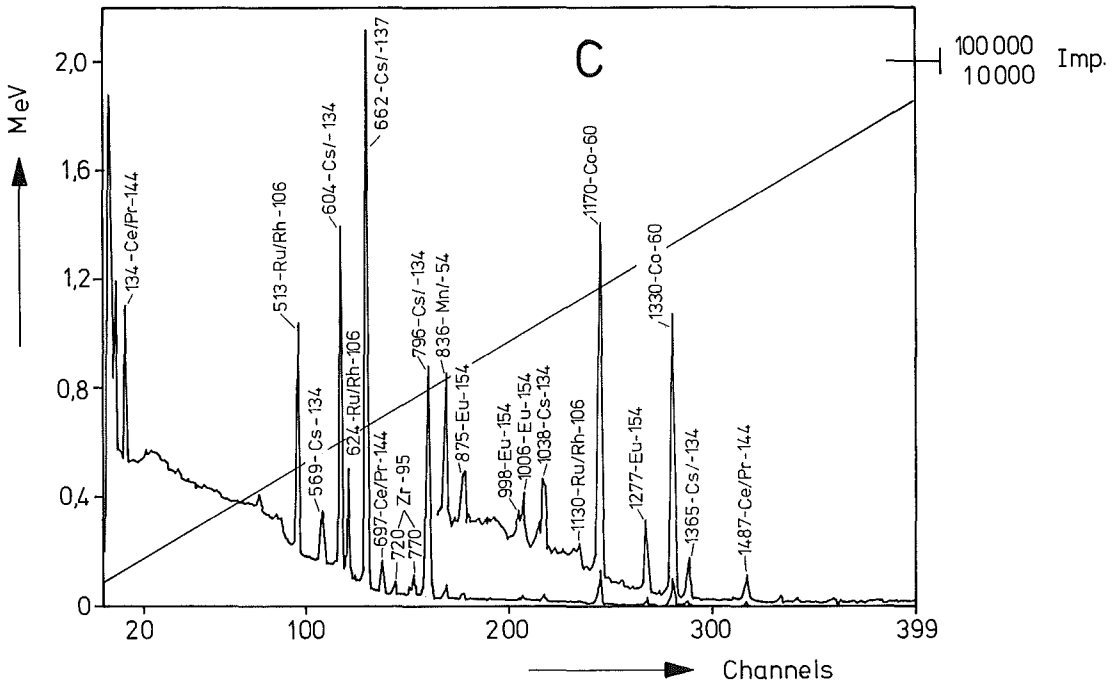

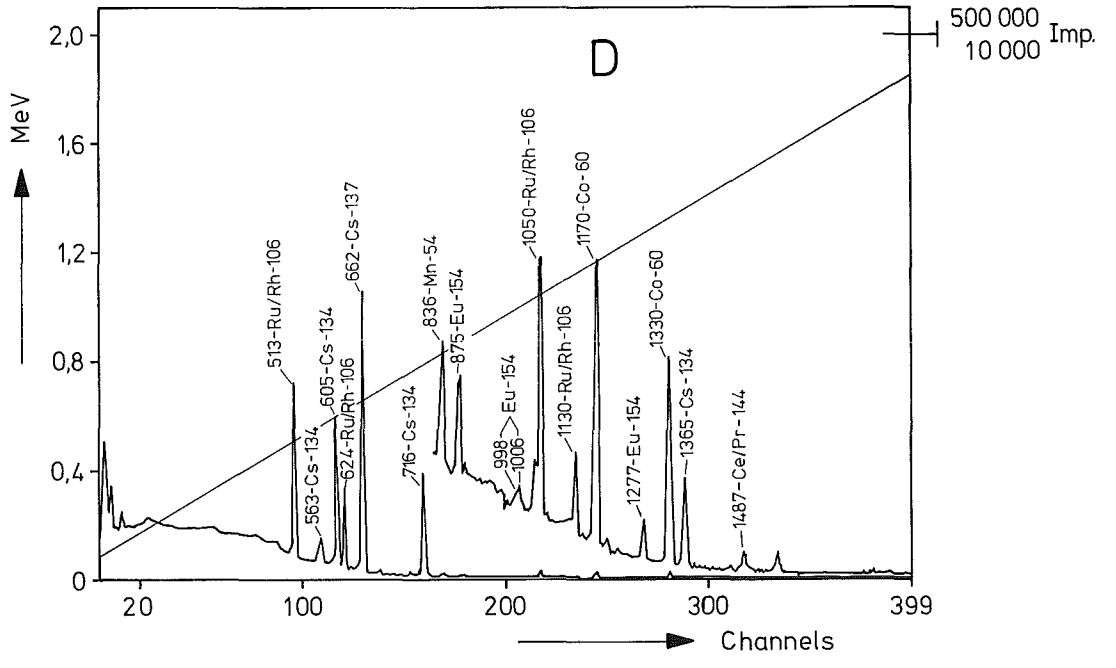

GfK Karlsruhe IMF/III	Pin Mol 8C-5 γ-Spectrum at Point C and D	Fig: 13

7. CERAMOGRAPHY AND AUTORADIOGRAPHY

7.1 Introduction

This chapter describes the cutting plan, the specimen preparation and the results of the subsequent ceramographic and autoradiographic examinations. The result obtained have been discussed in details with special emphasis on the following aspects of the pin:

I.) Internal and external conditions of the cladding material
II.) Fuel-clad gap or reaction zone [+)]
III.) Fuel
IV.) Blanket (two specimen only)
V.) Fission products
VI.) Central channel
VII.) α, β, γ-autoradiography

The characteristic restructuring irradiation behaviour of mixed oxide fuel exhibiting the formation of a) a central channel(c.c.,) b) a columnar grain growth (c.g.g.) region, c) an equiaxed grain growth (e.g.g.) region, d) an unrestructured outer region of fuel and e) numerous radial and circumferential cracks is seen. The salient features noted in each specimen are summarized in table 9. The clad outside appears to be in good condition whereas the clad inside upto 80 μm inthe central parts of the fuel has been damaged by either spalling off inner surface layer of the clad or by intergranular attack by the fission products etc. In certain places both these mechanisms appear to be operative.

A large reaction zone upto 130 μm is noticed and it appears that larger radial cracks exhibit some influence on the formation of reaction zone. Furthemore, it has been seen that the bridge with sharp edges observed in Betatron pictures is a metallic ingot formed by molten fission products and the bridge with diffused edges is the fuel itself. Some evidence of fuel melting in one specimen from the lower part of the pin is also seen.

+) Reaction zone signifies blocked gap as a consequence of fuel/fission products/clad chemical interactions.

Table 9 - Restructuring Data of several Specimens of pin C5.

Specimen No.	Clad damage thickness and mechanism. (/um)	Gap+) or reaction Zone thickness (/um)	Fuel Restructuring Data				Additional Remarks
			unrestruct. fuel region radius (mm)	e.g.g.region radius (mm)	c.g.g. radius (mm)	c.c. radius (mm)	
Mol 8C-5-1	5 - 10/um surface attack	70/um+)	a x i a l				A strong reaction of blanket pellet with fission product Cs and increase in its length are noted
Mol 8C-5-2	10/um thin layer spalling	70 - 100/um+)	a x i a l				An evidence of fuel melting at some parts is seen. The c.c. is irregular and is blocked by the fuel in the middle of the specimen.
Mol 8C-5-3	50 - 80 /um thin layer spalling	100 - 130/um	2.55 to 2.56	2.30 to 2.35	1.85 to 2.00	0.7-0.75	A large reaction zone with clad component rich and fission product rich areas is seen
Mol 8C-5-5	55 - 70/um thin layer spalling plus grain boundry attack	110/um	a x i a l				The central channel is blocked by a metallic ingot believed to be with high concentration of Ru/Rh fission products
Mol 8C-5-6	50/um same as above	100/um	2.55 to 2.58	2.35 to 2.40	1.90 to 1.97	0.85 to 0.90	A deep penetration of clad components into the fuel and some non-metallic precipitates considered to be BaO etc. are seen in the outer parts of the fuel. A large c.c. is seen
Mol 8C-5-7	50/um same as above	50/um	2.62	2.33 to 2.35	1.80 to 1.85	0.70 to 0.72	Even deeper penetration of clad components into the fuel than that noted above is seen.
Mol 8C-5-8	-	70/um	a x i a l				As noted for Mol 8C-5-1

The first blanket pellet on either side of the fuel column seems to have strongly reacted with the volatile fission product Cs forming some Cs-U-Phase in this region. The α-autoradiographs do not indicate any gross Pu migration, however, some of the β,γ -autoradiographs indicate higher concentration of fission products at a few places. The detailed discussion on each specimen is given in Art. 7.4 to 7.10.

7.2 Cutting Plan

The pin cutting plan was made after studying various γ-scans, betatron pictures, metrology profiles, temperature profiles, and external appearance of the pin. The centre of the reactor core was also taken into consideration. The cutting plan is shown in fig. 14. One axial specimen from each side of the fuel column has been taken to study the interaction of fission products and blanket pellets. Another two axial specimens were cut to study the fuel and two types of bridges (with sharp and diffused edges) observed in the Betatron pictures. Three radial specimens were made to study the fuel behaviour I) at reactor mid-plane II) at a point of measured high temperature and III) at a point considered to be representative of uniform burnup. Another specimen was taken for burnup analysis.

As mentioned above, the fuel temperature profiles were also taken into consideration while making the cutting plan. The temperature at the thermocouple contact points was recorded at regular intervals during all the twenty two irradiation cycles of the pin (cf. chapter 3). The average of the maximum temperatures in each cycle and the mean temperature of the irradiation cycles is shown in fig. 15.

Some important information about each specimen are summarized in table 10.

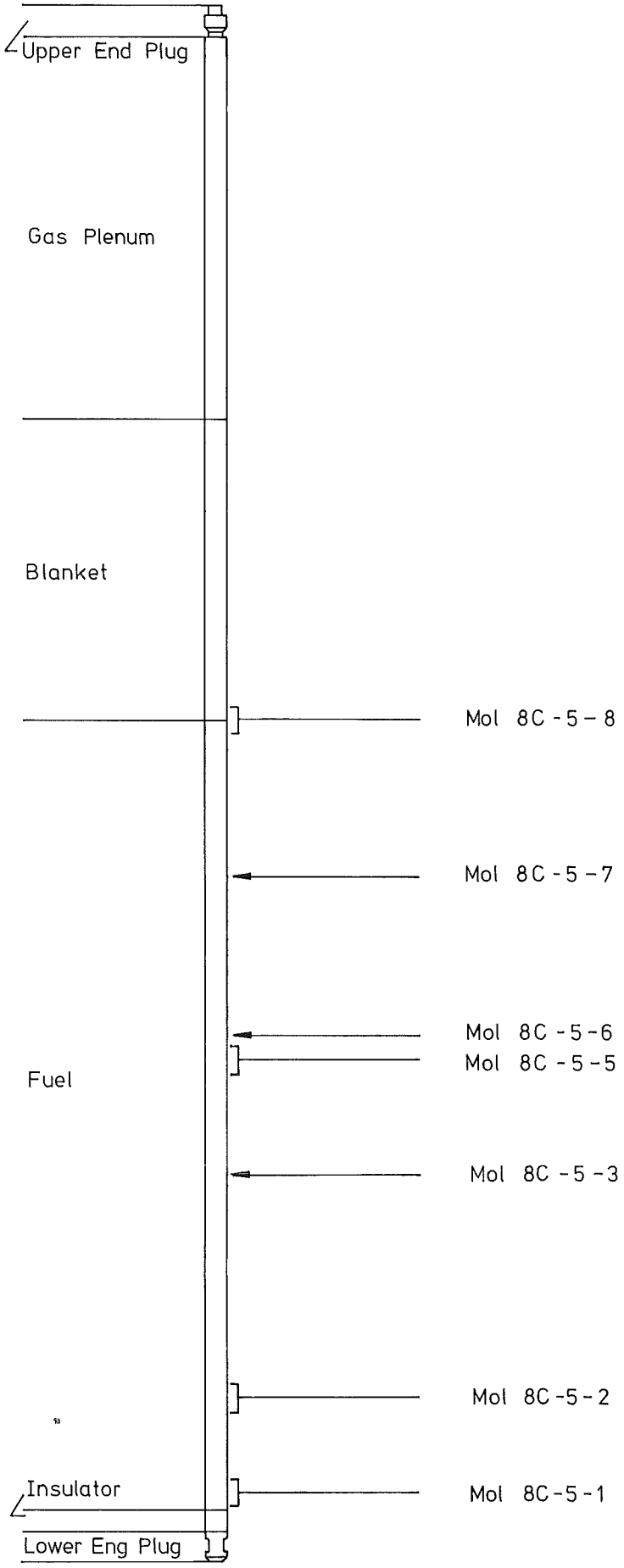

GfK Karlsruhe IMF/III	Cutting Plan for Fuel Pin Mol 8C-5	Fig. 14

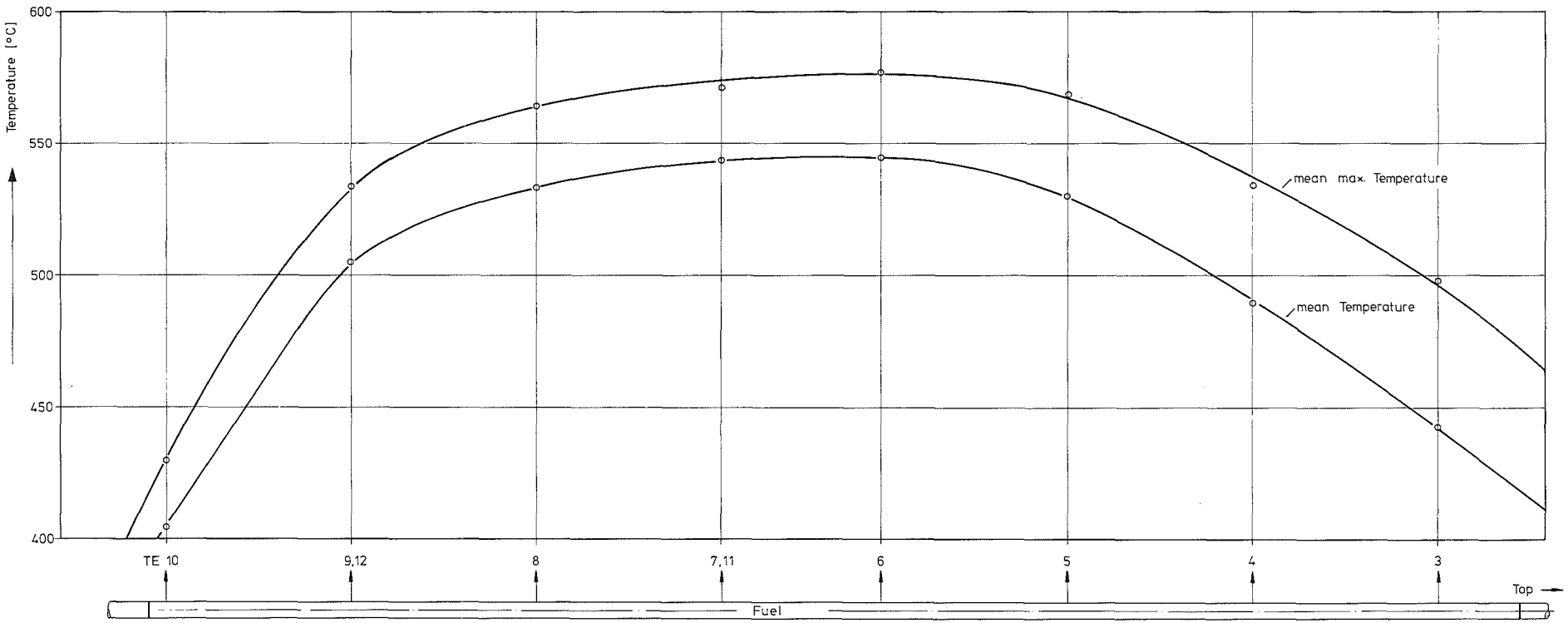

GfK Karlsruhe

IMF/III

Mean and Max Temperature for Mol 8C-5

Fig: 15

Table 10 Important Information about Specimens

Specimen No.	Type	Distance from lower end (cm)	Clad outside Mean Temp. (^{o}C)	Clad outside Average Max. Temp. (^{o}C)
Mol 8C-5-1	Axial	2.4	404	430
-2	Axial	6.7	455	490
-3	Radial	24.9	543	573
-4	Radial[+)]	30.8	545	577
-5	Axial	32.0	544	576
-6	Radial	33.9	540	574
-7	Radial	44.8	490	536
-8	Axial	54.4	427	480

+) for burnup analysis only

7.3 Specimen Preparation

The pin was cut dry by a 1,5 mm thick diamond wheel. The preliminary impregnation was made by ten parts of araldite H and one part of hardener HY 951 and the axial cutting was carried out after this impregnation. The specimen were mounted in Bakelite rings of 37 mm diameter with a mixture of ten parts of araldite D and one part of hardener HY 951.

Since some of the fission products are soluble in water, therefore, it was not used during grinding on silicon carbide papers of various (300, 400, 600) grades. They were again impregnated by the same araldite mixture as used in the preliminary impregnation. Diamond pastes upto 1/4 μm and organic lubricant decalin were used during polishing . The specimen were washed with propanol after polishing and dried with hot air.

7.4 Specimen Mol-8C-5-1 see Appendix pages I/3 to I/5

7.4.1 Clad

The Clad inside and outside appear to be in good condition, however, a small damage ranging from 5 - 10 μm on both sides of the clad in the lower part of the specimen is seen.

7.4.2 Gap

The fuel-clad gap has remained unchanged in its width with an average value of 70μm in the upper (fuel) part of the specimen. In the lower part (blanket), the gap has increased to over 250μm on the left side and almost closed on the right side of the specimen. No evidence of chemical interaction between various components is seen.

7.4.3 Fuel

The fuel restructuring with the formation of regions of different grain sizes but without central channel is seen. As noticed in the Betatron pictures, the central channel is starting here with a small diameter and, therefore, it is believed that the same has been lost during cutting and polishing etc. of the specimen. A few small radial cracks are also seen.

7.4.4 Blanket

The first blanket pellet appears to have strongly reacted with some volatile fission products condensed in this colder part of the pin. A high concentration of Cs in this region has been noticed in γ-spectrum of the fuel and, therefore, it is believed that Cs has strongly reacted with UO_2 forming some Cs-U phase. This phase appears to be in intimate contact with the clad, however, some porosity at the interface of this reaction product/blanket pellet is seen. Some metallic fission products are also visible in this phase. An increase in length of the first blanket pellet is also noted.

7.4.5 Autoradiography

The α-autoradiography of the fuel part of the specimen appears to be quite normal, thus indicating that no gross movement of Pu has taken place. However, a small enrichment of Pu in the upper part of blanket pellet close to the fuel pellet is seen. Similary a slight enrichment of Pu in Cs-U phase is also noticed. Therefore, it appears that the reaction product is some complex phase of Cs, U, Pu and some other fission products and also contains certain unreacted metallic fission products. As expected the γ-autoradiograph further substantiates the high concentration of fission product in the reaction phase. A small increase in γ-activity in the central part of the fuel is noted.

7.5 Specimen Mol-8C-5-2 see Appendix pages I/6 to I/9

7.5.1 Clad

In general, the clad outside appears to be in good condition, however, a small coarse surface believed to arise during cutting in the lower part of the specimen 8C-5-2/15 is seen. The clad inside also appears to be in good condition. The maximum clad loss of 10 μm is noted. A thin layer from the clad inside surface seems to have moved away from the clad and no evidence of damage as a consequence of other mechanisms such as grain boundary attack etc. is seen.

7.5.2 Gap

The fuel clad gap varies between 70 to 100 μm in thickness and is blocked by some gray coloured non-metallic fission product materials. This phase is in intimate contact with the fuel and clad and does not exhibit any grain structure. It is considered to be the oxides of fission products with high concentrations of Ba and Cs oxides. No evidence of chemical interaction, between fuel-clad, fuel-fission products and fission products-clad, is visible. A certain number of fuel particles fallen in the gap have been trapped here and the gray non-metallic phase on either side of the"spalled" clad surface layer is seen.(fig. 8C-5-2/14).)

7.5.3 Fuel

The fuel has restructured with the formation of an irregular central channel and various zones of different grain sizes. A strong evidence of fuel melting on either side of the central channel, except at one lower part of the specimen, characterized by the smooth dense fuel and large circular pores is seen in fig. 8C-5-2/11. The radius of the c.g.g.region varies between 1.90 to 2.05 mm. A number of large radial cracks with a few big voids is also seen.

7.5.4 Central channel

An irregular central channel starting with a smaller diameter at the top and ending with a larger diameter at the bottom is seen. The diameter varies between 0.35 to 0.8 mm and is blocked in the middle of the specimen. In the upper part of the central channel, the presence of molten fuel, metallic fission products and some other material are also seen. Figs. 8C-5-2/11, 8C-5-2/12, 8C-5-3/17. The light gray "needles" along the periphery of the melt indicative circular pores are considered to be of molten fuel. The dark phase is believed to be reaction product of molten fuel and some fission products. In certain cases /8/ a higher concentration of Ba, Sr and Si with small amounts of Mo and Nb in some similar phases has been reported. A few small ingots of metallic fission products are also seen.

The blocked part of the central channel corresponds to the "bridge" with diffused edges as seen in the betatron pictures and, therefore, it appears that the fuel itself is the "bridge" material.

7.5.5 Autoradiography

α-autoradiograph (fig.8C-5-2/1) of slightly different surface from fig. 8C-5-2/7 does not indicate any gross Pu migration. However, a small enrichment near the outer periphery and in the central part of the fuel is seen.

7.6 Specimen Mol-8C-5-3 see Appendix pages I/10 to I/13

7.6.1 Clad

Clad outside appears to be in good condition, however, some damage of 400 µm in length and about 50 µm in depth is seen near the 9 o'clock position as seen in fig. 8C-5-3/9.
This damage is believed to be of mechanical nature. The clad inside has been damaged ranging from 50 µm to 80 µm in depth arising from the inner surface layer removal of the clad material. No grain boundary attack of the clad inside surface is visible even upto x 500 magnification of certain areas as seen in fig. 8C-5-3/10.

7.6.2 Reaction Zone

A large reaction zone ranging from 100 - 130 µm is seen in fig.8C-5-3/10
The clad components have moved inside forming an Fe and Ni rich layer at the fuel/reaction zone interface. The thicker white layer near the clad surface is believed to be mostly Cr-rich zone with oxides of clad components and some fission products in small quantities. The bulk of the reaction zone consists mainly of oxides of fission products such as Cs, Te, Mo and to a lesser degree of oxides of other fission products and clad components.

7.6.3 Fuel

The fuel restructuring with the formation of various zones is visible. The radii of the c.g.g. region varies between 1.85 - 2.0 mm and that of c.g.g. + e.g.g. region varies between 2.30 - 2.35 mm. The unrestructured fuel beyond e.g.g. region is also visible. A large number of radial cracks is seen.

7.6.4 Fission products

Metallic fission products such as Pd, Mo, Ru, Rh etc. are mainly concentrated between radii 1.3 to 2.0 mm. This observation is further confirmed by $\beta\gamma$-autoradiograph.

7.6.5 Central channel

The central channel is well defined, circular and in the middle of the specimen and its diameter varies between 1.4 - 1.5 mm.

7.6.6 Autoradiography

The α-autoradiograph appears to be quite normal and without any gross Pu migration. However, a small enrichment around the central channel and a small depletion of Pu (in the annulus where higher metallic fission product concentration was observed) is seen. The α-autoradiography also appears to be quite normal. As expected the higher activity starts at a small distance away from the central channel and extends upto the middle of the specimen. Therefore, the fission products appear to be mainly concentrated in an annular segment of the fuel of radii 1.3 to 2.0 mm.

7.7 Specimen Mol-8C-5-5 see Appendix pages I/14 to I/17

7.7.1 Clad

In general the clad outside is in good condition, however, a small damage upto 25 μm at one place is seen in fig. 8C-5-5/14. The clad inside appears to have been damaged by a combination of surface layer removal and attack at the grain boundaries.

7.7.2 Reaction zone

The reaction zone up to 110 µm thick is seen. The various details described previously in art.7.6.2 as a consequence of the reaction between fission products, fuel and clad components are also noticed here.

7.7.3 Fuel

The fuel restructuring as described previously in art. 7.6.3 with the formation of a large number of radial cracks is visible.

7.7.4 Fission products

In general, the fission products follow the same pattern as noted in art. 7.6.4. A large metallic ingot of fission product is seen. This is in confirmity with the results obtained by γ-scanning of the fuel.

7.7.5 Central channel

The central channel is irregular and varies between 1.10 to 1.30 mm in diameter. In the upper part of the specimen, the central channel is blocked by a metallic ingot. The blocked part of the central channel corresponds to the "bridge" with sharp edges and, therefore, it appears that the molten metallic fission products tend to form "bridges" with sharp edges on both sides.

7.7.6 Autoradiography

The α-autoradiography is fairly normal and no special concentration of Pu is seen in the photograph. The lower part of the β,γ-autoradiograph exhibits the same characteristics as described previously, however, in the upper part a very high activity emanating from the metallic ingot is seen. The γ-spectrum results have indicated a high concentration of Ru / Rh fission products at this point.

7.8 Specimen Mol-8C-5-6 see Appendix pages I/18 to I/21

7.8.1 Clad

The clad outside surface appears to be in good condition, however, the last parts of the damage noted in specimen Mol-8C-5-3 are also seen here. The clad inside has been damaged upto 50 µm both by the surface layer removal and grain boundary attack of the material. The attack is not uniform inside and some irregularities of the clad thickness are seen.

7.8.2 Reaction zone

The reaction zone of 100 µm thickness is seen. The clad component rich and fission product rich areas as described in 7.6.2 are also seen here. At certain places some non-metallic precipitate considered to be BaO is also found at the reaction zone-fuel interface.

7.8.3 Fuel

The fuel restructuring is noted. The c.g.g. region varies between 1.87 to 1.95 mm and the c.g.g. + e.g.g. region varies between 2.35 to 2.40 mm. The unrestructured zone extends upto 2.58 mm. Numerous big voids indicating the loss of fuel and a large number of radial cracks are also visible. The clad components such as Fe and Ni seem to have penetrated deep into the fuel and some areas of higher concentration of these components in the outer periphery of the e.g.g. zone are noted.

7.8.4 Fission Products

The metallic fission products appear to follow the same general pattern as mentioned in 7.6.4. However, some non-metallic fission product precipitates such as BaO are seen at various places in the unrestructured zone of the fuel.

7.8.5 Central Channel

The central channel is smooth, round and in the middle of the specimen. Its diameter seems to have increased form that of specimen Mol-8C-5-3 and varies between 1.70 to 1.80 mm.

7.8.6 Autoradiography

Both α and β,γ-autoradiography indicate the same general behaviour of the fuel as noted in 7.6.6. A small Pu concentration in front of a large void is noted. This could be due to higher temperature in the inner side of the void. An annular concentration of fission products extending upto the middle of the specimen is also noted.

7.9 Specimen Mol-8C-5-7 see Appendix pages I/22 to I/24

7.9.1 Clad

Clad external surface appears to be in good condition. The mechanical damage noted in 7.6.1 and 7.8.1 is not visible anymore. The inside surface attack is much smaller and both thin surface layer removal and grain boundary attack are also noted. The maximum clad loss is 50 μm and the inside circumference appears to be quite regular.

7.9.2 Reaction zone

The reaction zone is much smaller than that described in 7.6.2 and 7.8.2 a maximum width of 50 μm is noted. The fission product rich area is smaller than the clad component rich area, thus, indicating a smaller amount of fission product radial movement at this position. A comparison with art.no. 7.6.2 and gross γ-scan of fuel fig. 10, thus, indicates that a smaller reaction zone should be expected where smooth γ-trace is seen.

7.9.3 Fuel

The fuel exhibits the same characteristics as noted previously. The c.g.g. region varies between 1.8 to 1.85 mm and c.g.g. plus e.g.g. region varies between 2.33 to 2.35 mm. The unrestructured zone extends upto 2.62 mm. The clad components such as Ni and Fe have penetrated even deeper into the fuel than what is noted in 7.8.3. Some high concentration of these components in a few parts of the fuel is also noted. A large number of radial cracks and big voids are visible. It appears that large quantities of fuel have moved away from this part of the pin.

7.9.4 Fission products

The behaviour is very similar to what has been noted for specimen Mo1-8C-5-6.

7.9.5 Central channel

The central channel has the same characteristics as noted previously. However, its diameter is smaller than that noted in 7.6.5 and 7.8.5 and varies between 1.40 to 1.45 mm.

7.9.6 Autoradiography

The appearance of both α and β,γ-autoradiographs is very similar to 7.6.6 and 7.8.6. However, the fission product annulus is relatively smaller here.

7.10 Specimen Mo1-8C-5-8 see Appendix pages I/25 to I/30

7.10.1 Clad

The clad outside is in good condition and,as expected,the clad inside also appears to be without any damage.

7.10.2 Fuel

The fuel and blanket pellets are not discernable because of the interaction of these pellets. The last part of the fuel may be seen in the lower end of the specimen.

7.10.3 Blanket

Besides the fuel/blanket interaction at the interface, the first blanket pellet also appears to have strongly reacted with some volatile fission products accumulated in this colder part of the pin. This has already been discussed in 7.4.4. Consequently, the unhomogeneous appearance of this blanket pellet and the reaction boundaries may be clearly seen. The lower part of the first blanket pellet has higher porosity and also appears to have some small unreacted regions within the reacted part of the pellet.

7.10.4 Autoradiography

A small Pu concentration in the lower part of the specimen, corresponding to the fuel part, is seen. Furthermore, the porous behaviour of the reacted material is also revealed in the autoradiograph . A small Pu concentration in the "halfmoon" shaped reaction boundary is also noted. As expected from the γ-scanning results (Fig.11), a very high β,γ-activity is seen here. This is believed to be mainly due to higher Cs-concentration in this part of the pin. The Cs reaction with the blanket pellet resulting in the appearance of a "halfmoon" shape may be indicative of the temperature profile of the first blanket pellet. However, it may be mentioned here that some additional study would be required to better understand this phenomenon.

8. FISSION GAS CALCULATION

The fuel pin was connected through a 3000 mm long capillary tube to the gas pressure measuring circuit outside the reactor core. The fission gas pressure at the end of each cycle was noted and the same has been shown in fig. 16. The total system volume was arising from the following parts of the measuring circuit.

$$V_{total} = V_{radial\ gap} + V_{plenum} + V_{capillary} + V_{measuring\ system}$$

The gas pressure at the end of irradiation was measured to be 30.7 kg/cm^2 and by taking the free volume of pin as 5.9 cm^3, the pressure inside the pin was calculated to be 46.3 kg/cm^2. The theoretical fission gas volume, by assuming that 30 % fission gas atoms were produced during fission, was calculated to be 262 cm^3. Since some of the fission gas produced is retained in the fuel in its pores and lattice therefore, the same has been measured by grinding and dissolving the fuel respectively. The results are given below:

gas	in pores (cm^3)	in lattic (cm^3)	total
Xe	8.923	2.66	11.58
Kr	1.247	0.31	1.56

Thus, the total gas retained by the fuel was 13.14 cm^3. Based on the theoretical fission gas released and the experimental value of the retained gases, the pin pressure arising from the released gas has been calculated to be 42.2 kg/cm^2. Thus, a good agreement between the measured and the calculated fission gas release is seen.

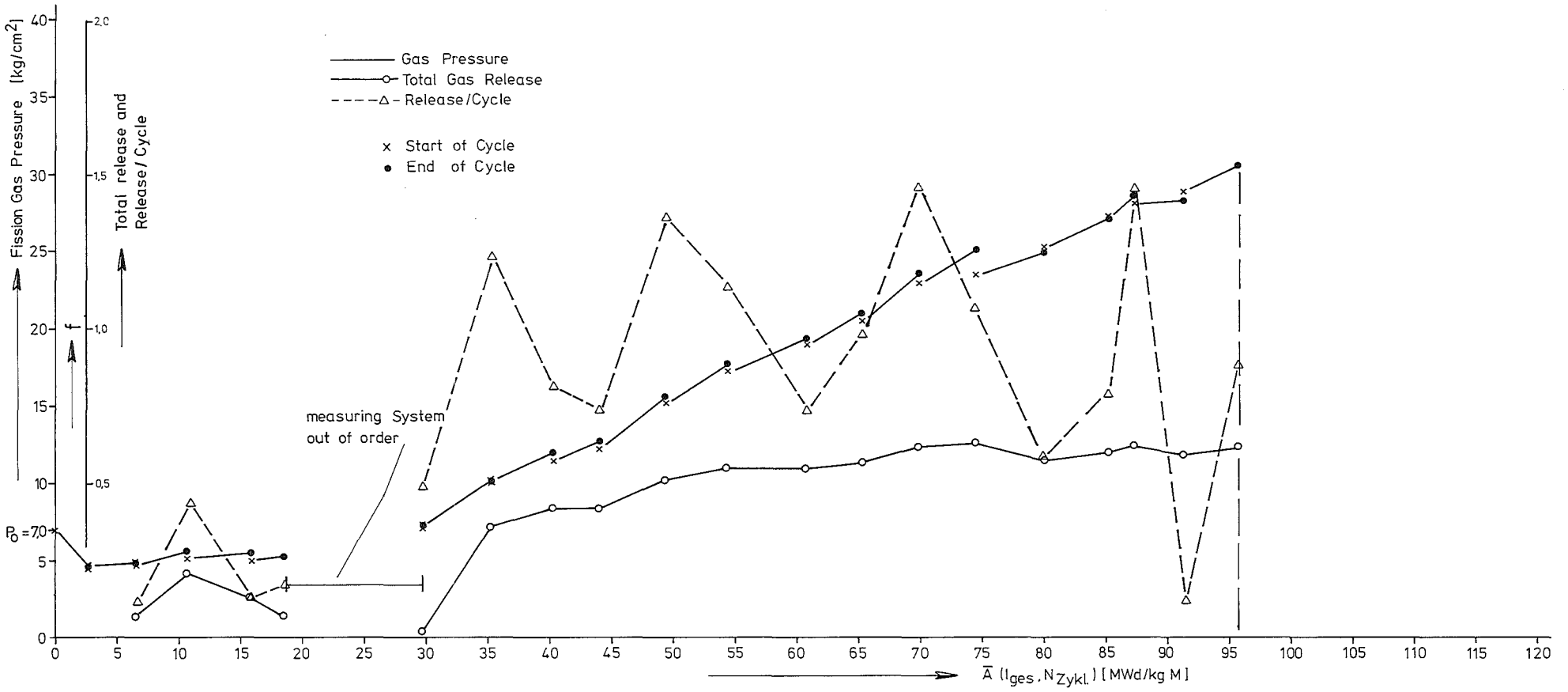

GfK Karlsruhe IMF/III	Fission Gas Release in each Cycle and Total Gas Release in Pin Mol-8C-5	Fig. 16

9. BURN-UP DETERMINATION

One of the specimen, Mo1-8C-5-4, was used to determine the absolute burn-up of fuel by its chemical analysis. The specimen was dissolved in HNO_3 and the fission product monitor and the heavy atoms were determined by the standard techniques. Burn-up was calculated as follows:

$$\text{Burn-up, } a/_oF = 100 \frac{A/Y}{H + A/Y}$$

where

$a/_oF$ = atom percent fission
A = determined number of atoms of fission product monitor
Y = effective fractional fission yield of A
H = determined number of residual heavy atoms.

Since in the mixed oxide fuel, different atoms are contributing to the fission reaction, it is, therefore, necessary to select a fission product monitor whose yield varies as little as possible with the fissioning nuclides. The table 11, compiled by Werténbach, shows the fission yield of Ce-144, Cs-137 and Nd-148 from varies nuclides.

Table 11 Fission yields of Ce-144, Cs-137 and Nd-148

Fissioning Nuclide	Mode of Fission +)	Fission Yield %			1 $a/_o$ = $MWD/_t$
		Ce-144	Cs-137	Nd-148	
U-235	Th	5.42	6.28	1.69	9500
Pu-239	Th	3.78	6.74	1.70	9800
Pu-241	Th	4.13	6.60	1.89	9000
U-238	F	4.74	6.28	2.18	9620

The half-life of these nuclides are as follows:

Ce-144 = 284 d
Cs-137 = 30.3 a
Nd-148 = stable

+) Th: Thermal
F: Fast

The fission product Cs-137 has long half life and almost equal fission yield from different nuclides; however, the post irradiation examination has established that this isotope migrates both in axial and radial directions and very high concentrations of Cs-137 have been seen in the colder parts of the fuel. The two other, isotopes i.e., Nd-148 and Ce-144 like most other rare earths do not migrate significantly and, therefore, the same were used as fission product monitors.

The fission monitor Nd-148 and total Nd atoms (143, 144, 145, 146, 148, 150) with 19.7 % fission yield were detemined by the isotope dilution mass spectrometry and Ce-144 was determined by γ-spectrometry. The total number of heavy atoms (U + Pu) after irradiation was determined by x-ray fluorescence spectrometry. The following results have been obtained:

U-atoms after irradiation / total heavy atoms before irr.	=	0.7127
Pu-atoms " " / " " " " "	=	0.1743
Fissioned atoms / " " " " "	=	0.1130
T o t a l		1.0000

Nd-148 / total heavy atoms before irradiation = 1.917×10^{-3}

Ce-144 / " " " " " = 2.242×10^{-3} (on 26.6.73)

By using the formula given above, the burn-up in atomic % was calculated

from Ce-144		11.27 $a/_o$
from Nd-148		11.34 $a/_o$
from total Nd		11.34 $a/_o$
Average burn-up	=	11.31 $a/_o$

10. SUMMARY AND CONCLUSIONS

1. The pin was found to be in excellent condition even after succesfully operating at greater than 9.6 $a/_o$ burnup at an average rod power of 393 W/cm. The irradiation programme has demonstrated that high burnup levels are feasible and the results obtained in this investigation thus provide further confidence in the stainless steel clad mixed oxide fuel concept.

2. The axial enlongation of the pin was seen to be less than 0.06 % and a maximum increase of 0.6 % in diameter at one point was observed. This sharp increase in diameter has been attributed to some external surface irregularities of the clad tube.

3. The total amount of fission gas yield was about 30 % of the total number of fissions. The total fission gas release was about 60 %.

4. The typical oxide fuel restructuring behaviour with the formation of various regions of different grain sizes and a central channel was seen.

5. The central channel was seen to be blocked at a few places by molten metallic fission product ingots with high Ru/Rh-106 concentrations.

6. Some evidence of fuel melting in the lower part of the pin (specimen Mol-8C-5-2) was seen.

7. The fission products were seen to have migrated in the axial and radial directions. A high concentration of Cs-137 was found at both ends of the fuel column and a strong interaction of this fission product with the blanket material was also seen.

8. No discernable effects of the blockage of central channel by metallic ingots or of a limited fuel melting or of gross migration of Cs-137 and of its interaction with blanket material on fuel pin performance could be seen.

9. The clad outside was in good condition whereas the clad inside upto 80 µm was damaged. The damage was seen to have been caused either by spalling of inner surface layer or by intergranular attack of the material. At certain places, the damage was also seen to have been caused by the combination of these mechanisms.

11. REFERENCES

/1/ A. Gerken and K. Kummerer:

Auslegung und Spezifikation des UO_2-PuO_2 Brennstab-Bestrahlungsversuches Mol-8C im BR-2, (Oct. 1968)
(Private Communication)

/2/ Th.Dippel and K. Kummerer:

Herstellung Pu-haltiger Prüflinge für die Versuchsgruppe 8C im Reaktor BR-2 in Mol, (Sept. 1973)
(Private Communication)

/3/ P. von der Hardt:

Technical Note No. 71/5466/02/P.vd.H. CEN-Mol
(Private Communication)

/4/ H. van den Boorn:

Bericht über die Bestrahlung von 10 Brennstäben der Versuchsreihe Mol-8C im BR-2, CEN/Mol
(Private Communication)

/5/ H.L. Krautwedel, D. Geithoff and H. Enderlein:
Kerntechnik 10, 494 (1968)

/6/ I. Tucek and R. Wiechers:
Kerntechnik 13, 2 (1971)

/7/ E. Smailos and D. Geithoff:

Die axiale Verteilung einiger Spaltnuklide in Brennstäben des Bestrahlungsexperimentes DFR-350, KFK 1648 (Okt.1972)

/8/ R. H. Hilbert et.al.:

Performance of Mixed Oxide Fuel Rods Irradiated to 13 $^{a}/_{o}$ Burn-up in EBR-II, GEAP-13538, (1973)

APPENDIX

Ceramography and Autoradiography Pictures

The orientation of all micrographic section is given in fig. 14.

Mol 8C-5-1

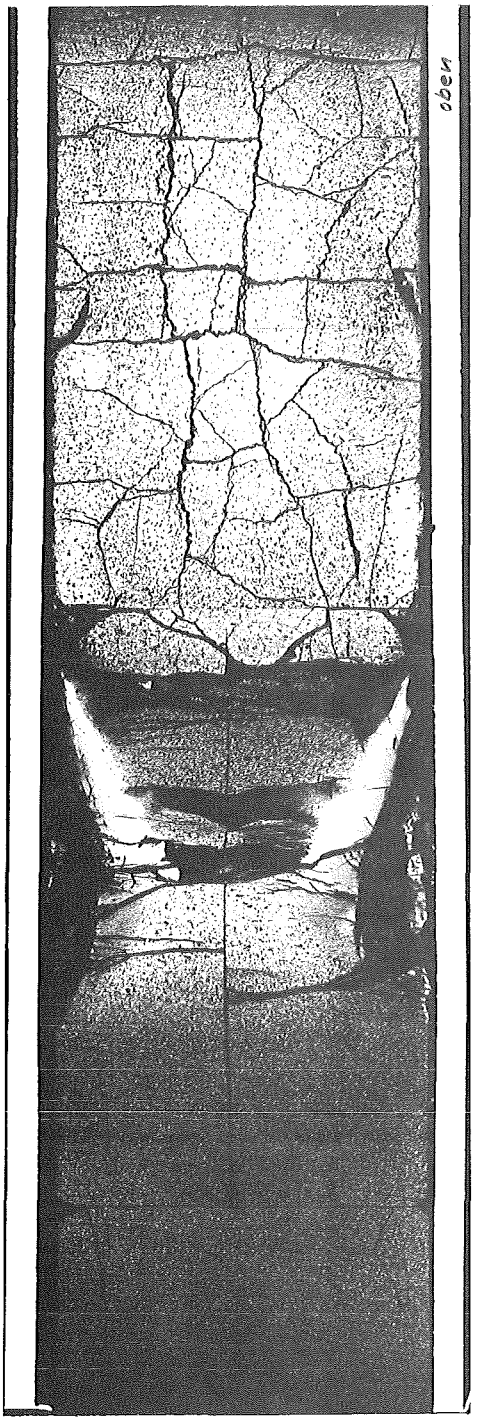

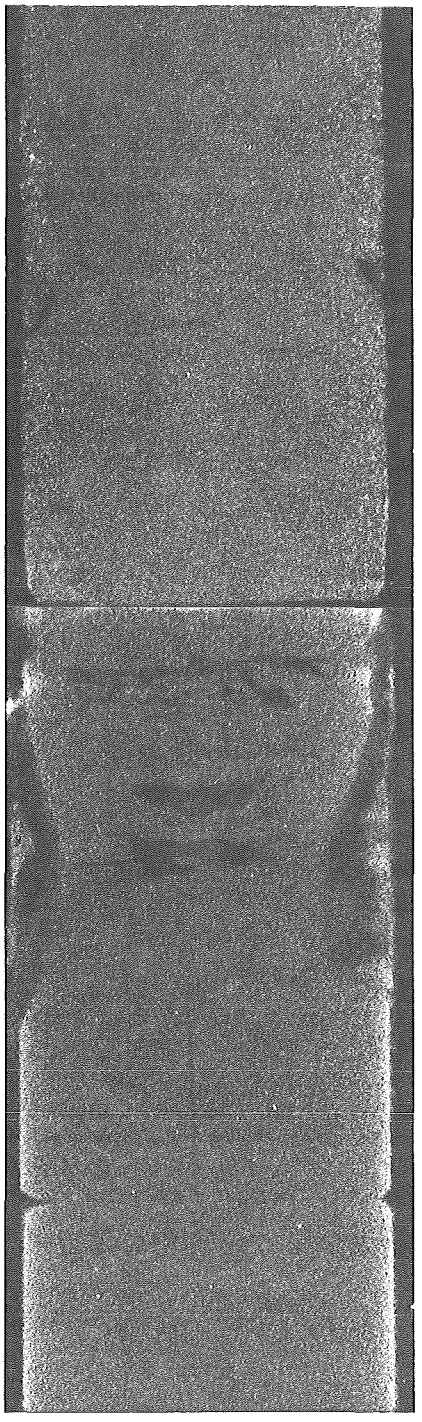

α - autorad.

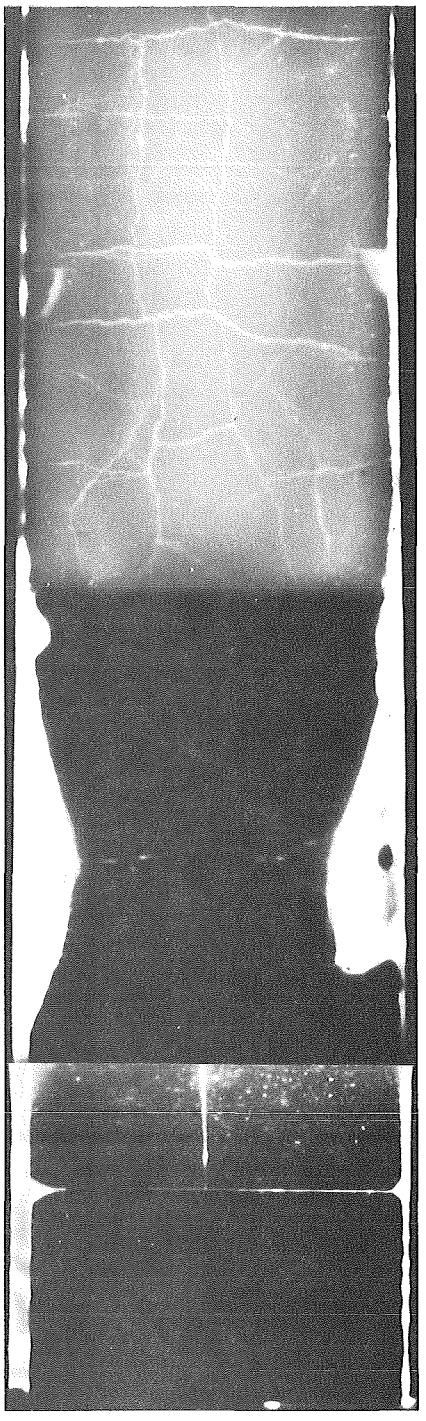

β-γ - autorad.

1mm

Mol 8C-5-1

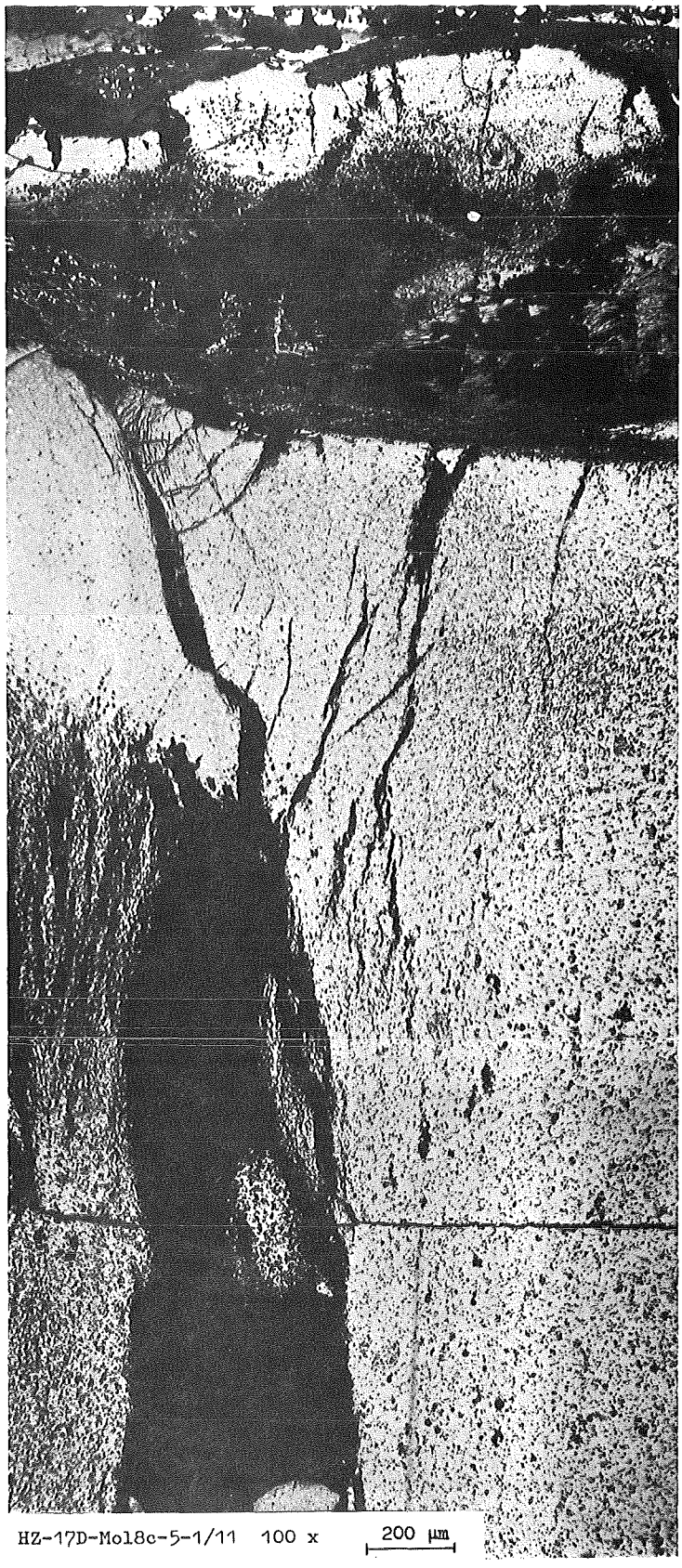

Mol 8C-5-1

Mol 8C-5-2

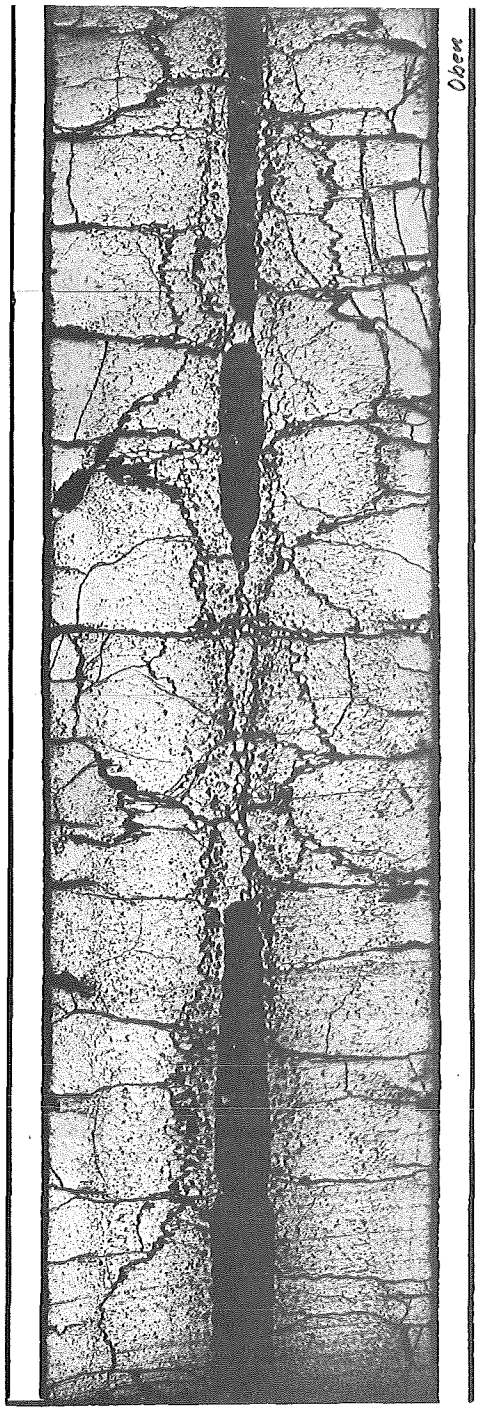

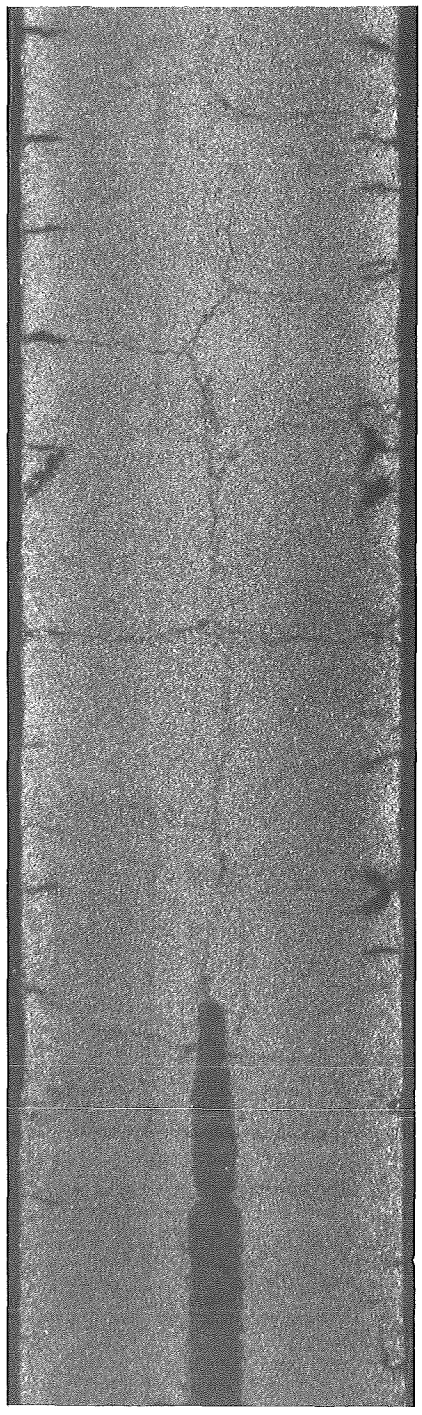

α - autorad.

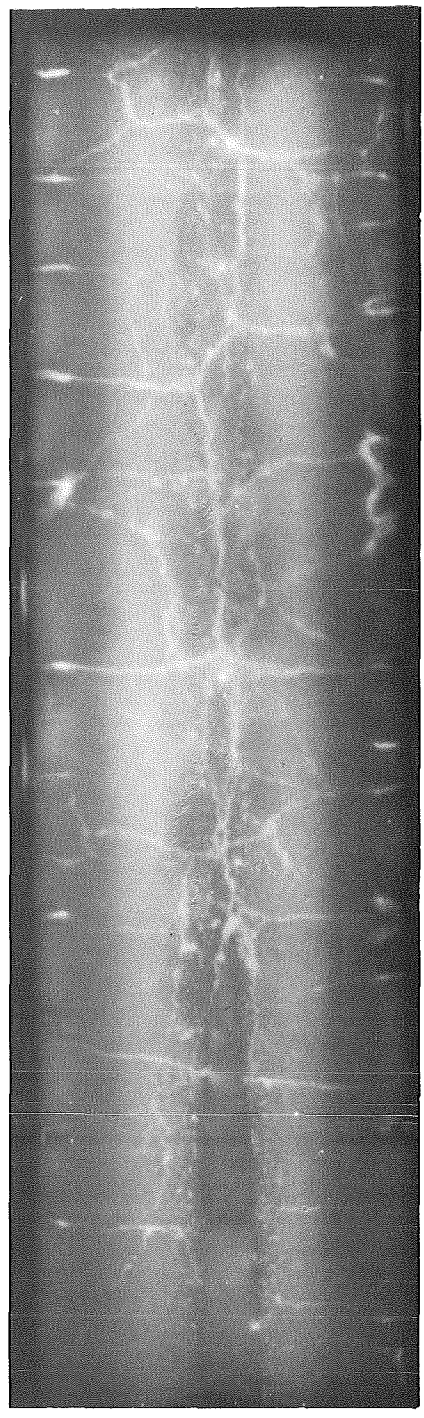

β-γ - autorad.

1mm

Mol 8C-5-2

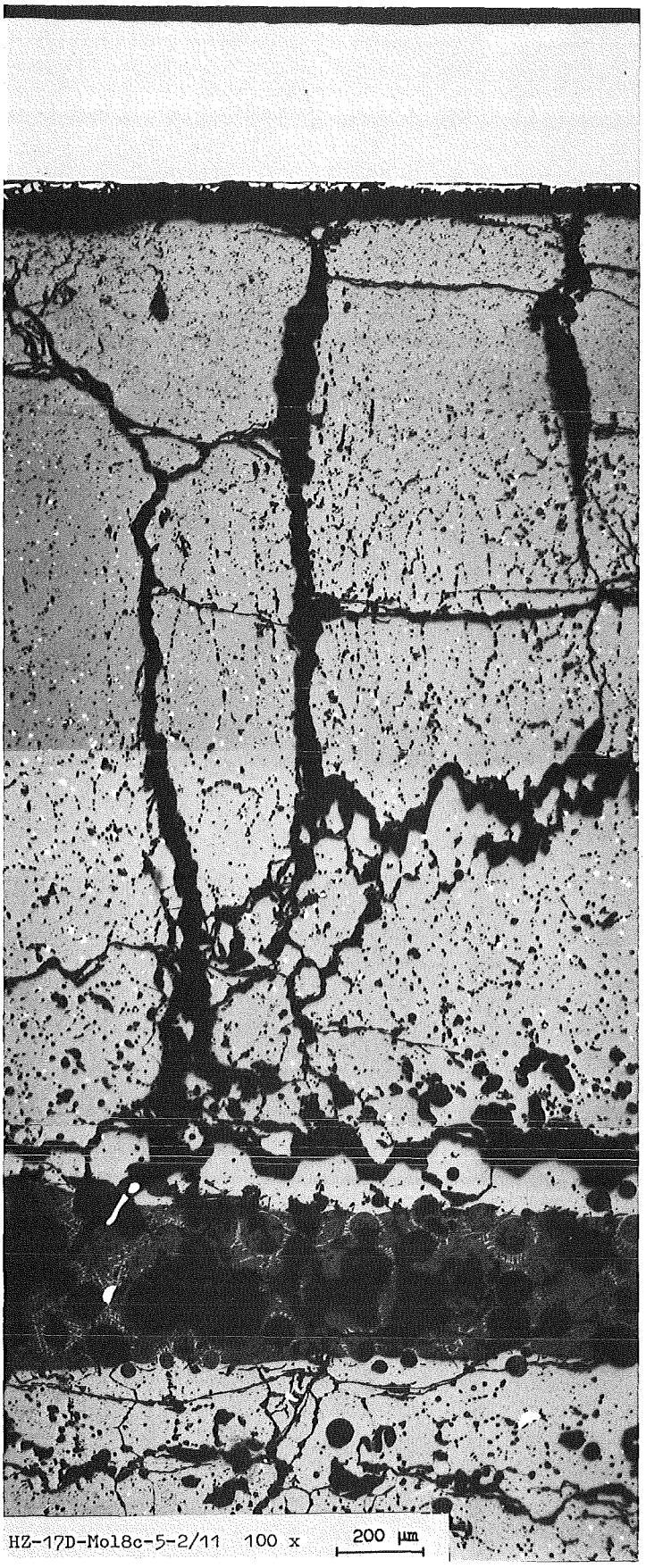

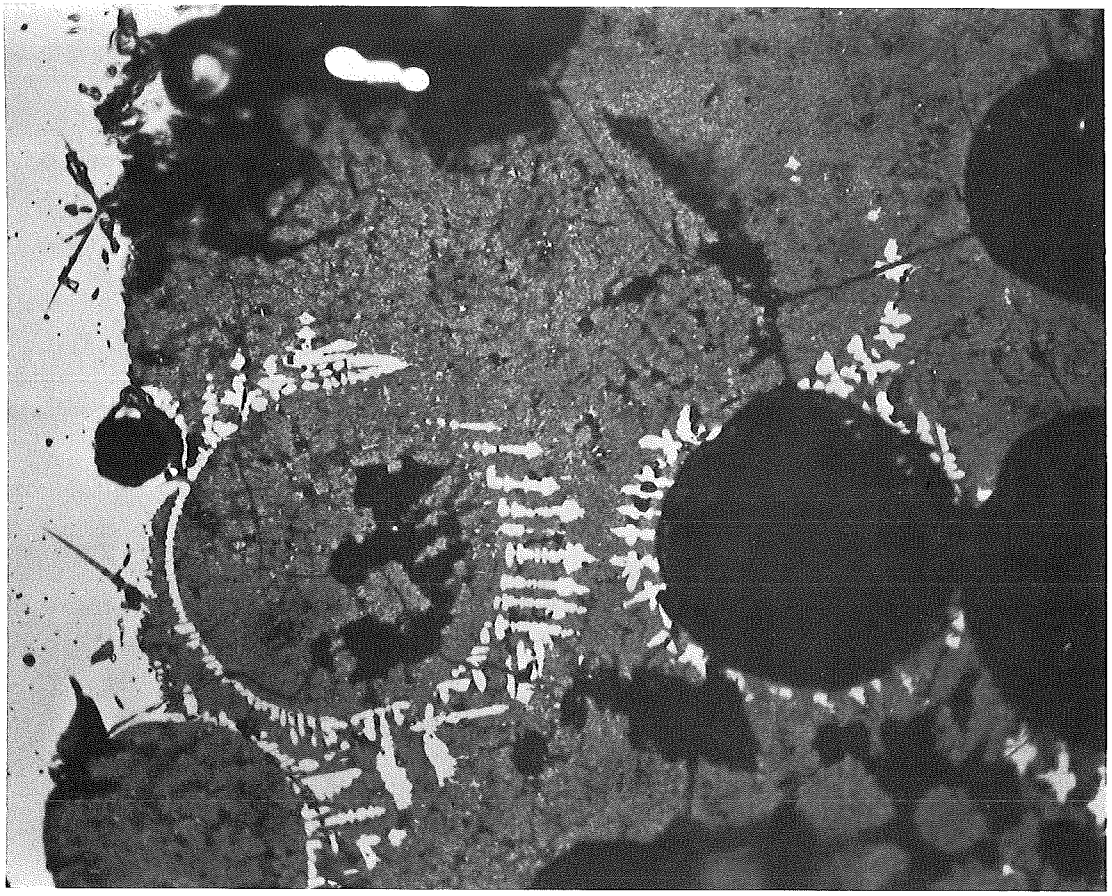

HZ-17D-Mo18C-5-2/12 500x 40 µm

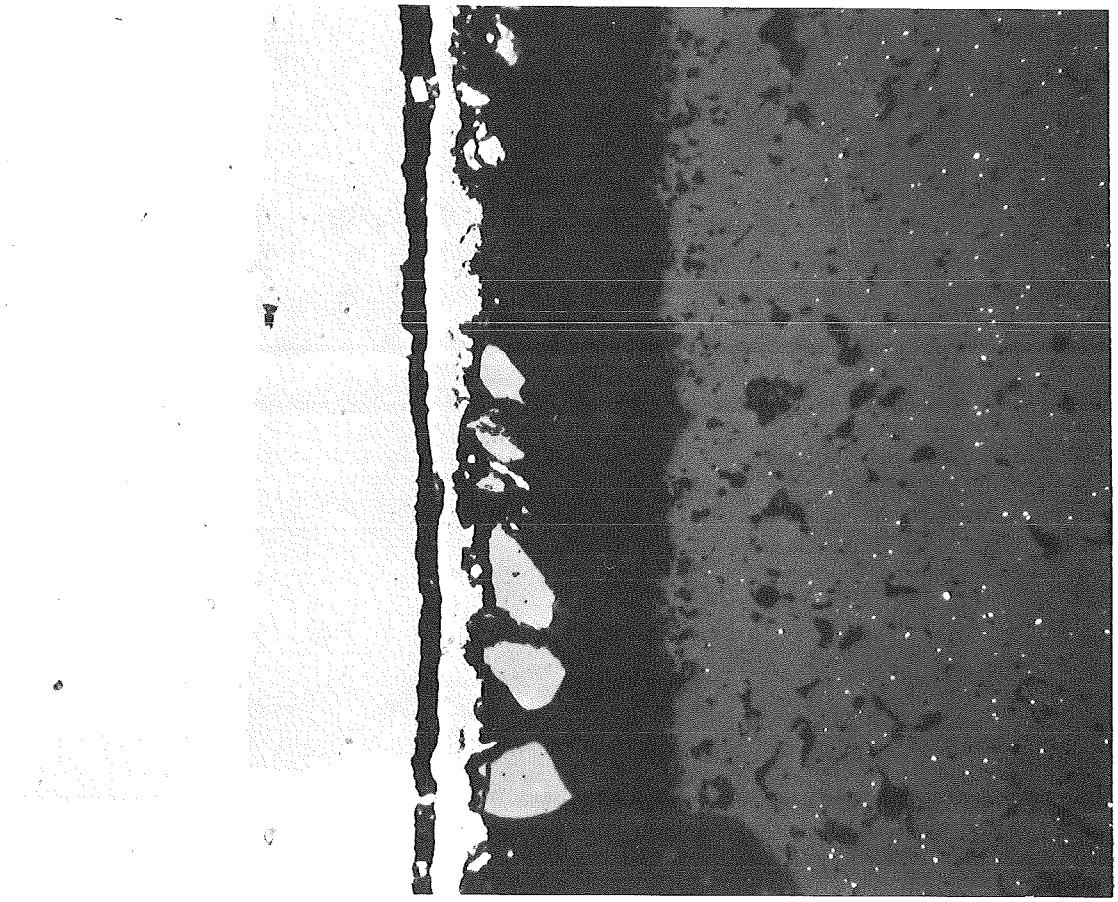

HZ-17D-Mo18C-5-2/14 500x 40 µm

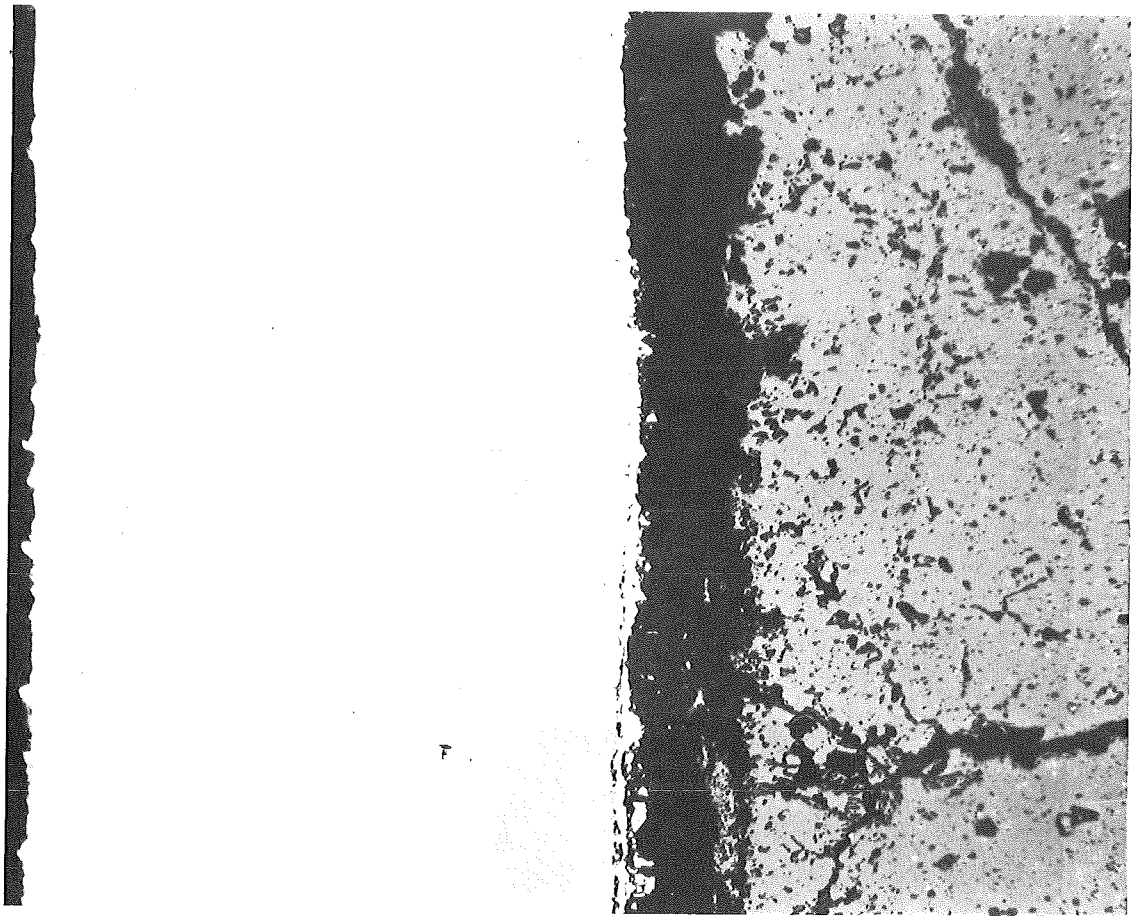

HZ-17D-Mo18C-5-2/15 200x 100 µm

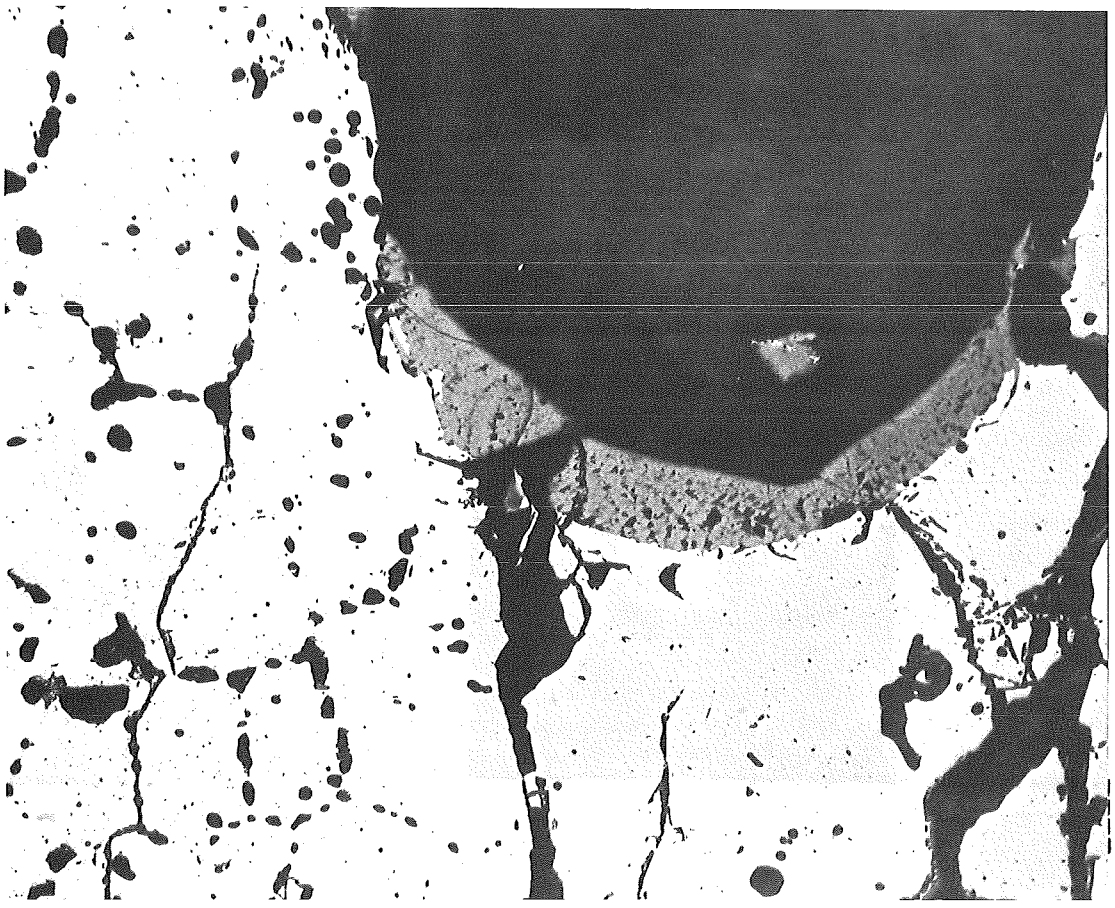

HZ-17D-Mo18C-5-2/17 200x 100 µm

Mol 8C-5-3

A

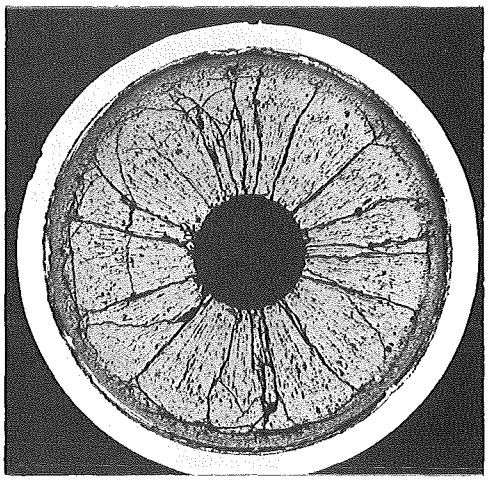

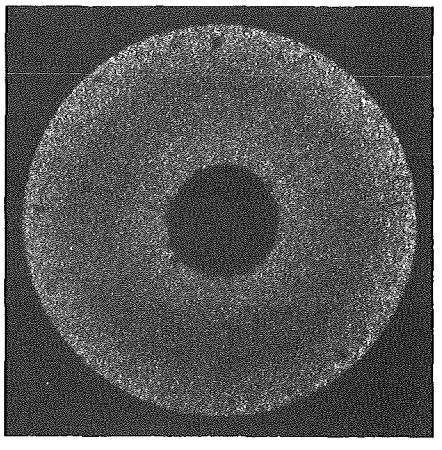

α-autorad.

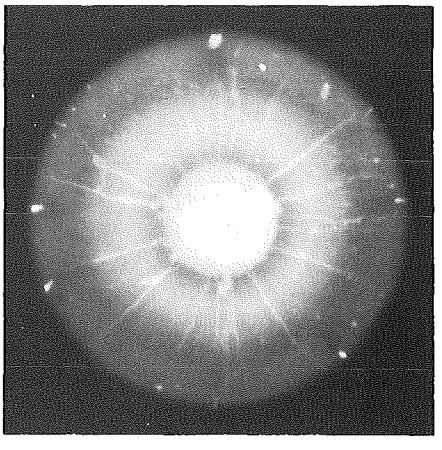

β-γ-autorad.

1 mm

Mol 8C-5-3

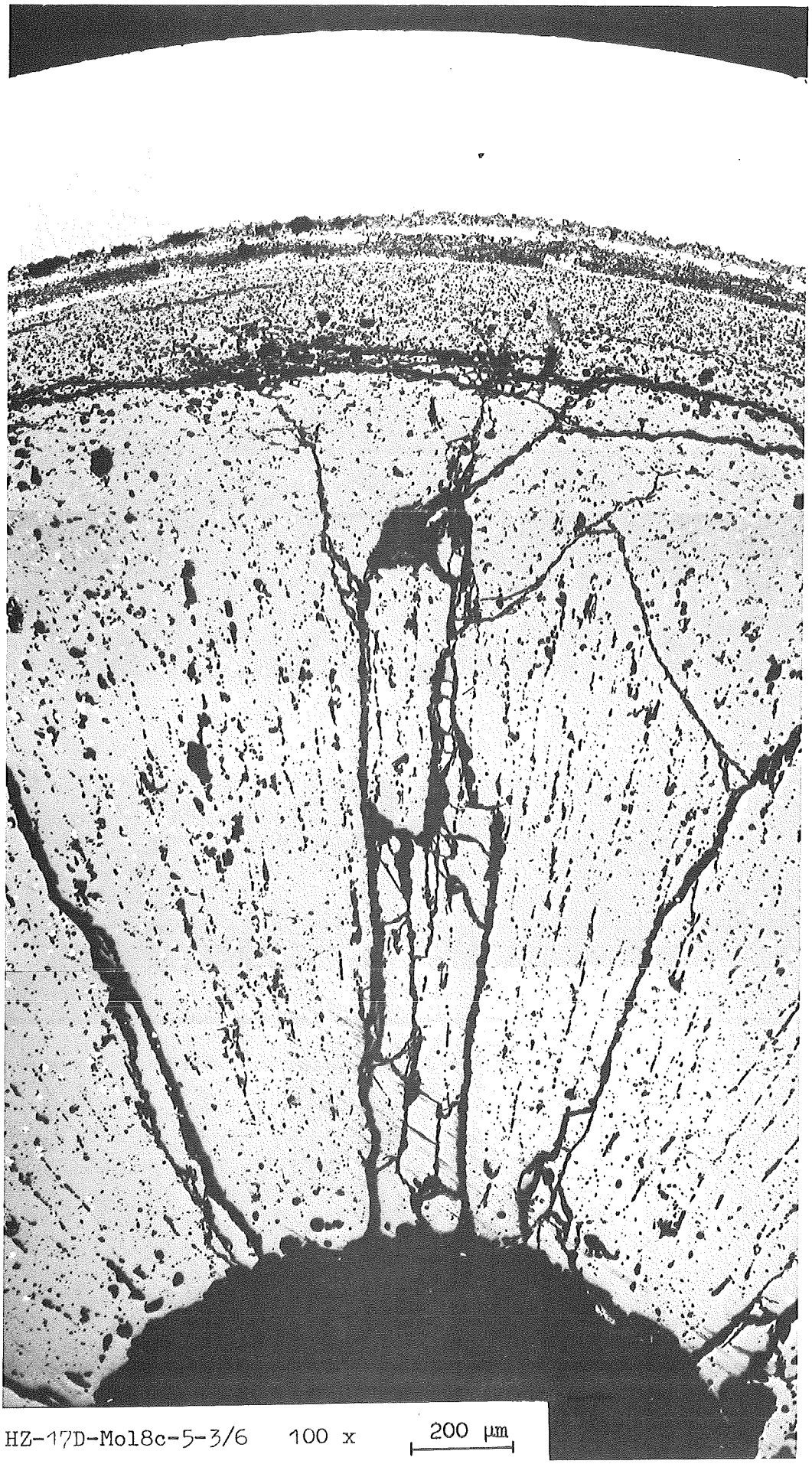

HZ-17D-Mol8c-5-3/6 100 x 200 µm

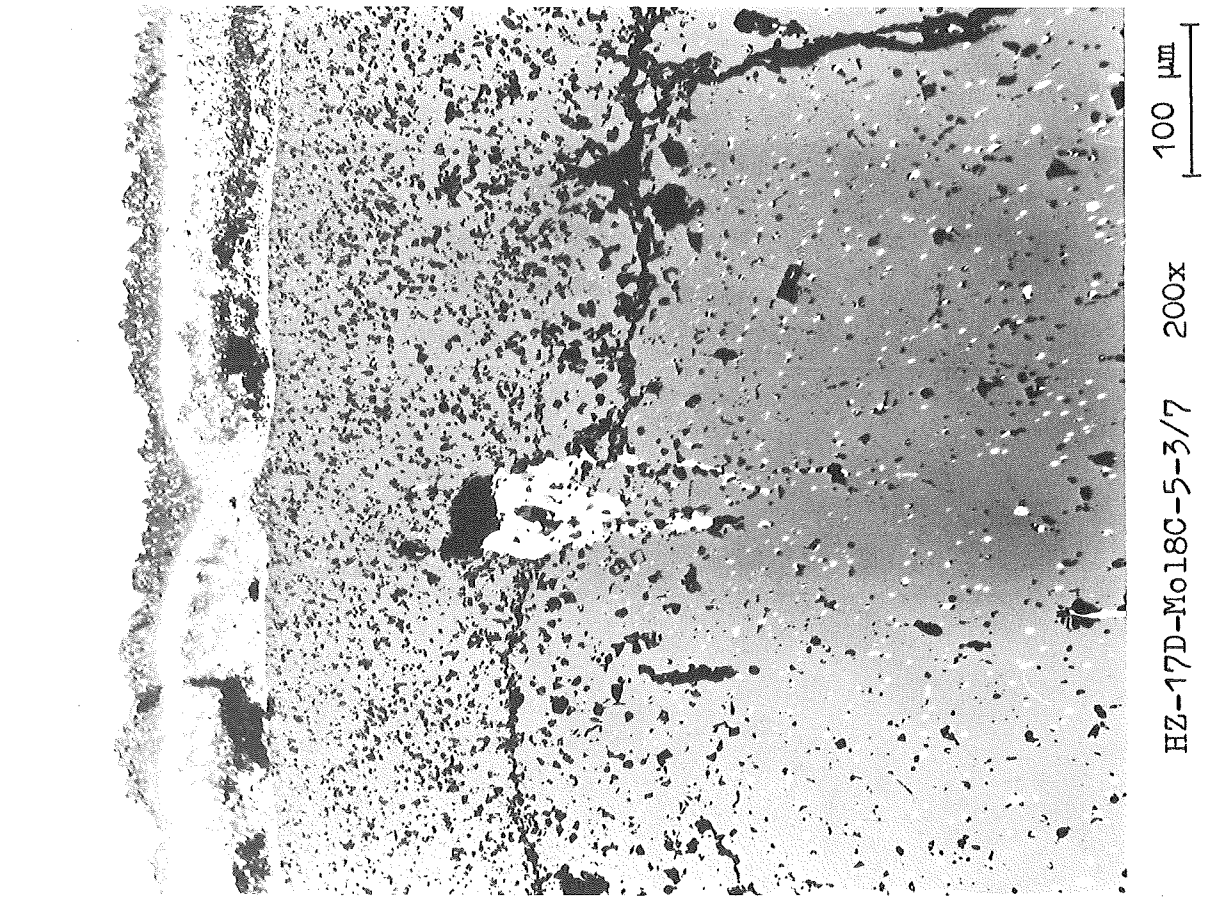
HZ-17D-Mo18C-5-3/7 200x
100 µm

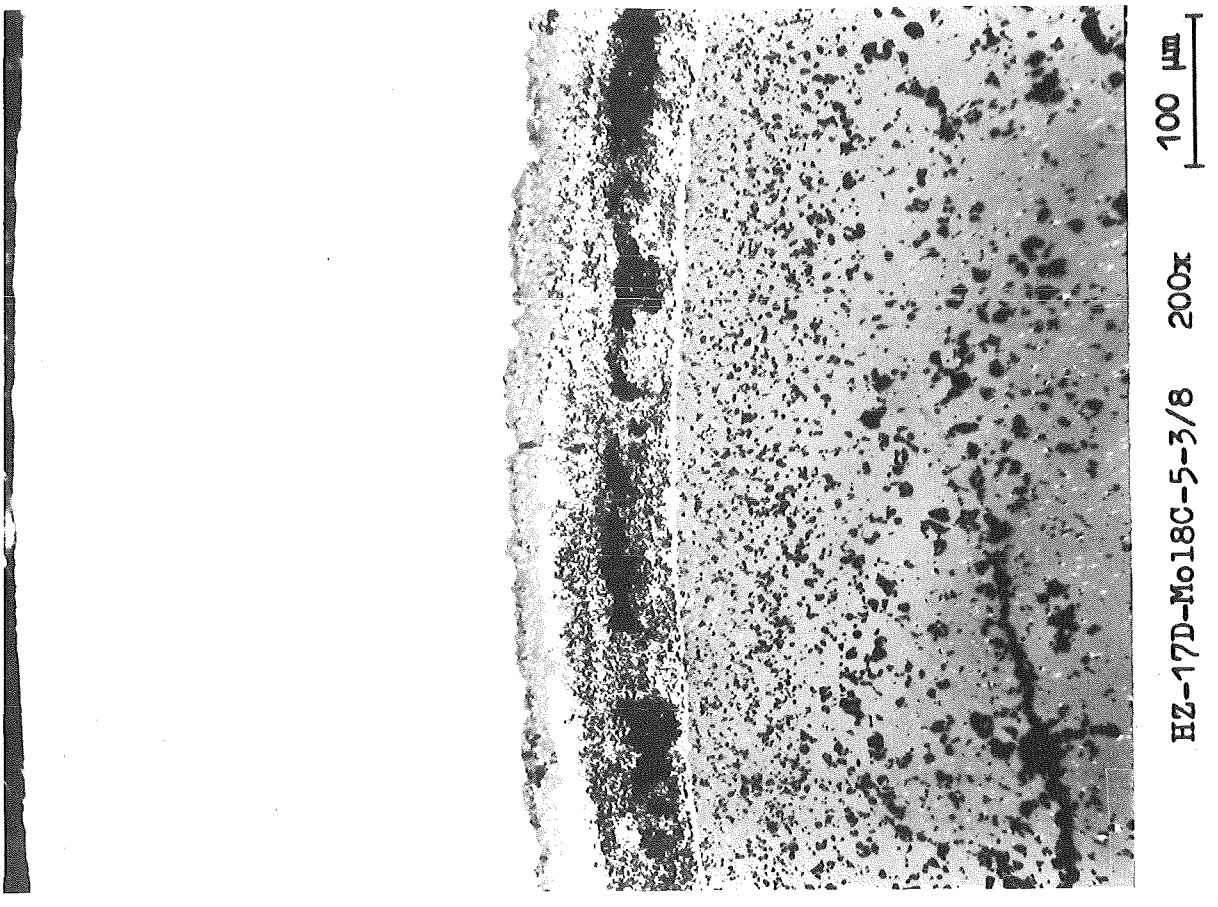
HZ-17D-Mo18C-5-3/8 200x
100 µm

Mol 8C-5-3

HZ-17D-Mo18C-5-3/9 200x 100 µm

HZ-17D-Mo18C-5-3/10 500x 40 µm

Mol 8C-5-5

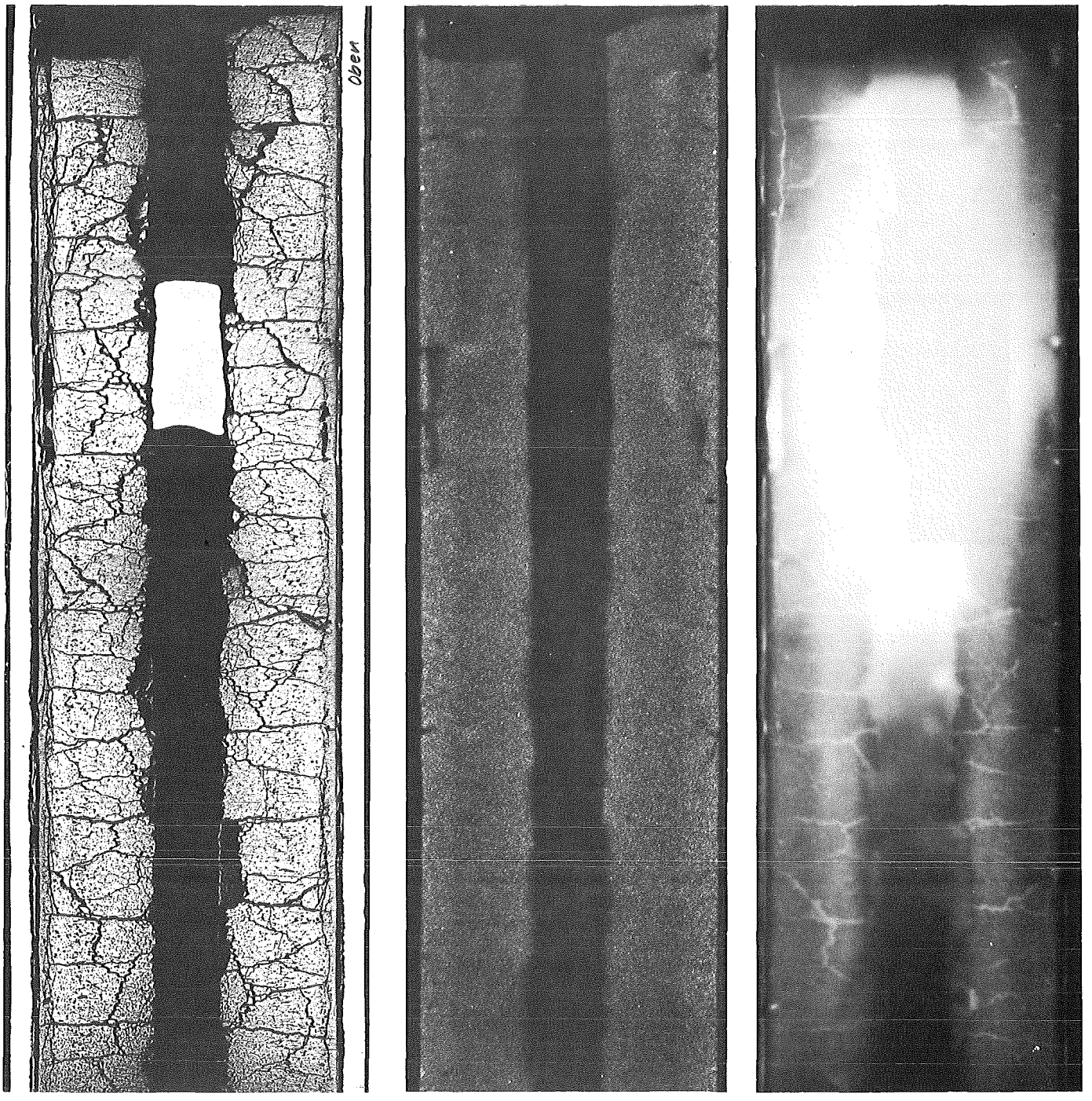

α - autorad.

β-γ - autorad.

1mm

Mol 8C-5 5

Mol 8C-5-5

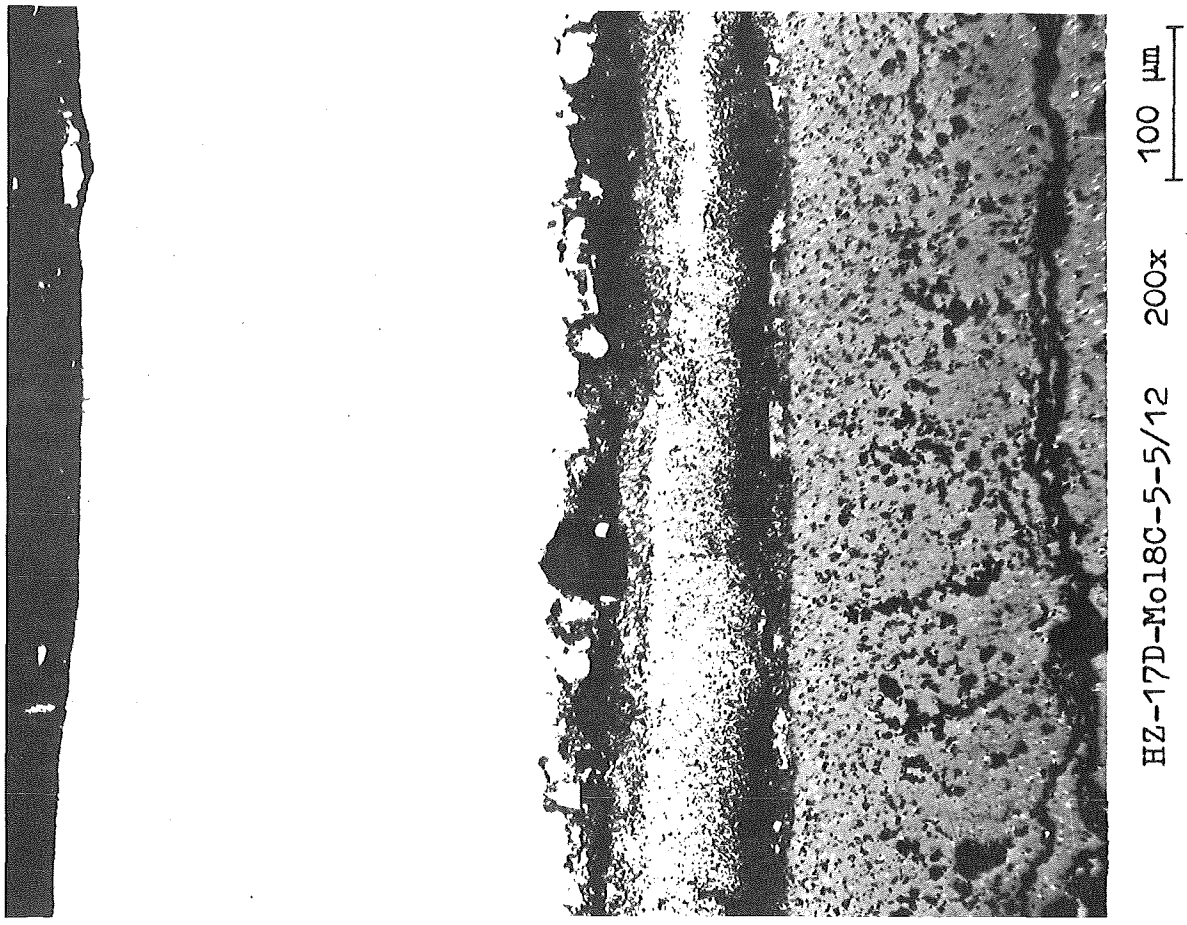

HZ-17D-Mo18C-5-5/12 200x 100 µm

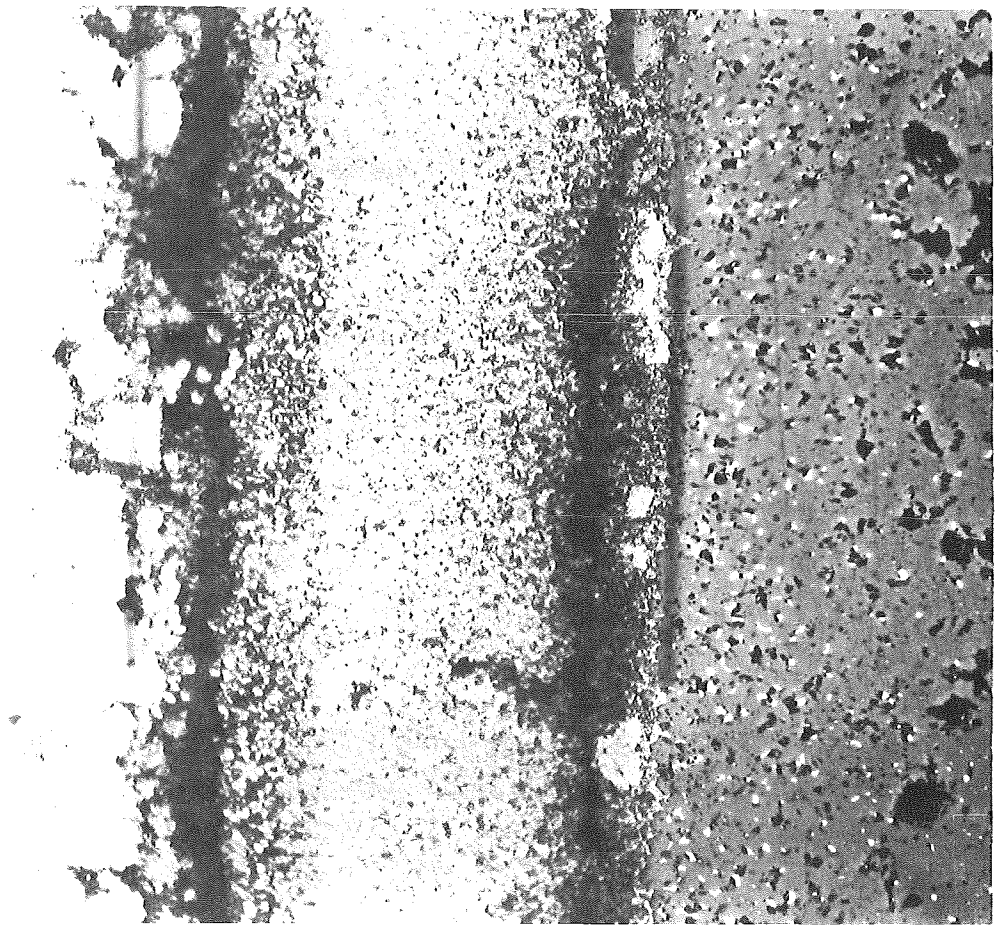

HZ-17D-Mo18C-5-5/13 500x 40 µm

Mol 8C-5-5

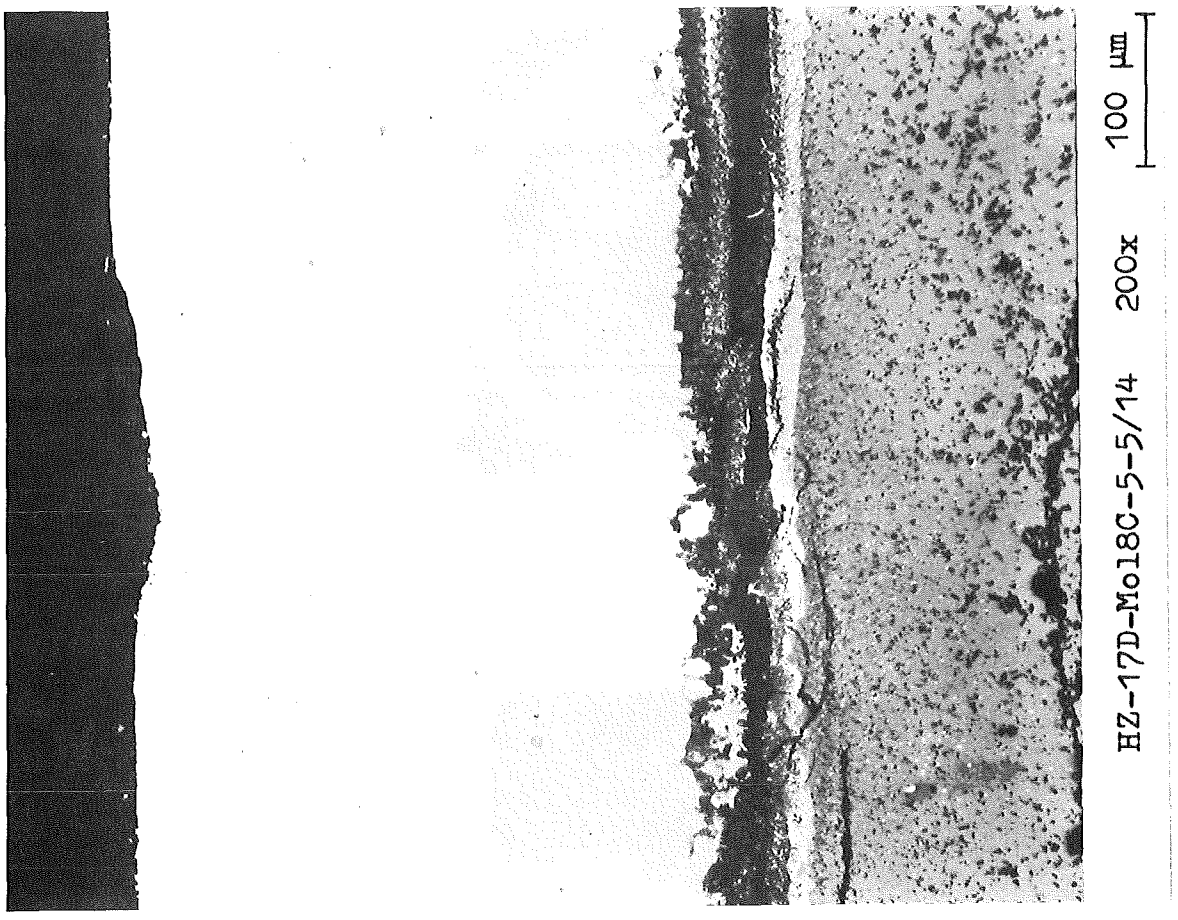

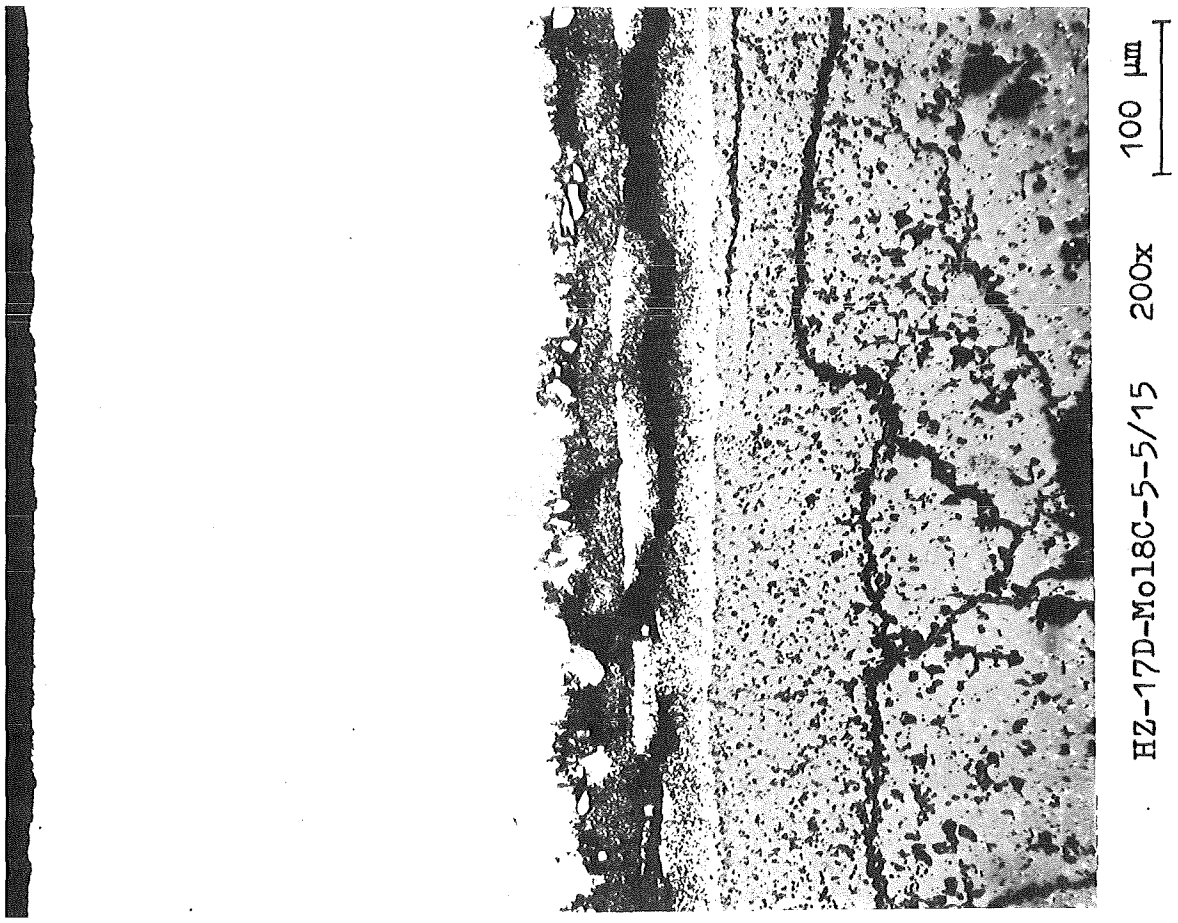

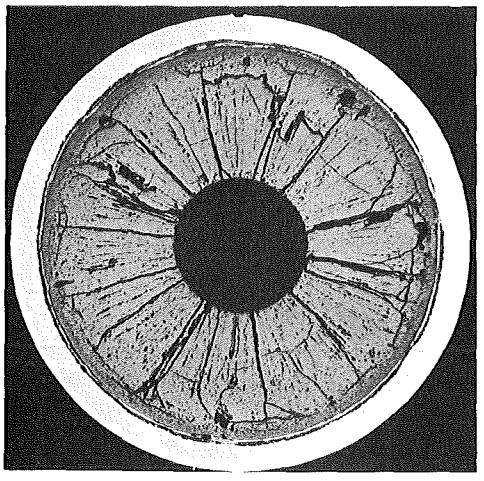

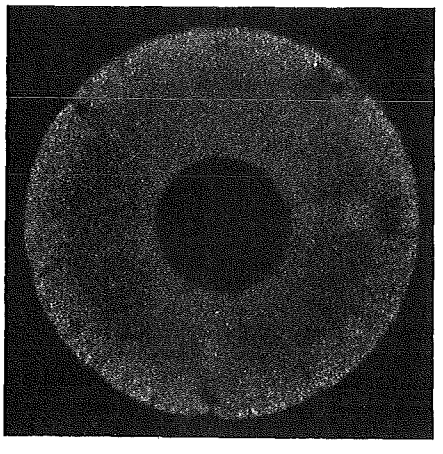

α-autorad.

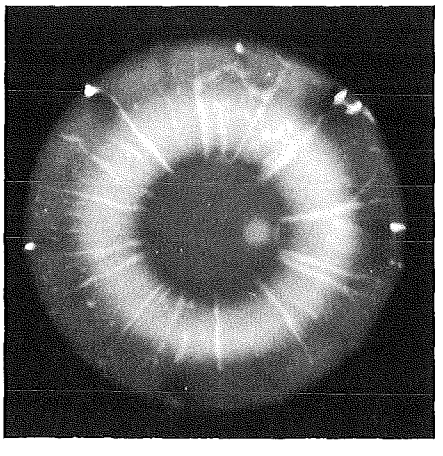

β-γ-autorad.

1mm

Mol 8C-5-6

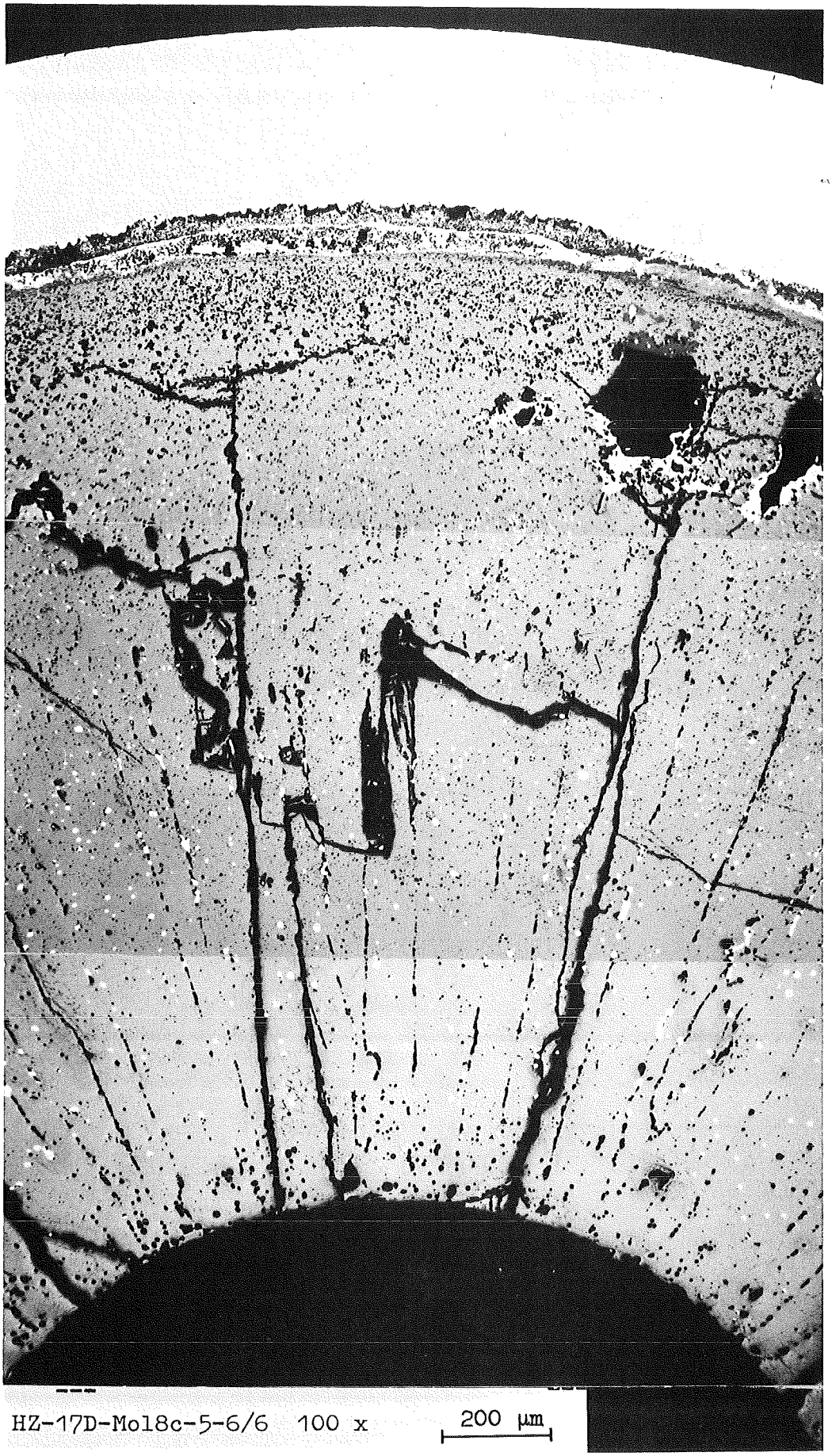

HZ-17D-Mol8c-5-6/6 100 x 200 µm

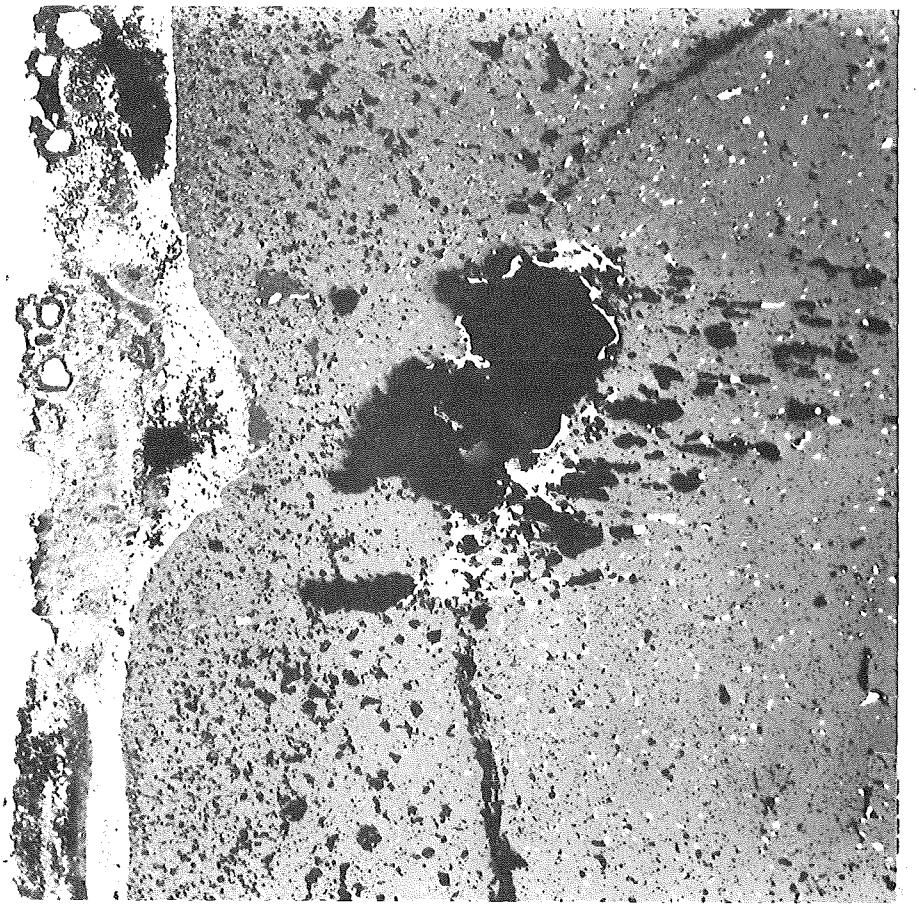

HZ-17D-Mo18C-5-6/7 200x 100 µm

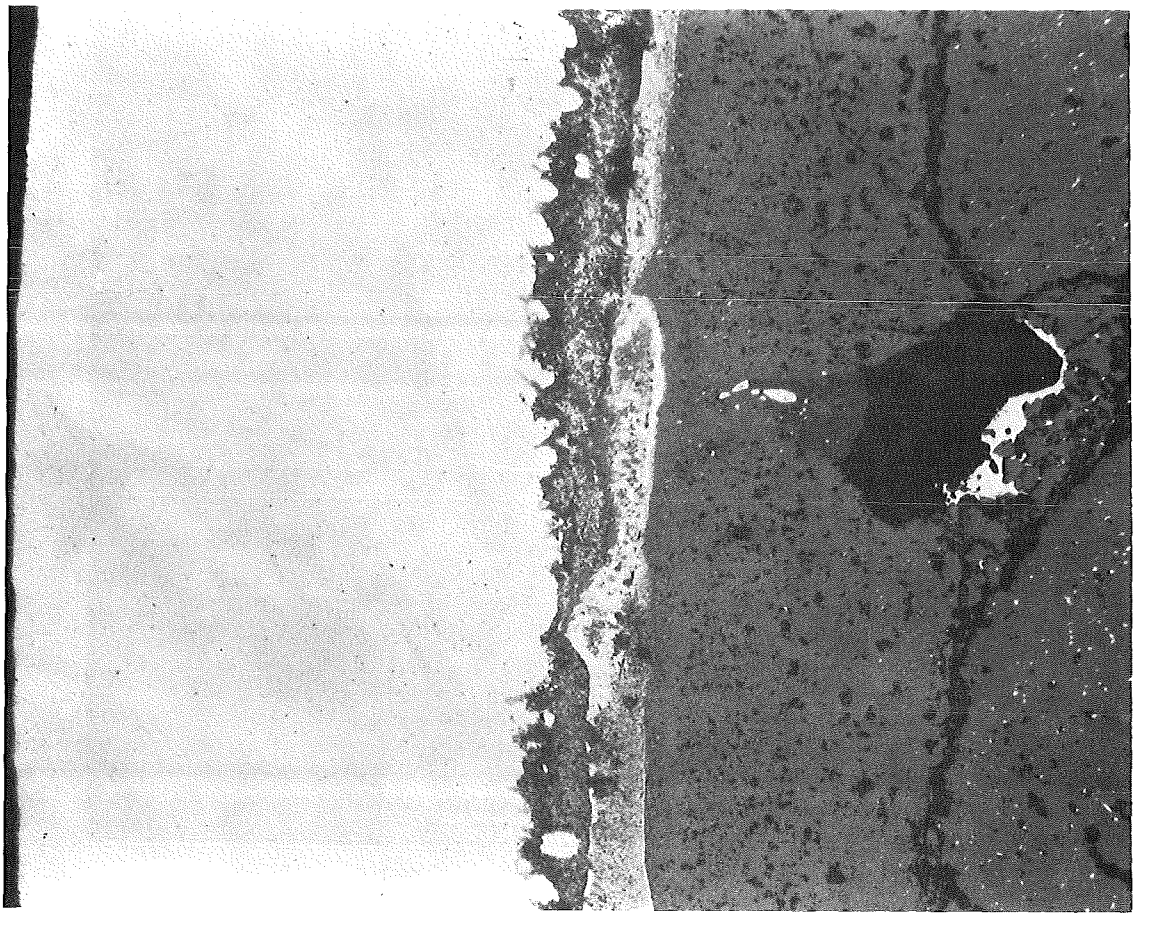

HZ-17D-Mo18C-5-6/8 200x 100 µm

Mol 8C-5-6

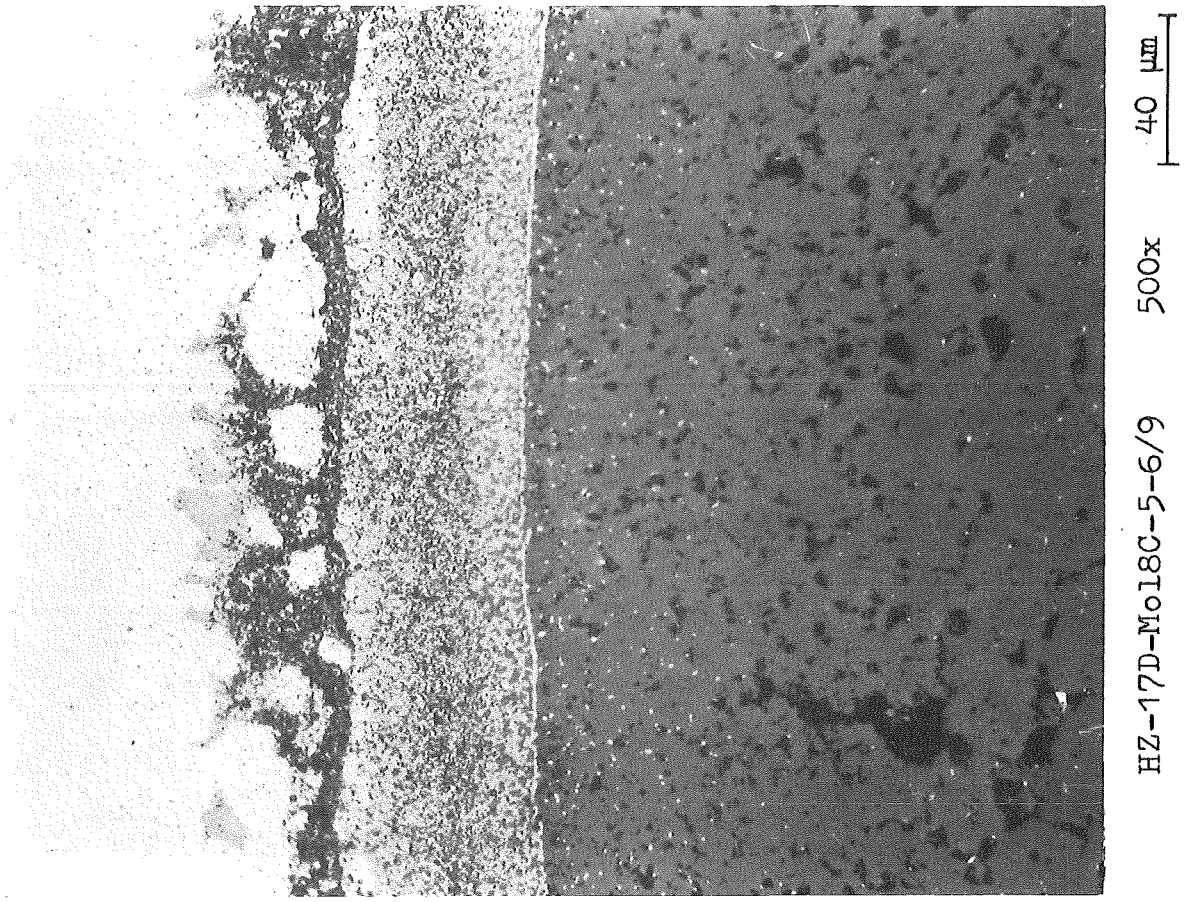

Mol 8C-5-7

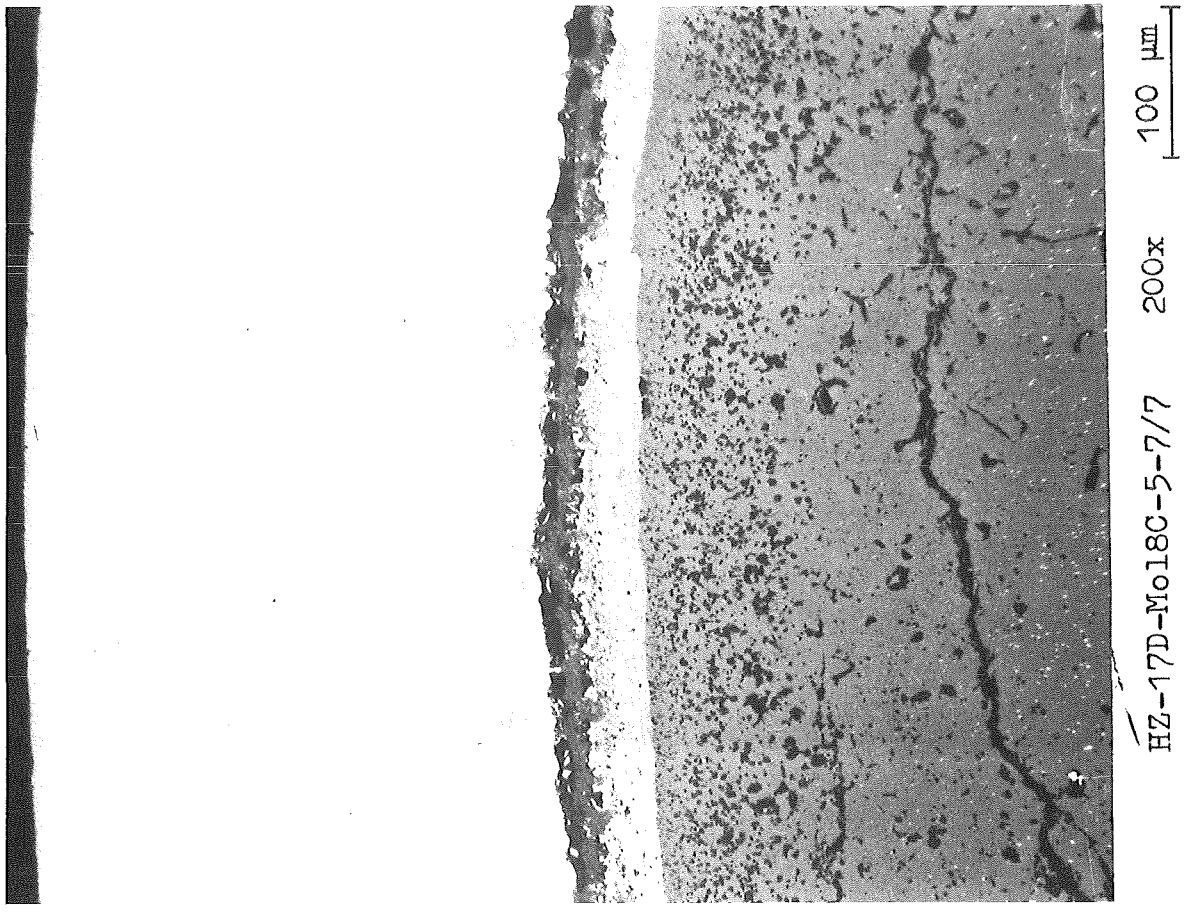

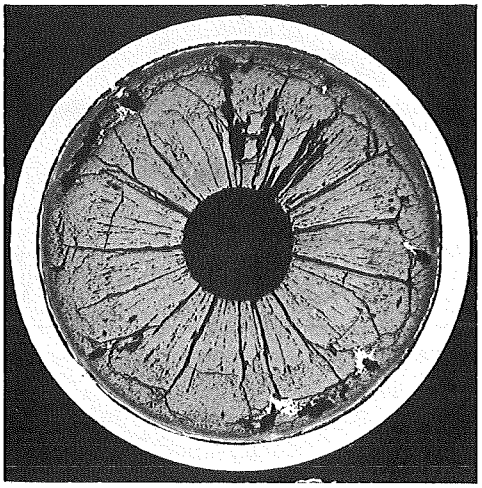

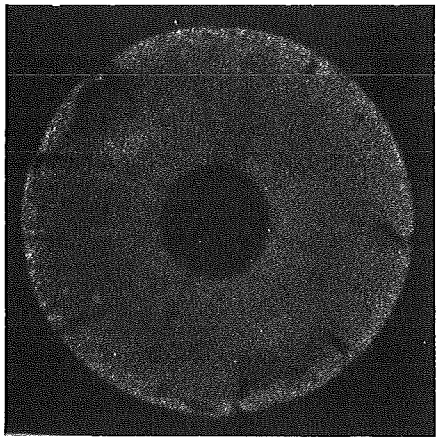

α-autorad.

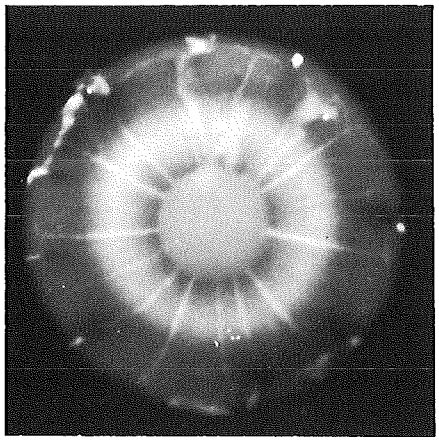

β-γ-autorad.

1mm

Mol 8C-5-7

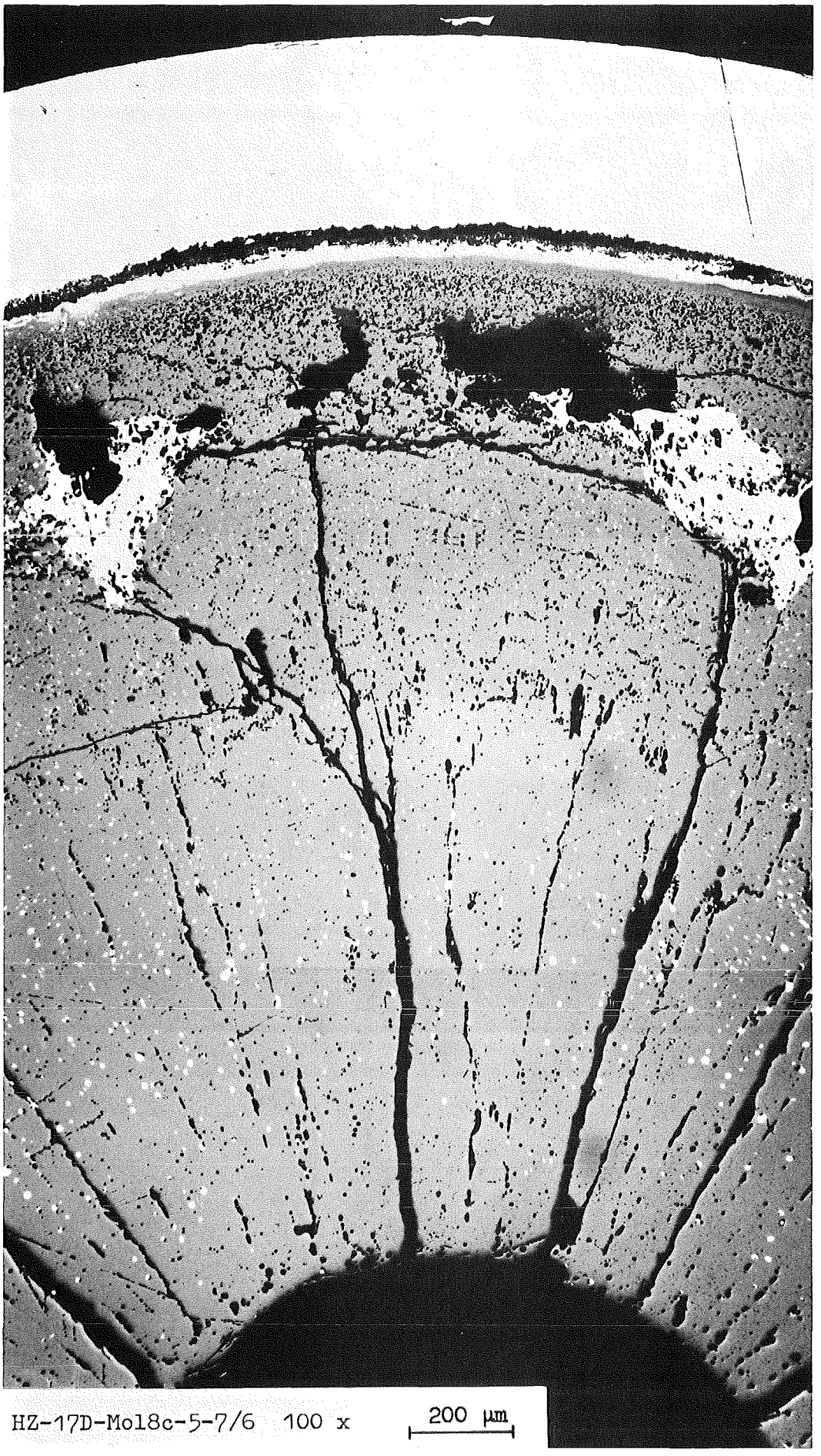

HZ-17D-Mol8c-5-7/6 100 x 200 µm

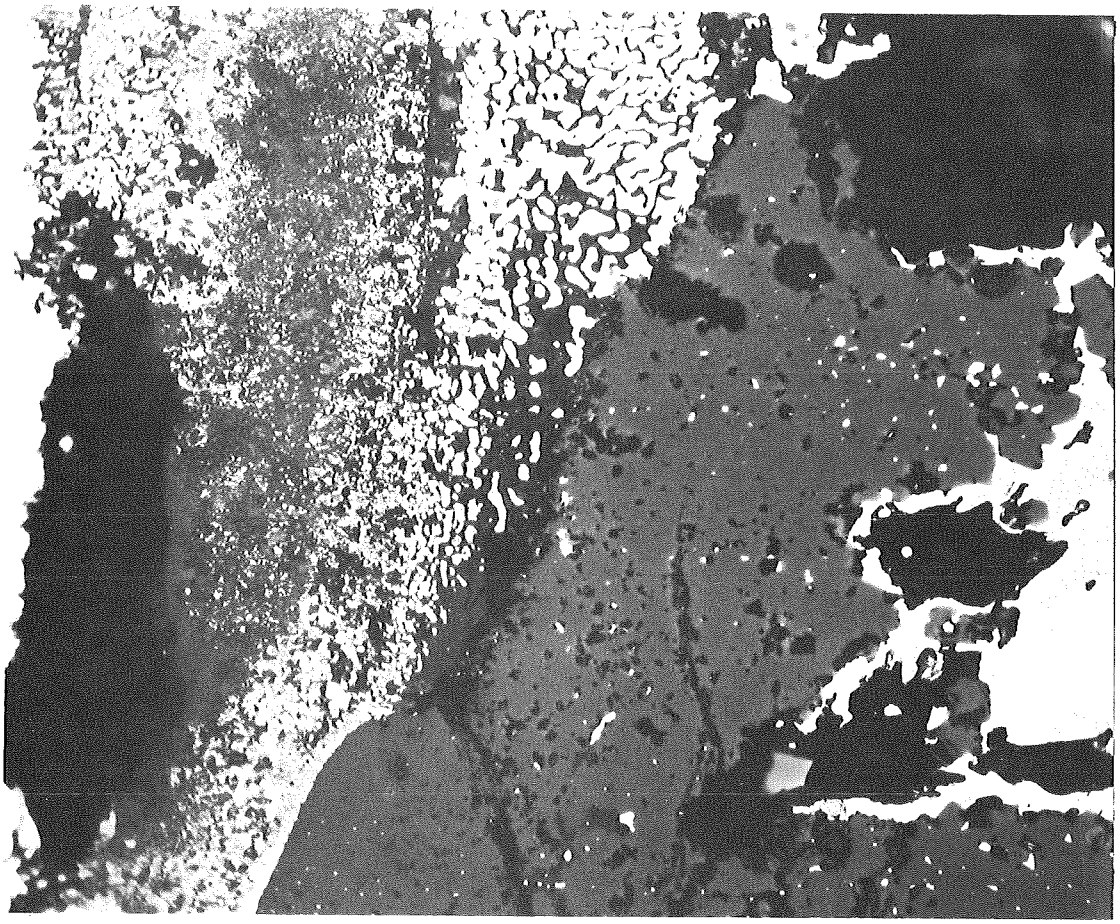

HZ-17D-Mo18C-5-7/8 500x 40 µm

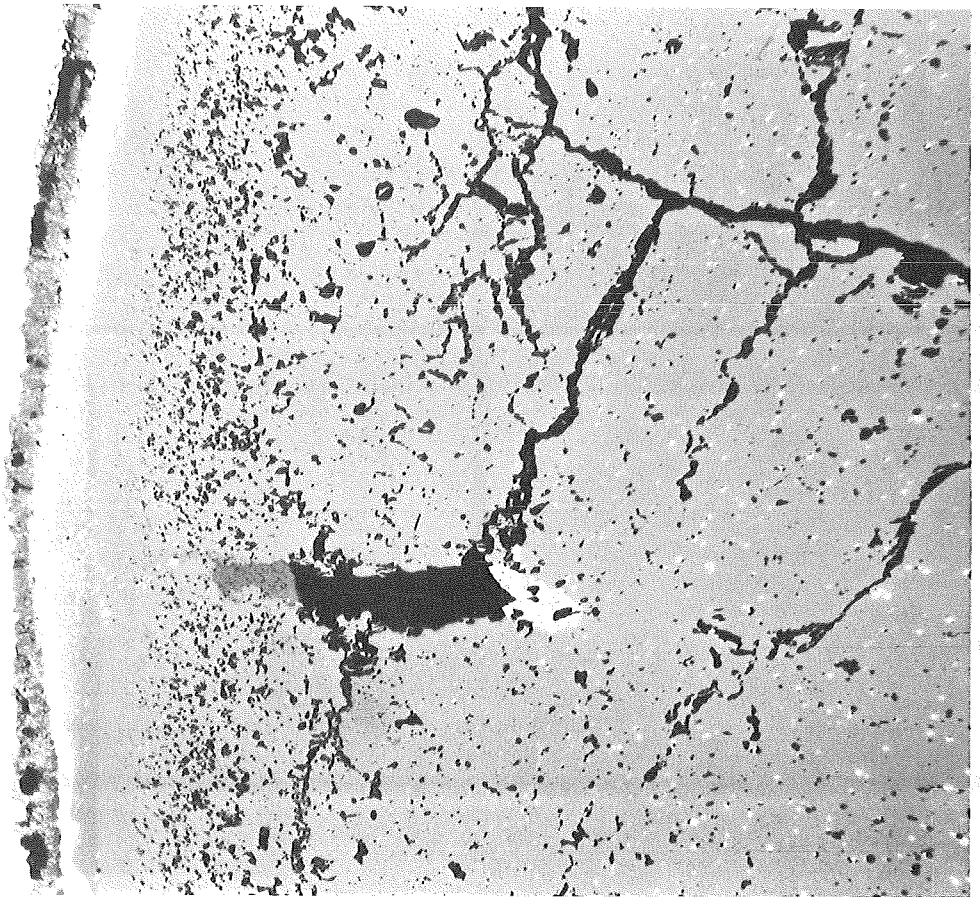

HZ-17D-Mo18c-5-7/9 100 x 200 µm

Mol 8C-5- -8

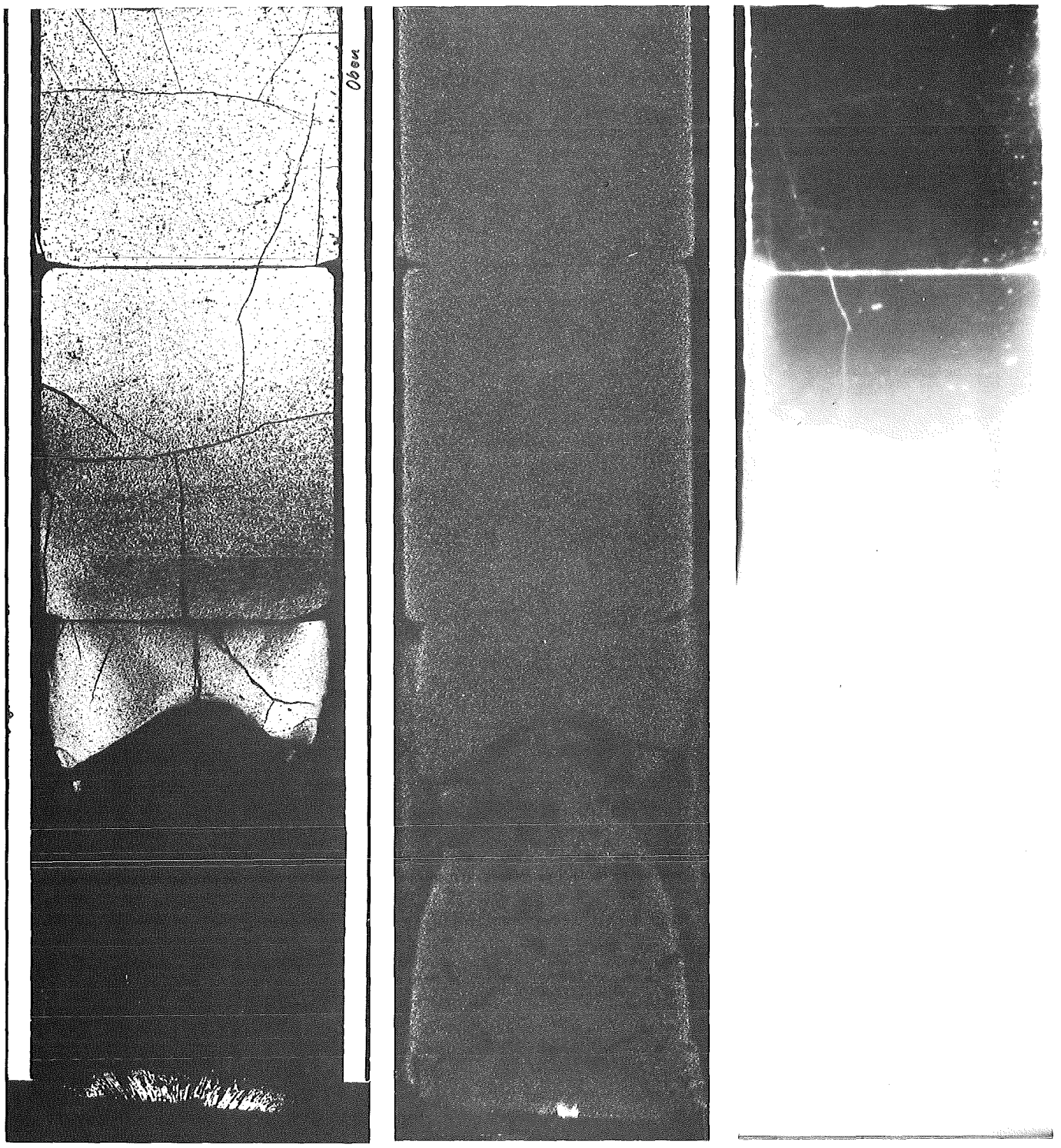

α-autorad.

β-γ-autorad.

1mm

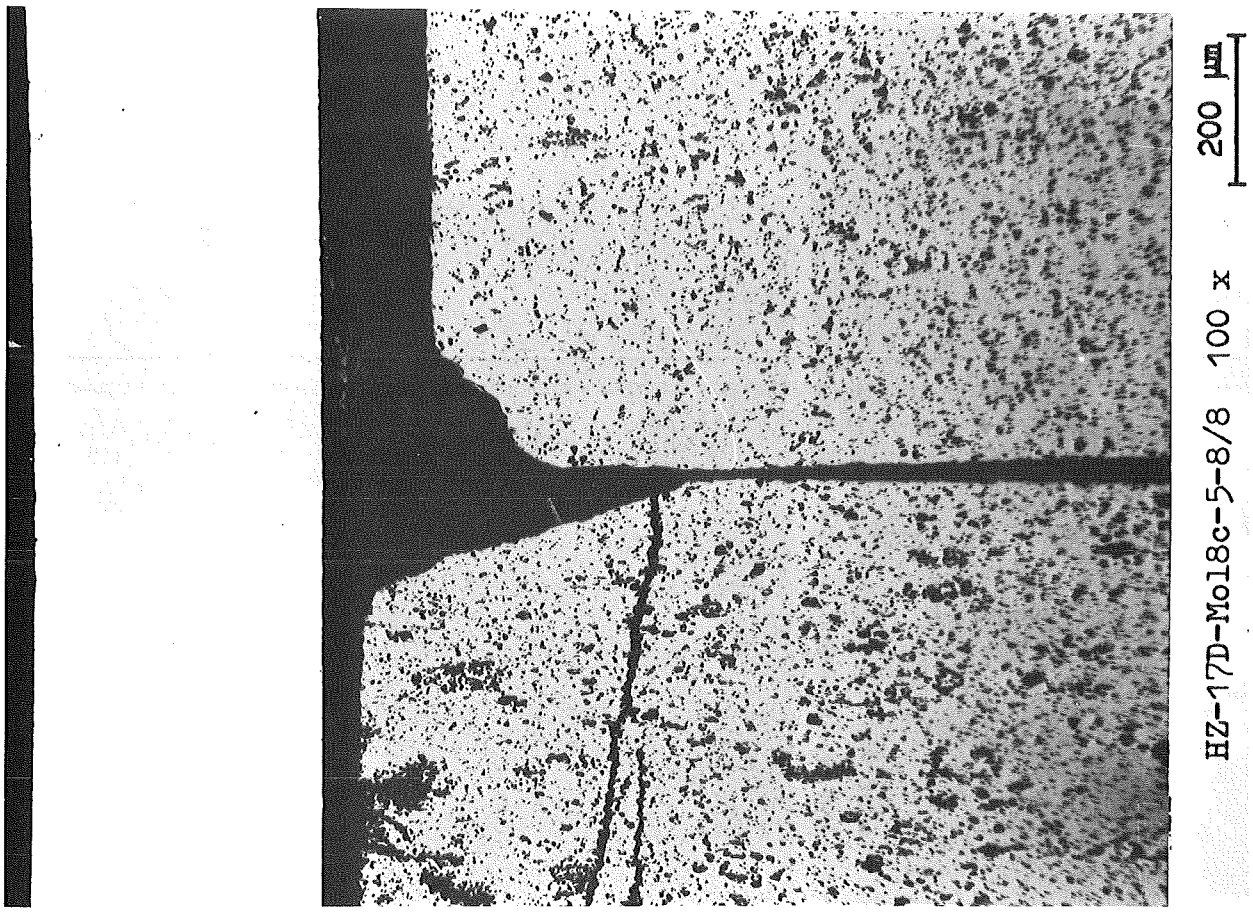
HZ-17D-Mo18c-5-8/8 100 x
200 µm

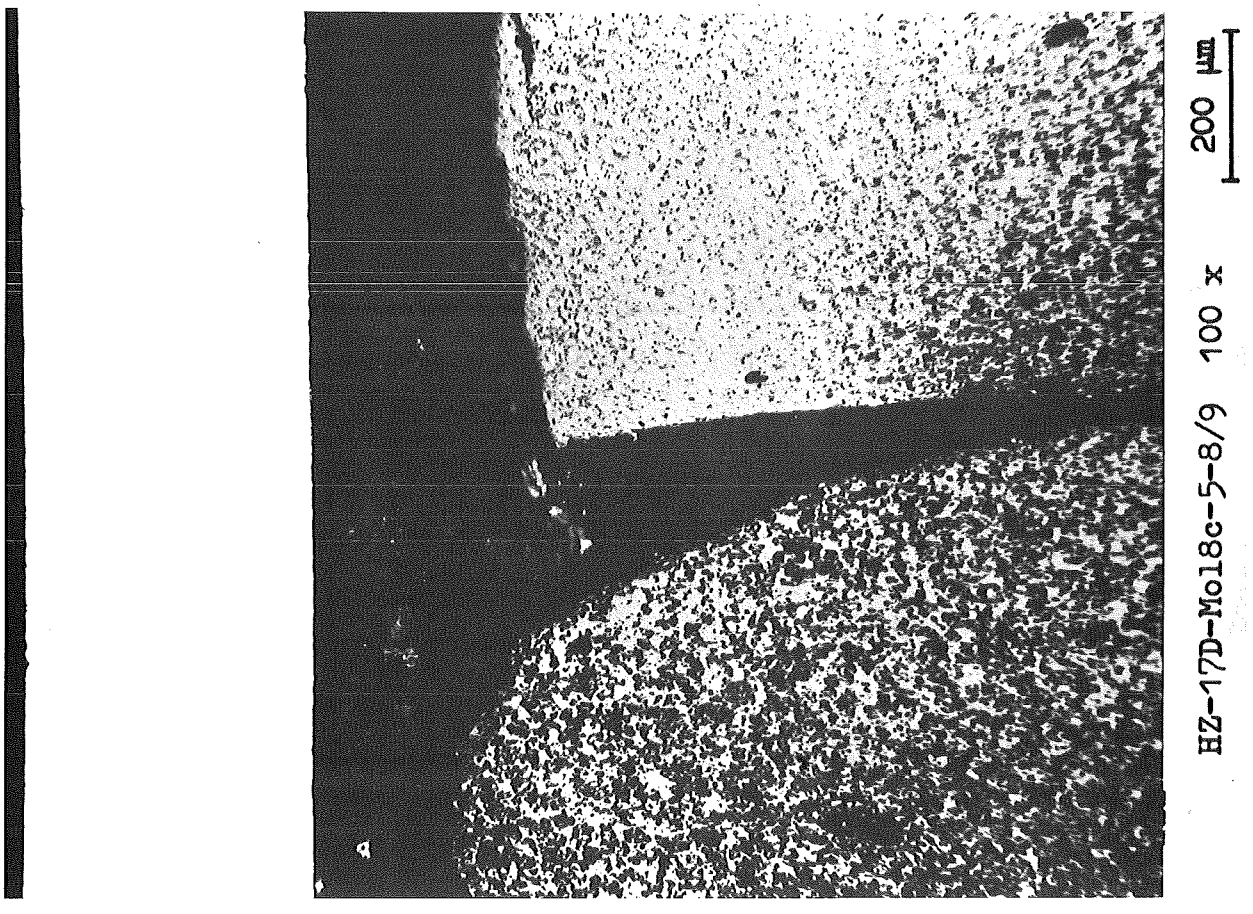
HZ-17D-Mo18c-5-8/9 100 x
200 µm

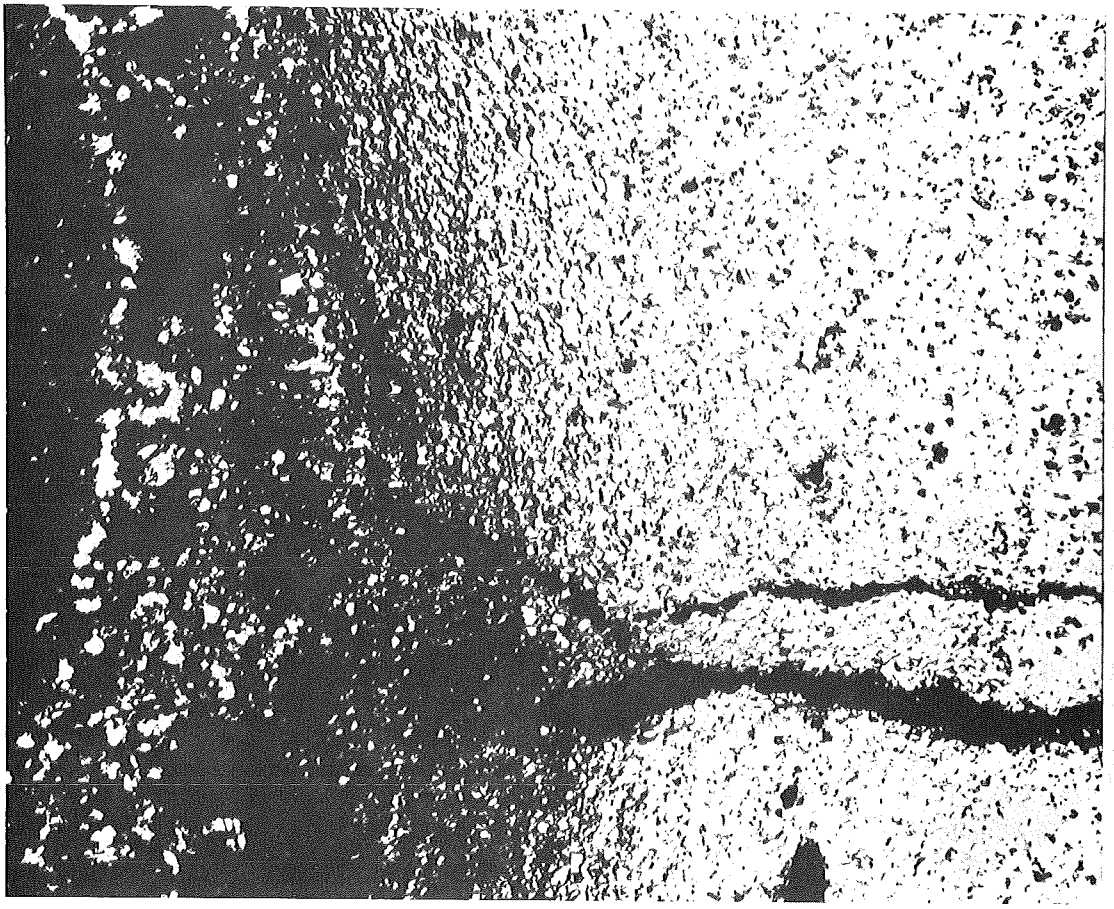

HZ-17D-Mo18C-5-8/10 200x 100 µm

HZ-17D-Mo18C-5-8/11 100x 200 µm

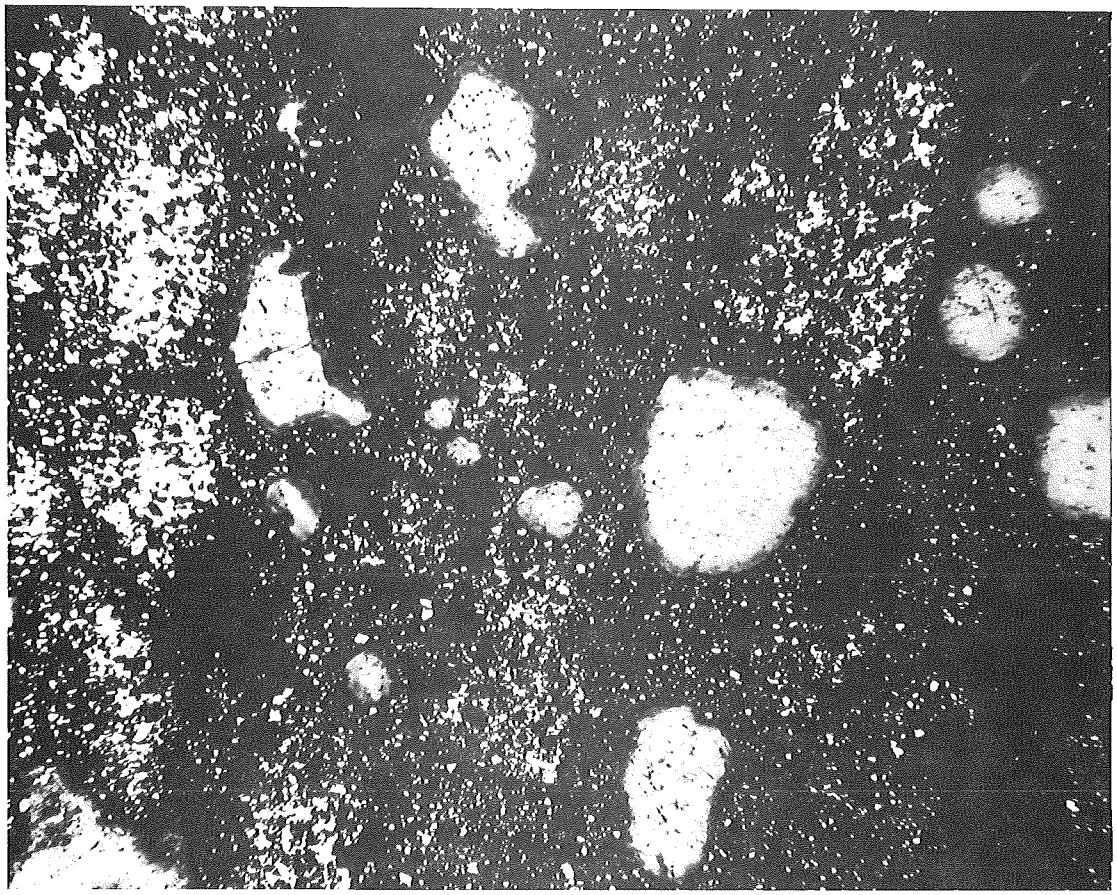

HZ-17D-Mo18C-5-8/12 100x 200 µm

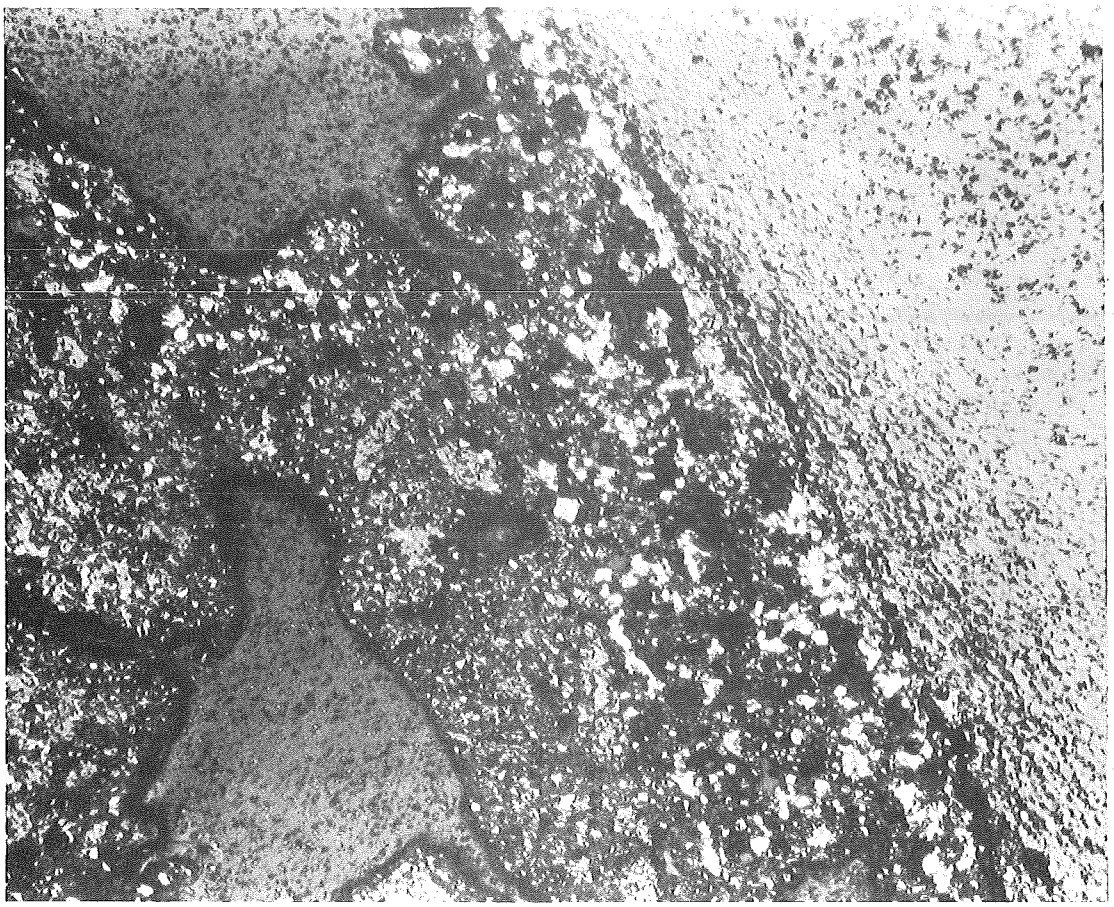

HZ-17D-Mo18C-5-8/13 200x 100 µm

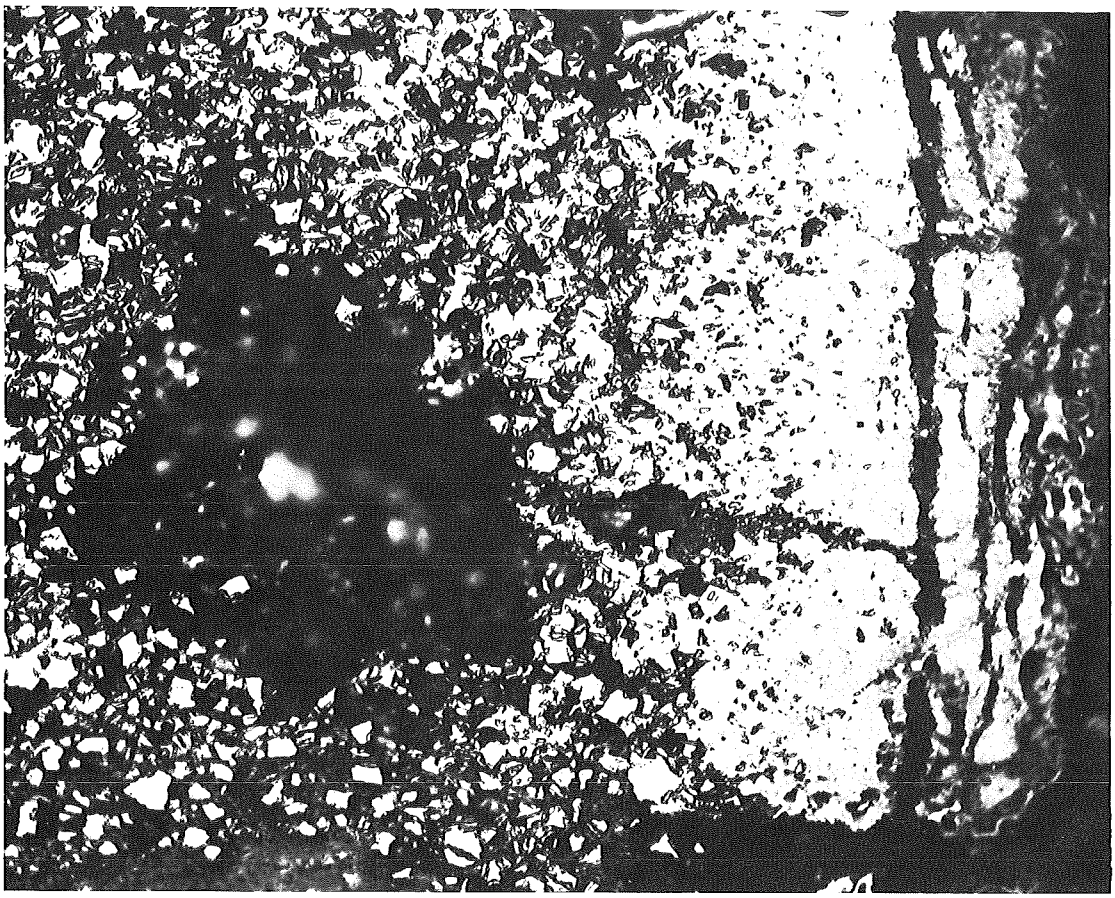

HZ-17D-Mo18C-5-8/14 500x 40 µm

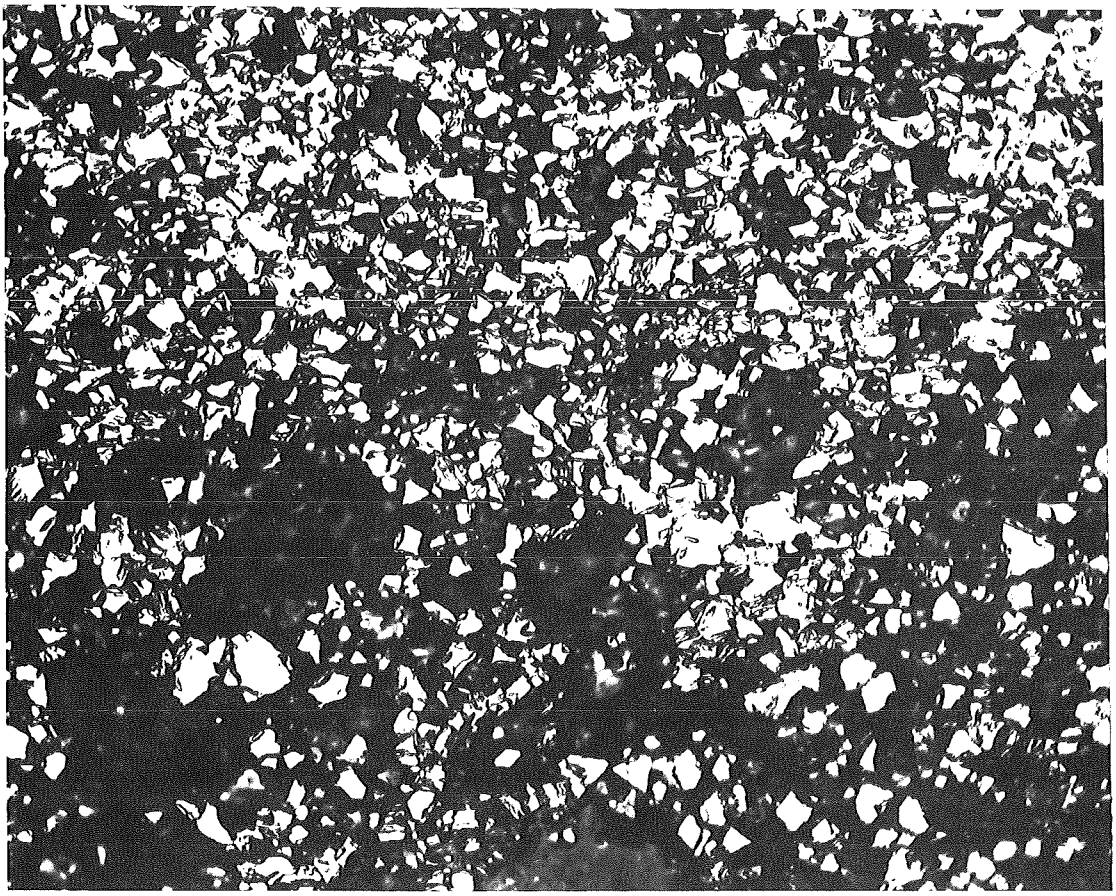

HZ-17D-Mo18C-5-8/15 500x 40 µm

Mol 8C-5-8

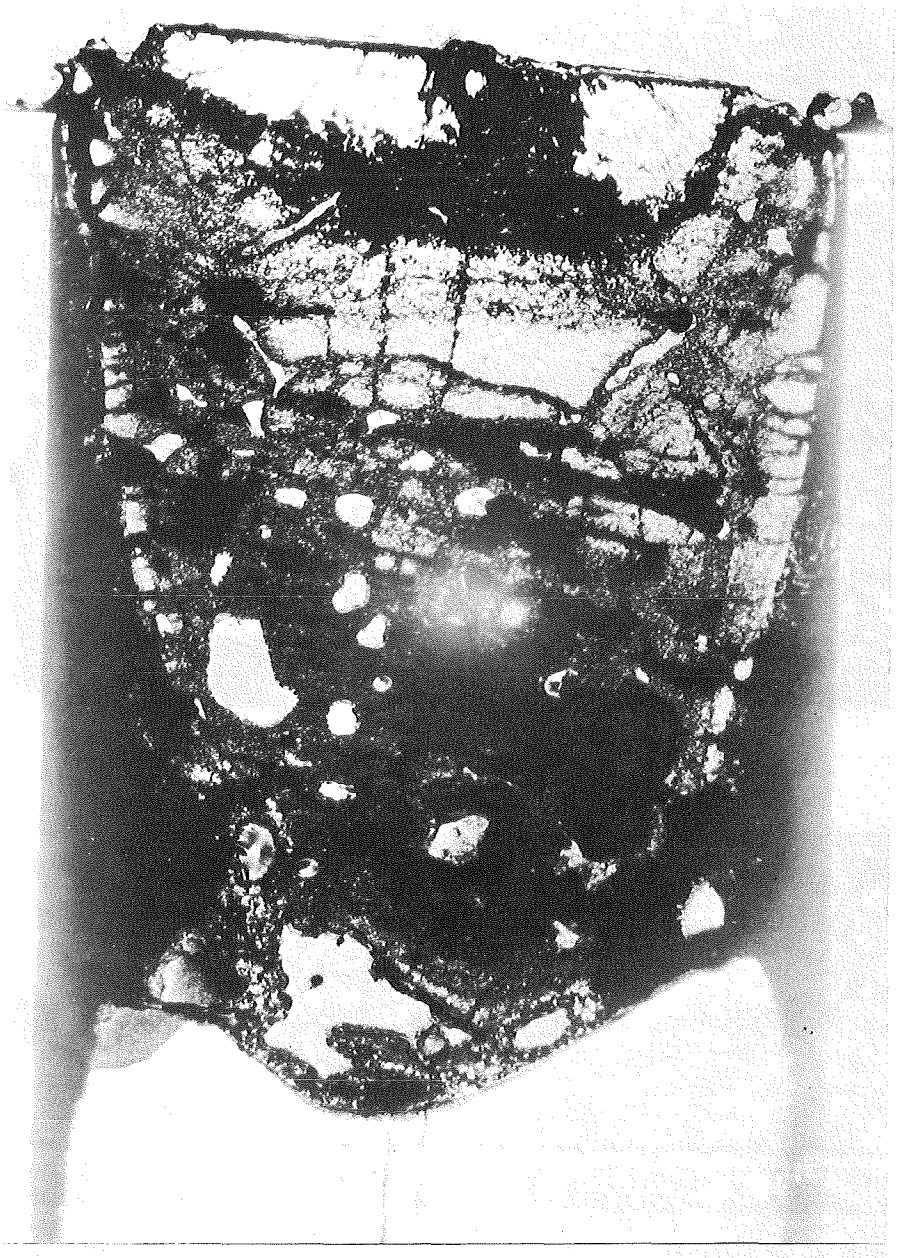

HZ-17D-Mo18C-5-8/16 20x 1 mm